DISSERTATIONES
CHIMICAE
UNIVERSITATIS
TARTUENSIS
164

KRISTEL JUKK

Electrochemical reduction of oxygen on platinum- and palladium-based nanocatalysts

DISSERTATIONES CHIMICAE UNIVERSITATIS TARTUENSIS
164

DISSERTATIONES CHIMICAE UNIVERSITATIS TARTUENSIS
164

KRISTEL JUKK

Electrochemical reduction of oxygen on platinum- and palladium-based nanocatalysts

UNIVERSITY OF TARTU
Press

Institute of Chemistry, Faculty of Science and Technology, University of Tartu, Estonia

Dissertation is accepted for commencement of the degree of Doctor of Philosophy in Chemistry on June 14, 2017 by Council of Institute of Chemistry, University of Tartu

Supervisors: Assoc. Prof. Kaido Tammeveski
Institute of Chemistry, University of Tartu, Estonia

Dr. Nadežda Kongi
Institute of Chemistry, University of Tartu, Estonia

Opponent: Prof. Enrique Herrero
Institute of Electrohemistry, University of Alicante, Spain

Commencement: August 22, 2017 at 10.00
Ravila Street 14a, Tartu (Chemicum), auditorium 1021

This work was supported by Graduate School of Functional materials and technologies receiving funding from the European Regional Development Fund in University of Tartu, Estonia.

ISSN 1406-0299
ISBN 978-9949-77-509-5 (print)
ISBN 978-9949-77-510-1 (pdf)

University of Tartu Press
www.tyk.ee

TABLE OF CONTENTS

1. LIST OF ORIGINAL PUBLICATIONS

This dissertation is based on the following original publications, which will be referred to by the corresponding Roman numerals in the text:

I **K. Jukk**, J. Kozlova, P. Ritslaid, V. Sammelselg, N. Alexeyeva, K. Tammeveski, Sputter-deposited Pt nanoparticle/multi-walled carbon nanotube composite catalyst for oxygen reduction reaction, *Journal of Electroanalytical Chemistry* 708 (2013) 31–38.

II **K. Jukk**, N. Kongi, A. Tarre, A. Rosental, A.B. Treshchalov, J. Kozlova, P. Ritslaid, L. Matisen, V. Sammelselg, K. Tammeveski, Electrochemical oxygen reduction behaviour of platinum nanoparticles supported on multi-walled carbon nanotube/titanium dioxide composites, *Journal of Electroanalytical Chemistry* 735 (2014) 68–76.

III **K. Jukk**, N. Kongi, P. Rauwel, L. Matisen, K. Tammeveski, Platinum nanoparticles supported on nitrogen-doped graphene nanosheets as electrocatalysts for oxygen reduction reaction, *Electrocatalysis* 7 (2016) 428–440.

IV **K. Jukk**, N. Kongi, K. Tammeveski, R.M. Arán-Ais, J. Solla-Gullón, J.M. Feliu, Loading effect of carbon-supported platinum nanocubes on oxygen electroreduction, (manuscript in preparation).

V **K. Jukk**, N. Alexeyeva, A. Sarapuu, P. Ritslaid, J. Kozlova, V. Sammelselg, K. Tammeveski, Electroreduction of oxygen on sputter-deposited Pd nanolayers on multi-walled carbon nanotubes, *International Journal of Hydrogen Energy* 38 (2013) 3614–3620.

VI **K. Jukk**, N. Alexeyeva, P. Ritslaid, J. Kozlova, V. Sammelselg, K. Tammeveski, Electrochemical reduction of oxygen on heat-treated Pd nanoparticle/multi-walled carbon nanotube composites in alkaline solution, *Electrocatalysis* 4 (2013) 42–48.

VII **K. Jukk**, N. Kongi, L. Matisen, T. Kallio, K. Kontturi, K. Tammeveski, Electroreduction of oxygen on palladium nanoparticles supported on nitrogen-doped graphene nanosheets, *Electrochimica Acta* 137 (2014) 206–212.

VIII **K. Jukk**, N. Kongi, K. Tammeveski, J. Solla-Gullón, J.M. Feliu, PdPt alloy nanocubes as electrocatalysts for oxygen reduction reaction in acid media, *Electrochemistry Communications* 56 (2015) 11–15.

IX **K. Jukk**, N. Kongi, K. Tammeveski, J. Solla-Gullón, J.M. Feliu, Electroreduction of oxygen on PdPt alloy nanocubes in alkaline and acid media, *ChemElectroChem* (2017, accepted for publication).

Author's contribution:

Paper I: The author has performed synthesis of catalyst materials, made all electrochemical measurements, analysed the data and participated in the writing of the paper.

Paper II: The author has performed all electrochemical measurements, analysed the data and participated in the writing of the paper.

Paper III: The author has performed synthesis of catalyst materials, made all electrochemical measurements, analysed the data and is mainly responsible for writing the paper.

Paper IV: The author has performed synthesis of catalyst materials, made all electrochemical measurements, analysed the data and is mainly responsible for writing the paper.

Paper V: The author has performed synthesis of catalyst materials, made all electrochemical measurements, analysed the data and participated in the writing of the paper.

Paper VI: The author has performed synthesis of catalyst materials, made all electrochemical measurements, analysed the data and is mainly responsible for writing the paper.

Paper VII: The author has performed synthesis of catalyst materials, made all electrochemical measurements, analysed the data and is mainly responsible for writing the paper.

Paper VIII: The author has performed synthesis of catalyst materials, made all electrochemical measurements, analysed the data and is mainly responsible for writing the paper.

Paper IX: The author has performed synthesis of catalyst materials, made all electrochemical measurements, analysed the data and is mainly responsible for writing the paper.

2. ABBREVIATIONS AND SYMBOLS

ALD	atomic layer deposition
AMFC	alkaline membrane fuel cell
A_r	real electroactive surface area
CNF	carbon nanofiber
CNT	carbon nanotube
$C_{O_2}^b$	concentration of oxygen in the bulk solution
CV	cyclic voltammetry
CVD	chemical vapour deposition
DCDA	dicyandiamide
DMF	dimethylformamide
D_{O_2}	diffusion coefficient of oxygen
E	potential
E_{onset}	onset potential
$E_{1/2}$	half-wave potential
$E°$	standard potential
ECSA	electrochemically accessible surface area
EDX or EDS	energy dispersive X-ray spectroscopy
EG	ethylene glycol
F	Faraday constant
fcc	face-centred cubic
GC	glassy carbon
GNS	graphene nanosheet
GO	graphene oxide
HR-SEM	high resolution scanning electron microscopy
HR-TEM	high resolution transmission electron microscopy
j	measured current density
j_d	diffusion-limited current density
j_{lim}	plateau current density
j_k	kinetic current density
k_i	heterogeneous electron transfer rate constant
K-L	Koutecky-Levich
MA	mass activity
MWCNT	multi-walled carbon nanotube
n	number of electrons transferred per oxygen molecule
NG	nitrogen-doped graphene
OA	oleic acid
OLA	oleylamine
ORR	oxygen reduction reaction
Pd/C	carbon-supported palladium nanoparticles
PdNP	palladium nanoparticle
PEMFC	proton exchange membrane fuel cell
Pt/C	carbon-supported platinum nanoparticles

PtNP	platinum nanoparticle
PVP	polyvinylpyrrolidone
R	universal gas constant
RDE	rotating disk electrode
rds	rate-determining step
RHE	reversible hydrogen electrode
SA	specific activity
SEM	scanning electron microscopy
SWCNT	single-walled carbon nanotube
T	temperature
TEM	transmission electron microscopy
TGA	thermogravimetric analysis
UPD	under potential deposition
v	potential scan rate
XPS	X-ray photoelectron spectroscopy
XRD	X-ray diffraction
v	kinematic viscosity of the solution
θ	electron take-off angle
ω	electrode rotation rate

3. INTRODUCTION

The oxygen reduction reaction (ORR) possesses great technological importance in electrochemical systems, like fuel cells, metal-air batteries and electrosynthesis of hydrogen peroxide. The reduction of O_2 occurs mainly via two-electron pathway or four-electron pathway. The 4-electron pathway is predominant on Pt-metals and silver, whilst 2-electron pathway takes place on carbon materials, gold and most of metal oxides.

Platinum (Pt) has highest electrocatalytic activity towards the ORR compared to other metals, but due to the high price and scarcity of this precious metal, alternative catalyst materials are needed. One opportunity to reduce the utilisation of platinum is to use nanostructured Pt (alloys, Pt/carbon composites etc.) or its complete replacement.

Platinum and palladium (Pd) have similar properties, for example, same face-centered-cubic crystal structure, similar atom size etc. Palladium is much more abundant in the Earth crust and its electrochemical activity towards the ORR is high, which makes Pd good substitute for Pt in the cathode catalyst of fuel cells. Therefore, in this PhD thesis palladium has been examined as Pt-Pd alloy and Pt-free catalyst for fuel cells.

The main aim of this work was to prepare different Pt- and Pd-based nanomaterials and to perform a detailed electrochemical characterisation of these composite materials towards O_2 reduction. The surface morphology and composition of the prepared catalysts were analysed using different physical methods (scanning and transmission electron microscopies, X-ray photoelectron spectroscopy, X-ray diffraction, energy dispersive X-ray spectroscopy and thermogravimetry). For electrochemical characterisation cyclic voltammetry, CO-oxidation and the rotating disk electrode (RDE) method were used.

In the first part of the work, platinum nanoparticles (PtNPs) were supported on different carbon-materials employing different preparation methods and these nanomaterials were used as electrocatalysts for O_2 reduction. Firstly, the magnetron sputtering technique was utilised for the preparation of PtNPs supported on multi-walled carbon nanotubes (MWCNTs) [I,II], secondly, sodium borohydride and ethylene glycol reduction of Pt-salt was used to synthesise Pt nanoparticles on nitrogen-doped graphene (NG) [III] and thirdly, chemical reduction of Pt-salt in the presence of oleylamine/oleic acid was applied to prepare Pt nanocubes supported on high-surface-area carbon [IV]. The studies of oxygen electroreduction on these nanostructured composite materials were carried out in acidic and alkaline media.

In the second part of present doctoral work, palladium nanoparticles (PdNPs) were anchored to MWCNTs and NG supports. Magnetron sputtering method was employed for the preparation of MWCNT-supported Pd catalysts [V] and the effect of annealing at three different temperatures [VI] on the ORR activity was explored. Nitrogen-doped graphene nanosheets were modified with PdNPs prepared by borohydride reduction [VII]. The electroreduction of oxygen on

these Pd-based composite materials was studied in sulphuric acid and potassium hydroxide solutions.

In the third part of doctoral thesis, the reduction of oxygen on PdPt alloy nanocubes synthesised in the presence of polyvinylpyrrolidone was investigated in acidic and alkaline solutions [VIII, IX]. Different Pd-to-Pt ratios were used and the electrocatalytic activity of PdPt catalysts for ORR was compared with that of cubic Pd and Pt nanoparticles.

4. LITERATURE OVERVIEW

4.1. The oxygen reduction reaction

The oxygen reduction reaction (ORR) is one of the most studied electrochemical reactions, being the most important reaction in energy conversion systems such as fuel cells and metal-air batteries, thus this reaction has been thoroughly studied on different materials [1–3]. The ORR proceeds in aqueous solutions mainly via two pathways: two-electron pathway (from O_2 to H_2O_2) or direct four-electron pathway (from O_2 to water).

In acidic media, the 4-electron pathway takes place as follows:

$$O_2 + 4H^+ + 4e^- \rightarrow 2H_2O \qquad E° = 1.229 \qquad (1)$$

The 2-electron pathway to H_2O_2:

$$O_2 + 2H^+ + 2e^- \rightarrow H_2O_2 \qquad E° = 0.67\ \text{V} \qquad (2)$$

which can be further reduced to water:

$$H_2O_2 + 2H^+ + 2e^- \rightarrow 2H_2O \qquad E° = 1.77\ \text{V} \qquad (3)$$

or catalytically decomposed:

$$2H_2O_2 \rightarrow 2H_2O + O_2 \qquad (4)$$

In alkaline media, the four-electron reduction proceeds:

$$O_2 + 2H_2O + 4e^- \rightarrow 4OH^- \qquad E° = 0.401\ \text{V} \qquad (5)$$

The 2-electron reaction yielding HO_2^-:

$$O_2 + H_2O + 2e^- \rightarrow HO_2^- + OH^- \qquad E° = -0.065\ \text{V} \qquad (6)$$

followed by subsequent reduction:

$$HO_2^- + H_2O + 2e^- \rightarrow 3OH^- \qquad E° = 0.867\ \text{V} \qquad (7)$$

or catalytical decomposition:

$$2HO_2^- \rightarrow 2OH^- + O_2 \qquad (8)$$

[1–4]. The standard potential ($E°$) values are given against the standard hydrogen electrode at 25 °C. The simplified reaction pathways are presented in Scheme 1 [3].

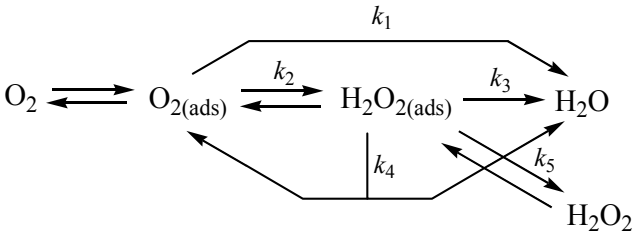

Scheme 1. Simplified scheme of the oxygen reduction reaction in acidic media. The rate constants for different pathways are shown as (k_i). Adsorbed states are subscribed by (ads).

The mechanism of the electrochemical O_2 reduction reaction is rather complex and involves many intermediates, primarily depending on the nature of the electrode material, catalyst and electrolyte [2, 3]. In fuel cells, O_2 reduction is the cathodic reaction, but the ORR kinetics are usually sluggish, therefore it is important to stimulate the reaction rate of O_2 reduction for practical applications in fuel cells, for that better cathode catalyst materials are needed.

4.2. Oxygen reduction on platinum electrodes

Platinum is the best metal catalyst for ORR [1] and this reaction has been widely studied on bulk Pt electrodes [1–3, 5]. Electroreduction of oxygen on platinum is the cathodic reaction in fuel cells and proceeds mainly through 4-electron pathway.

The ORR on different facets of Pt monocrystals has been systematically studied by Markovic research group [6–11]. They concluded that the structure-sensitivity of the ORR is mainly related to the structure-sensitive adsorption of anions (OH^-, HSO_4^-, ClO_4^-, etc.) on the Pt(hkl) facets that block the active centres and thus inhibit the O_2 reduction rate [11, 12]. In sulphuric acid solution, the structure-sensitivity towards the ORR is well-pronounced on the Pt(111) facet, because the surface geometry of Pt(111) fits well with the HSO_4^- anion structure, thus O_2 reduction is much more inhibited on Pt(111) compared to Pt(110) and Pt(100) monocrystals. The order of the electrocatalytic activities of oxygen reduction on Pt monocrystals in H_2SO_4 solution decreases as follows: Pt(110) > Pt(100) > Pt(111) [9]. The structure-sensitivity of Pt nanoparticles towards ClO_4^- and OH^- adsorption is less pronounced than HSO_4^- and thus the ORR activities in perchloric acid and hydroxide solutions are much higher compared to sulphuric acid. The electrocatalytic activity of O_2 reduction in 0.1 M $HClO_4$ decreases in the order Pt(110) > Pt(111) > Pt(100), whilst in 0.1 M KOH, it follows the order of Pt(111) > Pt(110) > Pt(100) [8]. On the stepped Pt surfaces it was found that the ORR activity in sulphuric and perchloric acid on Pt(111) was the lowest [13, 14]. The O_2 reduction activity of Pt(110)–(1 × 1) was found

to be lower than that of disordered Pt(110)–(1 × 2) in 0.1 M $HClO_4$ by 30–40 mV on the basis of the half-wave potential ($E_{1/2}$) value [15].

The structure-sensitivity of the ORR on Pt(hkl) low-index facets should lead to particle size effects according to the cubo-octahedral model of Pt particles [16]. Several efforts have been made to understand the Pt particle size effect on the ORR kinetics [17–28]. Mayrhofer et al. have reported in their early studies that the specific activity (SA) for O_2 reduction increases when the particle size increases [20, 21]. This change in activity is related to the enhanced surface coverage by oxygen-containing species, which block the active sites more strongly when the Pt particle size decreases. Sheng et al. also studied the size-dependence of the ORR activity of Pt nanoparticles (size below 5 nm) on high-area carbon support in acidic electrolytes [22]. However, their results did not express any influence of the size on the specific and mass activities (MA) for O_2 reduction. Whilst the study by Sheng et al. resulted in independent relationship between Pt particle size and oxygen reduction activity, it has been reported by Shao and co-workers that both SA and MA are dependent on the Pt particle size, if the particle diameter is under 10 nm [23]. These authors suggested that this behaviour is related to the oxygen binding energies on different Pt sites, which get accessible when the particle size changes. Furthermore, Shinozaki et al. [27], who varied the Pt particle diameter from 2 to 10 nm, showed that in 0.1 M $HClO_4$ solution the SA increased from 0.8 to 1.8 mA cm^{-2} with increasing particle size, and for particles bigger than 10 nm the activity plateaued to 2.7 mA cm^{-2} at 0.9 V vs RHE. It has been suggested by Mukerjee and McBreen that the decrease in the ORR activity of the smaller Pt particles (size below 5 nm) is related to the increase of Pt low-coordination sites on the surface of platinum nanoparticles, which inhibits the electroreduction of O_2 due to the strong adsorption of OH^- above 0.8 V vs RHE [19]. The particle-size effect has been assigned to the geometric factors, associated with the crystal facets distribution on the surface of the nanoparticle [16], or to the alteration in the electronic structure of smaller particles that raise the adsorption energy of oxygenated species [19, 20].

The ORR kinetics on platinum also depends on the coverage of surface oxides. It has been established that in the wide range of potentials the surface of Pt electrodes is covered by oxygen-containing groups [5, 29]. Depending on the oxide coverage, the Tafel slope changes when the reduced Pt-surface covers with surface oxides. At low overpotentials Tafel slope is approximately –60 mV and it changes to –120 mV at high overpotentials in acidic and alkaline media [29]. Damjanovic and Brusic have suggested that the first electron transfer to O_2 molecule is the rate-determining step (rds) in both acidic and alkaline solutions [29]. They showed that the same rds controls the kinetics of O_2 reduction in both Tafel regions. The rate equation was expressed as follows [29]:

$$i = nFkC_{O_2} \exp(-aEF/RT) \exp(-\beta\gamma\Theta/RT) \quad (9)$$

where γ is the measure of the change in the energy of adsorption with oxygen coverage Θ.

4.3. Oxygen reduction on PtNPs supported on CNTs and graphene

Carbon-supported platinum catalysts (Pt/C) have been under investigation in numerous studies as potential ORR electrocatalysts with improved activity and stability. Due to their unique electrical and structural properties carbon nanotubes (CNTs) are an attractive support material for Pt nanoparticles (PtNPs). Carbon nanotubes demonstrated the ability to carry large current densities and fast electron-transfer kinetics when used for electrochemical applications [30]. In 1998, Che et al. synthesised carbon nanotubes by chemical vapour deposition (CVD) method as support materials for Pt nanoparticles and used these as membranes for O_2 reduction electrocatalysis in 0.05 M H_2SO_4 [31]. They observed a large O_2 reduction wave at potentials similar to those characteristics for Pt electrocatalysts in acid solution. Other pioneering studies have pointed out that PtNPs supported on CNTs show an excellent electrocatalytic activity [32–34] and high stability in electrochemical conditions [35, 36].

Various catalyst preparation strategies have been proposed to attach Pt nanoparticles onto the sidewalls of carbon nanotubes. Uniform Pt metal deposition onto high-surface-area carbon supports is a key challenge of developing successful efficient catalyst materials with high durability. Chemical synthesis provides covalent bonding of Pt to CNTs through linking atom [37] and non-covalent bonding, namely van der Waals interaction between metal and carbon. Polyol method is one of the most frequently used for synthesis of Pt/C catalyst materials [38–46]. Modification of carbon surface by introducing hydrophilic groups is essential for successful anchoring of metal nanoparticles [38, 47]. It has been proposed, that microstructure of the catalyst support material can influence the ORR process [48]. By varying synthetic conditions it is possible to achieve changes in the microstructure and morphology of catalyst materials. Chen and co-workers deposited phosphonate functionalised platinum nanochains onto the surface of multi-walled carbon nanotubes (MWCNTs) covered by polyallylamine using the thermal decomposition method [49]. Catalyst particles with improved morphology were formed via self-assembly process with the aid of electrostatic interactions between functionalised materials. Vinayan et al. synthesised the Pt-based electrocatalysts by a conventional sodium borohydride reduction method and modified polyol reduction method and stated that the modified polyol reduction yields more uniform dispersion, higher loading and optimum particle size of Pt and Pt_3Co alloy nanoparticles over the MWCNT surface compared to the conventional sodium borohydride reduction method [42]. The effect of the functionalisation degree of MWCNTs on the synthesis and catalytic performance of Pt/MWCNT has been studied by Hernandez-Fernández et al. [43]. They found that increasing metal dispersion is favoured on severely treated carbon nanotubes, because that treatment provided nucleation sites and enhanced the hydrophilicity of the carbon surface. Kohl and co-workers used ethylene glycol for the synthesis of PtNPs supported on oxygen and nitrogen functionalised CNTs for oxygen reduction and found that

the performance of the catalyst for ORR is dependent on the type of the functional groups on the CNTs and these nanomaterials are also more effective in hybrid fuel cells than commercial Pt/C [46].

Electrodeposition is another widespread method for the preparation of carbon nanotube-supported Pt nanoparticles [50–56]. Girishkumar used electrodeposition for the preparation of PtNPs supported on single-walled carbon nanotubes (SWCNTs) modified electrodes for methanol oxidation and oxygen reduction [51]. These nanocomposites showed higher catalytic activity for methanol oxidation and oxygen reduction than unsupported Pt. The higher catalytic activity was attributed to larger surface area provided by the carbon nanotube architecture and decreased overvoltage for these reactions. Electrodeposition was also used for the preparation of hierarchical Pt nanoparticles supported on CNT coated carbon fiber as electrocatalysts for oxygen reduction by Sharma and Kar [56]. The overall ORR activity of this nanocomposite was enhanced synergistically by the presence of Pt-nanoparticle clusters on the defective CNT surface.

Physical preparation techniques, such as pulsed laser deposition [57], microwave-assisted [58–60], chemical vapour deposition [61], atomic layer deposition (ALD) [62, 63] techniques were successfully utilised for the preparation of highly effective, pure and uniform cathode catalysts for ORR. Roy and Hsieh used a comprehensive pulse microwave-assisted polyol synthesis method to deposit Pt catalysts onto MWCNTs and found that by the microwave-assisted deposition well-dispersed Pt particles over the CNT support were achieved and these catalyst materials delivered an improved electrocatalytic activity and excellent stability not only for hydrogen oxidation reaction but also the ORR kinetics [58]. Atomic layer deposition was employed for the preparation of uniform Pt layers on aligned CNTs as catalyst materials and were demonstrated to be applicable as efficient fuel cells catalysts and also the functionalisation of the surface was directly affecting their performance towards the ORR [62]. Magnetron sputtering technique is another physical method for the preparation of catalyst materials for O_2 reduction [64–67]. Magnetron sputtering has a number of advantages over other physical methods, such as ease of sputtering any metal, alloy or compound onto different substrates providing high-purity films, good adhesion to substrate with accurate control of metal loading [64]. Pham et al. investigated the use of the graphene-carbon nanotube hybrids as the magnetron sputtered Pt support in proton exchange membrane fuel cells (PEMFCs) and showed that these catalysts exhibit high intrinsic catalytic activity and superior electrochemical stability compared to a commercial carbon black supported Pt catalyst [66].

In the past decade, graphene-based supports have shown several advantages over traditional carbon supports, displaying remarkable charge transfer properties, high surface area, chemical inertness and mechanical flexibility [68–74]. It has been also stated that the fast electron transport properties of graphene can facilitate the reduction of O_2 and therefore increase the efficiency of fuel cells [68]. Graphene exhibits several advantages over CNTs, such as lower cost,

larger surface area and simple preparation. Very important advantage is that graphene synthesised from graphite powder does not contain metallic impurities, which could alter electrochemical properties. It has been also found that metal nanoparticles are more uniformly and well-distributed on graphene-based supports, which also enhance the electrochemical activities. Ghosh et al. synthesised graphene and functionalised graphene as support materials for Pt nanoparticles and found that these materials exhibited higher surface area and better electrochemical activity than commercial Pt/C, enhancement was attributed to well-distributed PtNPs on the prepared graphene supports [75]. Platinum nanoparticles embedded on reduced graphene-oxide were used as electro-catalysts by Ha et al., who concluded that these nanomaterials showed much higher electrochemical surface area and greater catalytic activity towards O_2 reduction than 75% Pt/C [76]. The superior activity was also ascribed to uniform particle distribution and also to small Pt particle size. As a highly efficient catalyst support for oxygen reduction, the core-shell graphene nanosheet (GNS) and amorphous carbon composite was used [77], where GNS-shell showed excellent conductivity, high surface area and corrosion resistance and thus PtNPs deposited on the carbon support demonstrated good catalytic activity and higher electrochemical stability than state-of-the-art Pt/C catalyst. Maia work-group investigated the ORR on electrodeposited Pt nanoclusters with porous dendritic structures on top supported on different carbon nanomaterials as graphite, MWCNTs, graphene oxide, graphene oxide nanoribbons, chemically converted graphene and graphene nanoribbons [73]. The results showed that the electrocatalytic activity depends quite strongly on the support material and the best results were obtained with Pt electrodeposited onto graphene nanoribbons and graphene, whilst others exhibited poor electrocatalytic activity, due to the better synergistic effects between Pt nanoparticles and support.

Furthermore, the incorporation of heteroatoms (nitrogen, sulphur, boron or others) into the graphitic structure has enabled to improve the chemical and physical properties of carbon-based support materials [78], e.g. carbon nano-tubes [79–83], carbon nanofibers [84–86] and graphene materials [87–89]. The doping by heteroatoms is considered to activate neighbouring carbon atoms for oxygen adsorption followed by reduction [90]. As a result of heteroatom incorporation, the O_2 molecules can be efficiently reduced on the doped carbon surface. It has been reported that nitrogen doping also prevents the agglo-meration and improves the distribution of metal nanoparticles on carbon support [79–81]. According to previous studies, N-doped carbon supports not only facilitate the dispersion of metal nanoparticles but tender them highly durable by introducing more binding sites to the carbon surface that anchor metal precursor or metal nanoparticles. Ramaprabhu and co-workers used graphene nanoplatelets and N-doped graphene nanoplatelets as a catalyst support for PtNPs for ORR in PEMFCs [91]. Both composite materials showed improved power densities, but the one containing nitrogen showed slightly higher fuel cell performance. The enhancement in the power density was attributed to the increased electrical conductivity and improved carbon-catalyst binding. Pt

nanoparticles supported on nitrogen-doped reduced graphene oxide (NRGO) were prepared for use as PEMFC catalysts by He et al [92]. Uniformly distributed PtNPs on NRGO were in evidence and cyclic voltammetry revealed lower losses of the electrochemically accessible surface area (ECSA) and higher ORR catalytic activity was found for this novel Pt/NRGO catalyst in comparison to those of the platinum/graphene oxide and conventional Pt/C catalysts. Nitrogen-doped graphene was used as a support material for PtNPs by Liu et al., who used this catalyst material for the studies of methanol oxidation and oxygen reduction [93]. These nanomaterials showed excellent electrocatalytic activities toward these two reactions and they found that nitrogen-doped graphene supported platinum is promising alternative. Pt nanoparticles anchored on N-doped reduced graphene oxide nanomaterials were used as electrocatalysts for ORR and it was found that these composites exhibit very high electrocatalytic activity and excellent stability towards O_2 reduction [94]. The increase in the ORR activity was assigned to the synergistic catalytic effect of both N-doped carbon matrix and PtNPs.

4.4. Oxygen reduction on palladium electrodes

The most active electrocatalyst for ORR is platinum [1]. Platinum and palladium have similar properties, but Pd is much more abundant in the Earth crust than Pt [95]. In acidic and alkaline media the O_2 reaction mechanism on Pd is similar to that of platinum and the ORR proceeds mainly through 4-electron pathway [96–99].

The electroreduction of oxygen on palladium surface depends on the metal structure. It has been suggested that the adsorption of anions on Pd is stronger than on Pt and this is one of the reasons for a lower ORR activity of Pd catalysts as compared to Pt electrode in acid media [99]. Palladium is more structure-sensitive for anion adsorption than Pt, because of stronger interactions between Pd surface and adsorbed anions (Cl^-, ClO_4^-, HSO_4^-, etc). Strongly adsorbed anions on palladium surface block the active sites for O_2 adsorption, thereby preventing O=O bonds for breaking and thus resulting in a slower reduction of oxygen on palladium than on Pt surface in acidic media [99]. This is the main reason why Pd is not frequently used for PEMFC applications [95]. In alkaline media, inversely to acidic media, where Pd is unstable and less active, the electrocatalytic activity towards O_2 reduction is comparable to that of platinum. In the presence of OH^- anions, the inhibiting effect of anion adsorption is much lower, therefore the oxygen reduction activity is enhanced [99].

Hoshi and co-workers studied the structure-sensitivity of the ORR on Pd monocrystals in perchloric acid using the RDE technique [100]. They reported the following order of activities for low-index Pd single crystal planes: Pd(110) < Pd(111) < Pd(100). Therefore, it is of considerable interest to study the ORR on shape-controlled Pd nanoparticles (PdNPs) [99, 101–103]. Shao et al. explored the electrocatalysis of O_2 reduction on cubic and octahedral Pd nanocrystals

[101]. They demonstrated that the Pd cubes with (100) facets were one order of magnitude more active than octahedric Pd with (111) facets in 0.1 M $HClO_4$. Erikson et al. investigated the ORR on cubic PdNPs [102, 103]. They found that Pd nanocubes showed enhanced ORR activity compared to spherical PdNPs and bulk Pd in acid and alkaline solutions, this effect was explained by the predominance of Pd(100) surface sites. Lee and co-workers successfully synthesised various sizes Pd nanocubes (27, 48 and 63 nm) composed of Pd(100) [104]. Cubic PdNPs exhibited good electrocatalytic activity for ORR in alkaline media. These authors also studied the ORR activity and methanol tolerance of Pd nanocubes in acid solution [105]. The specific activity for O_2 reduction was higher on Pd nanocubes compared with regular PdNPs (9 nm).

In early work, Damjanovic et al. studied the potential dependence of the Tafel slopes on palladium and found that at more negative potentials than 0.8 V vs. RHE the Tafel slope value is −120 mV and at more positive potentials than 0.8 V vs. RHE the slope value is −60 mV [96, 97]. The change in the Tafel slope value at 0.8 V vs. RHE is related to the adsorption of the surface oxides to Pd surface. Although the kinetics of the ORR is affected by surface oxides, the mechanism remains the same, and the rate-determining step for O_2 reduction reaction is the transfer of the first electron to the oxygen molecule. Depending on the surface-oxide adsorption, the ORR proceeds on oxide-free palladium surface mainly through four-electron pathway, but on PdO-covered surface partly via peroxide intermediate step [106].

4.5. Oxygen reduction on PdNPs supported on CNTs and graphene

A lot of work has been made to find electrocatalytically active Pd-based material for oxygen reduction to overcome the low activity of bulk palladium in acidic media [95]. For that reason, the electrocatalytic properties of nanostructured Pd catalysts have received an increasing attention. Carbon-supported Pd (Pd/C) composite materials are widely studied as promising catalyst materials for ORR to replace expensive and scarce platinum [99, 107–110].

In general, Pd-based catalysts have larger particles than Pt-based catalysts and as a result, have smaller specific surface area and thus show lower electrocatalytic activity. Usually, the particle size on carbon support changes in the following order: Pd > PdPt > Pt [111–114], which is related to the different metal nanoparticle nucleation mechanism for Pd/C and Pt/C catalysts. The differences in the nucleation mechanism also cause the dissimilar distribution of PdNPs and PtNPs on carbon support [95]. Jiang et al. investigated the Pd particle size effect on the ORR activity using carbon-supported Pd catalysts [115]. They found that with smaller size (3–5 nm) Pd is highly active in alkaline media and the electrocatalytic activity for ORR is similar for bulk Pd and Pt. Carbon-supported Pd was also explored by Senthil Kumar et al. and these authors found that Pd/C

catalysts show rather high O_2 reduction activity, but it was greatly influenced by the pre-treatment of carbon supports [109].

For the preparation of carbon-supported Pd-based catalysts, chemical and physical methods have been employed. In the case of chemical methods, different reducing agents and Pd precursors have been used [71, 102, 110, 116–121]. Alvarez et al. studied the effect of different conditions of synthesis of Pd/C nanocomposites on their electrocatalytic properties [110]. They found that the highest electrocatalytic activity towards the ORR in alkaline media can be achieved when using ethylene glycol as a reducing agent. Lee and co-workers attached PdNPs to different carbon nanomaterials by self-regulated reduction of sodium *n*-tetradecyl sulphate and sodium *n*-dodecyl sulphate [118, 119]. It was found that the newly prepared Pd/SWCNT, Pd/MWCNT and Pd/graphite nanofibers possess high activity for oxygen reduction and Pd/CNT showed even higher activity than Pd/graphite nanofibers. This unique method for synthesising PdNPs on carbon support was suggested to yield in extraordinary physical and chemical features that are useful in advanced applications.

Another effective method for the preparation of Pd-based catalysts is electrochemical deposition of metal nanoparticles to carbon support [107, 122–124]. Good advantage using electrodeposition is the control of the loading of metal on the surface of different carbon substrates [107]. Janes and co-workers used galvanostatic electrodeposition for the fabrication of Pd nanocubes on SWCNTs [122]. They suggested that this technique provides unique opportunities to control the size and shape of metal nanoparticles. Hsieh et al. used a pulse electrodeposition approach for the synthesis of Pd nanocatalysts supported on graphene oxide sheets [123]. They suggested that this technique offers a promising route in synthesising highly crystalline Pd clusters and the presence of graphene oxide sheets renders multi-functional roles in promoting the dispersion of Pd clusters, ionic diffusion and charge transfer.

As physical methods, chemical vapour deposition [125], atomic layer deposition [126, 127], magnetron sputtering [128, 129] etc. have been employed [58, 130]. Liang et al. synthesised PdNPs supported on carbon nanofibers by the two-step metal organic chemical vapour deposition, which resulted in uniformly distributed and small Pd nanoparticles all over the nanofiber, making the used method attractive for the preparation of catalyst materials [125]. For the synthesis of PdNP/MWCNT hybrid materials microwave irradiation was used [130]. It was reported to be simple and fast method for preparing PdNPs supported on CNTs with different Pd content, varying from 1 to 40 wt%.

Zheng et al. used an incipient wetness impregnation method for the preparation of Pd-based catalysts supported on activated carbon, platelet carbon nanofibers (p-CNF) and fish-bone carbon nanofibers (f-CNF) containing 5 wt% of palladium and studied the effects of the microstructure of CNF on the ORR activities [131]. It was found that the p-CNF has a higher ratio of edge atoms to basal atoms and therefore the palladium supported on this carbon nanomaterial has more positive ORR onset potential and ORR peak potential than for Pd

supported on f-CNF and also it was noted that the supporting materials also have influence on the reaction process.

As for Pt-based electrocatalysts, also for palladium graphene-based supporting materials are becoming more attractive [71, 123, 132–137]. Seo et al. explored the electroreduction of oxygen on graphene-supported PdNPs and an excellent ORR activity was observed [71]. An electrostatic attraction method was utilised for anchoring 10 nm Pd nanocubes on reduced graphene nanosheet surfaces by Liu et al. who employed this nanomaterial as electrocatalysts for ORR in alkaline media [134]. They found that the support material with greater number of physical defects facilitated greater active sites of these cubic PdNPs due to its higher surface area and thus better promoted ORR.

Heteroatom-doped graphene supports are showing also promising results as support materials for PdNPs [121, 138, 139]. Vinayan et al. synthesised triangular shaped PdNPs decorated N-doped graphene and explored their catalytic properties [121]. Nitrogen-doping of the support material lead to the formation of highly dispersed anisotropic nanoparticles over the graphene support and this nanocomposite showed good electrocatalytic activity towards the ORR and stability in acidic media due to the strong binding between PdNPs and graphene support as a result of N-doping. Recent study by Chen workgroup focused on oxygen electroreduction catalysed by PdNPs supported on N-doped graphene quantum dots [138]. The as-prepared catalysts showed enhanced activities towards O_2 reduction in alkaline media compared to that of PdNPs supported on undoped graphene quantum dots and commercial Pt/C catalysts, the improvement was explained by the enhanced electron withdrawing effects of the pyrrolic nitrogen centres that manipulated the electronic interactions between palladium and oxygen reduction intermediates.

4.6. Oxygen reduction on palladium-platinum alloys

The high price and scarcity of Pt forces researchers to find a way to reduce its amount in the catalyst materials. One strategy for lowering the Pt content is to replace it partially by other metals. Palladium is a promising substitute due to the similar properties to the Pt (same group of the periodic table, similar atomic size and crystalline structure) [95, 99]. Advantages for using Pd are the abundance of it in the Earth crust and also the fact that palladium improves the alloy stability in acidic media.

Li et al. designed and prepared Pt-Pd/C catalyst for ORR and found that the addition of small content of Pd to the catalyst, improved the catalytic activity compared with Pt/C catalyst [111]. Beard et al. used electroless deposition of Pt onto the Pd surface for the preparation of carbon supported Pt-Pd electrocatalysts and found that alloyed catalysts showed comparable ORR activities with that of commercially available Pt/C, it was suggested that there is little interaction between two metals which enhances the catalytic behaviour [140]. The decoration of MWCNTs with Pt-Pd alloy electrocatalysts of three different

compositions and their electrocatalytic performance towards the ORR were described by Ghosh et al. [141]. They showed that nanocomposite with 1:1 metal ratio outperformed other nanoparticles and Pt black, the combined effect of the electrocatalyst and its support and synergistic effect between the metals is believed to enhance the overall electrocatalytic activity.

Catalytic properties of alloy nanostructures are substantially affected by the shape, size, composition and surface structure [142–144]. Controlling the shape and facets of nanocrystals is a productive method to improve the performance in catalytic reactions [142–144]. In recent years, several researches have been focused on the preparation of shape-controlled Pt-Pd nanoalloys for electrocatalytic application: nanodendrites [144–146], nanoflowers [144, 147–150], concave particles [144, 151–154], nanowires and -rods [155–159], poly- and octahedral shapes [160, 161], nanocubes [144, 162, 163], etc. Pd-Pt bimetallic nanodendrites were synthesised by Xia workgroup, who used these nanostructured materials as electrocatalysts for O_2 reduction [145]. Pd-Pt nanocrystals exhibited relatively large surface areas and particularly active facets toward the ORR, being almost three times more active than state-of-the-art Pt/C catalyst. Chen and others studied oxygen reduction on Pt-Pd alloy nanoflowers and found that these catalysts possess superior electrocatalytic activity and remarkable methanol-tolerance in acidic media [150]. The advancement was proposed to be related to the change of the binding energy of Pt (electronic effect), decrease in the Pt-Pt bond length (geometric effect) and also with the unique porous nanostructure. Wang and co-workers also prepared Pt-Pd nanoflowers as electrocatalyst material for ORR [147–149]. These nanocatalysts displayed enhanced electrocatalytic ORR performances as compared to commercially available Pd/C and Pt/C catalysts, which could be due to unique structures of Pt-Pd nanoflowers and bimetallic synergistic effects between these precious metals. These authors also prepared Pt-Pd nanocubes anchored to reduced graphene oxide, which were found to exhibit improved ORR activity and stability compared with commercial 10 wt% Pt/C [162]. Zhang et al. used bromide-induced galvanic replacement reaction for the preparation of Pd-Pt nanocrystals with different composition and a concave structure [152]. They found that the Pd-Pt sample with the lowest Pt content exhibited the largest specific electrochemical surface area and four times higher mass activity than commercial Pt/C catalyst for the ORR. The improvement in the activities was related to the enrichment of Pt nanoparticles on the catalyst surface. Many advantages were found when using PtPd porous nanorods as catalyst materials for O_2 reduction [158]. Firstly, the porous structure was suggested to effectively improve the surface area and lower the utilisation of noble metal, secondly the larger surface area and synergistic effect between Pd and Pt, resulted in higher activities than Pt/C and thirdly, these kinds of nanomaterials were presented to exhibit excellent durability.

Several research groups have prepared core-shell type Pd-Pt catalysts [143, 164–176]. Yang et al. prepared carbon-supported pseudo-core-shell Pd-Pt nanoparticles as electrocatalysts for O_2 reduction by galvanic replacement reaction

[164]. The Pd-Pt/C catalysts showed good activity in acidic solution even in the presence of methanol and it was found that the best overall composition was $Pd_{70}Pt_{30}/C$, explained in terms of the weaker OH_{ads} binding on the Pt sites and the combination of preferable electronic and strain effects. Three-dimensional Pd@Pt core-shell nanostructures with controllable shape and composition were synthesised and their electrocatalytic properties towards oxygen reduction were evaluated [175]. Pd@Pt nanocatalysts showed higher catalytic activity than pure Pd and Pt catalysts for ORR and the enhancement was explained by the increase of Pd/Pt molar ratio, more and more PtNPs were formed on the surface of Pd nanocube. Pt monolayer shell-Pd tetrahedra core electrocatalysts towards the ORR were examined [167]. It was shown that Pt monolayer on Pd tetrahedra resulted in good ORR activity, due to the predominant Pt(111) facets on the Pd tetrahedral surface and the clean surface of Pd nanoparticles ensured a favourable Pd-Pt core-shell interactions, which was essential to improve the kinetics of the ORR. Alia et al. studied the O_2 reduction reaction on platinum coated palladium nanotubes, which displayed good activity compared to Pd nanotubes and Pt nanotubes [174]. Lee et al. established a method for the preparation of truncated Pd nanocubes and their further coating with multi-armed Pt shells [172, 173]. These Pd-Pt core-shell nanomaterials were employed for ORR electrocatalysis in alkaline media. Pd-Pt nanocubes and Pd nanocubes displayed greater mass activity than Pt nanoparticles, its greater activity was associated to the better accessibility of Pd(100) planes. Liu's work-group prepared carbon-supported Pt-Pd alloy catalysts with core-shell structure with Pt as the shell using room-temperature electron reduction method and studied their electrocatalytic behaviour towards the ORR [176]. They found that these nanostructures are highly active and stable catalyst materials for this reaction, because of the smaller particle size (~2.6 nm) the binding with oxygen is weaker and this kind of structure promotes the O-O bond breaking and desorption of OH^-, which resulted in almost 4 times higher mass activity for core-shell structure than for the commercial Pt/C.

5. EXPERIMENTAL

5.1. Electrode preparation

Glassy carbon (GC), bulk polycrystalline palladium and platinum electrodes were fabricated by mounting GC (GC-20SS, Tokai Carbon), Pd (99.95%, Alfa Aesar) or Pt (99.5 %, Alfa Aesar) disks into Teflon holders. In some parts of the doctoral work, commercial GC electrodes (geometric area 0.071 cm^2, Radiometer), were used. The surface of the working electrodes was polished to a mirror finish using 1.0 and 0.3 μm Al_2O_3 (Buehler) water suspension and for bulk Pd and Pt electrodes, additional polishing on 0.05 μm alumina slurry was used. The polishing residues were removed by sonicating the electrodes in Milli-Q water (Millipore Inc.) for 5 min.

The commercial 20 wt.% Pt/Vulcan XC-72 catalysts were purchased from E-TEK, Inc. (Framingham, MA, USA) and used for comparison purposes.

5.2. Preparation of catalyst materials

5.2.1. Acid-treatment of carbon nanotubes

The acid-treatment of multi-walled carbon nanotubes (purity >95%, diameter 30 ± 10 nm, length 5–20 mm, NanoLab Inc.) was carried out using previously published procedure [177]. First, carbon nanotubes were treated by refluxing in a mixture of concentrated sulphuric and nitric acids (1:1, v/v) for 2 h at 55 °C and then for 3 h at 80 °C. Afterwards, the nanotubes were washed with Milli-Q water (Millipore, Inc.) using repeated centrifugation (3000 rpm, 10 min), and resuspended in Milli-Q water. Finally, the MWCNTs were vacuum dried for 15 h. MWCNTs were dispersed in dimethylformamide (DMF) (1 mg mL^{-1}) and then sonicated for 30 min to give a homogeneous suspension.

5.2.2. Preparation of nitrogen-doped graphene nanosheets

Graphene oxide (GO) used in this work was synthesised from graphite powder (Graphite Trading Company) by a modified Hummers' method as described elsewhere [178]. Dicyandiamide (DCDA, Aldrich) was used as a precursor for nitrogen doping. Briefly, GO was dispersed in deionised water and ethanol solution (3:1) with the aid of ultrasonic agitation. Nitrogen precursor was added to form GO/DCDA mixture with ratio of 1:20. Small amount of polyvinyl pyrrolidone (PVP) was added to reaction media and mixture was sonicated for 2 h. The resulting mixture was dried at 75 °C in vacuum. Subsequent pyrolysis of the prepared material was performed in argon atmosphere at 800 °C for 2 h.

5.2.3. Preparation of sputter-deposited PtNP/MWCNT catalysts

For modification of GC electrodes with MWCNTs, a 12.3 μL drop of MWCNT/DMF suspension was placed on the GC surface (geometric area 0.126 cm^2) for further magnetron sputtering procedure. Subsequent anchoring of Pt nanolayers of different loading onto MWCNTs was performed by sputter-deposition with a Pt target in argon atmosphere. The nominal Pt film thicknesses were 4, 8 and 16 nm, corresponding to Pt loadings of 8.6, 17.2 and 34.4 μg cm^{-2}, respectively (calculated per geometric area of the GC substrate). In what follows, the prepared catalysts are designated as 1-PtNP/MWCNT, 2-PtNP/MWCNT and 3-PtNP/MWCNT, respectively.

5.2.4. Preparation of Pt-TiO_2/MWCNT catalysts

GC disk electrodes (geometric area of 0.196 cm^2) were coated with vertically aligned multi-walled carbon nanotubes prepared by chemical vapour deposition. The catalysts for MWCNT synthesis, namely 1 nm Al_2O_3 and 0.5 nm Fe layers were deposited on GC by electron beam evaporation. MWCNTs were grown at 780 °C in a cold-wall atmospheric pressure CVD system, similar to that described earlier [179], by adding 1% of acetylene to the flow of 50:50 mixture of hydrogen and helium gases. In order to remove the metal catalyst (Fe and Al_2O_3) particles remained from MWCNT preparation by the CVD method, the MWCNT/GC samples were etched in 1 M HCl, followed by rinsing in heated deionised water for 3 times, and drying in ambient atmosphere for several days. To form TiO_2 clusters on the MWCNT surface, atomic layer deposition from $TiCl_4$ and H_2O vapours was applied. The ALD precursors supply and purging times were 10 and 30–50 s, respectively. The deposition temperature was 250 °C. Finally, the TiO_2/MWCNT supports were coated with Pt nanolayers of different thicknesses (2, 4 and 8 nm, corresponding to Pt loading of 4.3, 8.6 and 17.2 μg cm^{-2}, respectively) using the magnetron sputtering technique. In what follows, these composite catalysts are designated as 1-Pt-TiO_2/MWCNT, 2-Pt-TiO_2/MWCNT and 3-Pt-TiO_2/MWCNT, respectively.

5.2.5. Preparation of Pt/NG catalysts

The Pt/NG catalysts were prepared using two synthetic procedures. By the first method, PtNPs were synthesised by chemical reduction of hexachloroplatinic acid ($H_2PtCl_6 \times H_2O$, 99.9%, Aldrich) using sodium borohydride ($NaBH_4$, 99%, Aldrich) as a reducing agent. Briefly, a suspension of 20 mg of NG and 10 mM H_2PtCl_6, equivalent to 20 or 40% weight ratio of Pt to carbon support, was prepared by sonication in 80 mL Milli-Q water. Subsequently, the Pt precursor was simultaneously reduced and supported on the N-doped graphene nanosheets using $NaBH_4$. The suspension was then vacuum-filtered and rinsed several times with water and ethanol. The final product was dried at 60 °C for 12 h. The prepared catalyst materials are designated as 20-Pt/NG_{BH} and 40-Pt/NG_{BH}.

In the second approach, PtNPs were anchored onto NG support using procedure described elsewhere [180]. In this case, 0.059 g of $H_2PtCl_6 \times H_2O$ was added to 5 mL of ethylene glycol (EG, 99.5%, Sigma-Aldrich) that contained 0.15 M NaOH. The solution was mixed in a 50-mL three-neck flask at 1200 rpm for 30 min, followed by reflux of the mixture at 160 °C (achieved within less than 20 min) for 3 h at 1200 rpm. During the reduction process, the colour of the mixture changed from yellowish-brown to black. After the mixture was cooled down, 100 or 40 mg of NG was added to the mixture yielding a 20 or 40 wt% Pt/NG catalyst. Using 1 M HNO_3, the pH of the solution was adjusted and the final mixture was stirred for 24 h at room temperature. The suspension was then vacuum-filtered and washed several times with water and ethanol. The final product was dried overnight at 60 °C. The prepared catalyst materials are designated as 20-Pt/NG_{EG} and 40-Pt/NG_{EG}.

5.2.6. Preparation of Pt nanocubes supported on Vulcan XC-72R carbon

Cubic Pt nanoparticles were synthesised using a procedure previously reported [181, 182]. The initial synthesis recipe was scaled up by a factor of 6 in order to obtain a higher amount of product, so that the only variable is the loading. Briefly, 0.12 g of platinum (II) acetylacetonate ($Pt(acac)_2$), 48 mL of oleylamine (OLA) and 12 mL of oleic acid (OA) were added into a 3-necked flask and heated up to 130 ºC in argon atmosphere, while stirring at 500 rpm. At this temperature, 0.3 g of tungsten hexacarbonyl ($W(CO)_6$) was added to the reaction mixture, followed by raising the temperature to 240 ºC for 30 min at 200 rpm. When the reaction was finished, the black dispersion was cooled down to room temperature and the Pt nanoparticles were collected by centrifugation at 6000 rpm for 10 min. After decanting the supernatant, the residue was re-suspended in 50 mL of hexane.

For the preparation of Pt/C catalyst materials, the amount of carbon and Pt was calculated to obtain 35 mg of carbon-supported Pt catalyst. Thus, the suitable amount of nanoparticles suspension was mixed with the proper mass of Vulcan XC-72R (Cabot Corp.) carbon to obtain the 10, 20, 30, 40 and 50 wt% Pt/C catalysts. The samples were then magnetically stirred for 30 min. The as-prepared catalyst materials were then washed following a protocol described elsewhere [182]. First, the samples were washed twice with a mixture of hexane and ethanol. The precipitates were then re-dispersed in 20 mL of methanol and a pellet of NaOH was added to the dispersion, which was sonicated for 10 min. After the catalyst precipitated, the alkaline solution of methanol was removed and the carbon-supported particles were washed with acetone. This procedure was repeated at least three times, and after that, the catalyst particles were vacuum-filtered and rinsed with ultrapure water and ethanol. Final products were dried in an oven at 70–80 °C for 12 h.

5.2.7. Preparation of sputter-deposited PdNP/MWCNT catalysts

Prior to magnetron sputtering procedure, GC electrode was modified with MWCNTs. For that, a 12.3 μL drop of MWCNT/DMF ink was placed onto GC electrode surface (geometric area 0.126 cm^2). Then, the MWCNTs were coated with Pd nanoparticles of different loading by sputter-deposition with a Pd target in argon atmosphere. The nominal Pd film thicknesses were 5, 10 and 15 nm, which correspond to Pd loading of 6, 12 and 18 μg cm^{-2}, respectively. In what follows, the prepared catalysts are designated as 1-PdNP/MWCNT; 2-PdNP/MWCNT and 3-PdNP/MWCNT, respectively.

5.2.8. Preparation of heat-treated PdNP supported on MWCNTs

Three drops of 100 μL of multi-walled carbon nanotubes dispersed in DMF ink were placed on a glassy carbon plate for further magnetron sputtering procedure. Acid-treated MWCNTs on the small GC plates were placed in the sputtering chamber and the coating with Pd nanolayers was conducted by sputter-deposition with a Pd target in argon atmosphere. For each experiment, the same amount of Pd was deposited on MWCNTs. The nominal Pd film thickness was 15 nm, which corresponds to Pd loading of 18 μg cm^{-2}. PdNP/MWCNT composites were further annealed in argon using a tube oven at 300 °C, 400 °C and 500 °C for 30 min.

5.2.9. Preparation of Pd/NG catalysts

Anchoring of Pd nanoparticles to N-doped graphene nanosheets was performed using the following procedure. First 0.1 g of $PdCl_2$ (Aldrich) with 0.1 mL of concentrated HCl was added to 60 mg of NG dispersed in 60 mL of deionised water. The suspension was sonicated for 15 min and then 0.021 g of $NaBH_4$ was added during agitation. The suspension was sonicated for additional 15 min, filtered and washed with ethanol solution. The resulting powder was dried at 60 °C for 2 h. The prepared catalyst materials were designated as Pd/NG.

5.2.10. Preparation of cubic PdPt alloy nanoparticles

PdPt-alloy nanocubes were synthesised using a similar methodology to that described elsewhere [183]. Briefly, 20 mM potassium tetrachloropalladate (K_2PdCl_4, >99.99%, Sigma-Aldrich), 20 mM potassium tetrachloroplatinate (K_2PtCl_4, >99.99%, Sigma-Aldrich), 75 mg of sodium iodide (≥99.99%, Sigma-Aldrich) and 160 mg of polyvinyl pyrrolidone (MW≈55000, Sigma-Aldrich) were mixed together with 10 mL N,N-dimethylformamide (Sigma-Aldrich) in a glass vial and the mixture was sonicated for 2 min. The resulting homogeneous mixture was capped, transferred to an oven and heated at 130 °C for 3 h before cooling down to room temperature. The colloidal products were collected by

centrifugation and washed several times with an ethanol-acetone mixture and finally stored in ultrapure water. In order to synthesise PdPt-alloy nanocubes with different composition, the amount of K_2PdCl_4 and K_2PtCl_4 was varied accordingly. The nominal PdPt alloy compositions were 34/66, 50/50 and 66/34.

5.3. Surface characterisation

The surface morphology of carbon nanotube-supported Pd- and Pt-based catalysts were characterised by high-resolution scanning electron microscopy (HR-SEM) using Helios NanoLab 600 (FEI) instrument, where GC disks were used as substrates for the nanocatalysts. Transmission electron microscopy (TEM) was used to explore the surface structure of the as-prepared Pd/NG, Pt/NG, Pt/C and PdPt nanocatalysts. TEM measurements were performed on a Tecnai 12 instrument operated at 120 kV accelerating voltage, a probe corrected G2 80–200 FEI Titan operating at 200 kV or JEOL, JEM-2010 working at 200 kV equipped with an X-ray detector OXFORD INCA Energy TEM 100 for microanalysis (EDX) instrument. The TEM samples were prepared by placing an aliquot of diluted dispersions onto a Formvar-covered copper grid.

X-ray diffraction (XRD) analysis for heat-treated PdNP/MWCNT and PtNP/MWCNT composite materials was carried out on a Bruker D8 Advance difractometer (Cu Kα radiation of 0.154 nm, 2θ range 15–100° with LynxEye linear detector, $U = 40$ kV and $I = 40$ mA).

X-ray photoelectron spectroscopy (XPS) measurements were carried out with a SCIENTA SES-100 spectrometer using nonmonochromatised Al Kα X-ray radiation (1486.6 eV), a take-off angle of 90° and a source power of 400 W. The pressure in the analysis chamber was less than 10^{-9} Torr. For collecting the survey scans, the following parameters were used: energy range 800–0 eV (for Pt-TiO_2/MWCNT materials) or 600–0 eV (for Pd/NG and Pt/NG materials), pass energy 200 eV, and step size 0.5 eV. In specific regions, high-resolution scans were performed with the pass energy of 200 eV and the 0.1 eV steps.

Thermogravimetric analysis (TGA, Mettler-Toledo TGA/SDTA851 thermobalance) was used to experimentally determine the Pt loading (% in weight) of the prepared carbon-supported Pt nanocubes. The experiments were carried out in an oxidative atmosphere, N_2:O_2 (4:1) raising the temperature from 25 to 850 °C at a heating rate of 10 °C min^{-1}.

5.4. Electrochemical measurements

Electrochemical measurements were performed either in 0.5 M H_2SO_4, 0.1 M $HClO_4$ or 0.1 M KOH solutions. Electrolyte solutions were prepared using sulphuric acid (Suprapur®, Merck), perchloric acid (Aldrich) or potassium hydroxide (p.a. quality, Merck) and Milli-Q water. Solutions were saturated with pure oxygen (99.999% AGA), argon (99.999% AGA) or carbon monoxide (99.97%, AGA).

The electrochemical measurements were conducted in a three-electrode glass cell, where reversible hydrogen electrode (RHE) was used as a reference electrode and a Pt wire as a counter electrode. Autolab potentiostat/galvanostat PGSTAT30, PGSTAT128N or PGSTAT302N (Metrohm-Autolab B. V.) controlled with General Purpose Electrochemical System (GPES) software were used to record cyclic voltammograms, CO oxidation and O_2 reduction polarisation curves. Also, in some cases, a VMP3 multichannel potentiostat (BioLogic) was employed, these measurements were conducted using the *N*Stat configuration mode in which 6 GC rods (diameter 3 mm) as working electrodes were simultaneously employed sharing the same counter and reference electrodes. The counter electrode was again a Pt wire and the reference electrode a reversible hydrogen electrode connected to the cell through a Luggin capillary.

An EDI101 rotator and a CTV101 speed control unit (Radiometer) were typically employed for the RDE measurements, but in the work of Pt-TiO_2/ MWCNT catalyst an AFMSRX rotator and MSRX speed controller from Pine Research Instrumentation were used. The background currents in all the studies were also recorded at the same conditions as used to measure the ORR polarisation curves in Ar-saturated electrolyte and were subtracted from the experimental ORR current. All the electrochemical measurements were carried out at room temperature (23±1 °C).

6. RESULTS AND DISCUSSION

6.1. Oxygen reduction on sputter-deposited PtNP/MWCNT composites

Magnetron sputtering technique was employed to prepare Pt nanoparticles supported on multi-walled carbon nanotubes as electrocatalysts for O_2 reduction [I]. Three different nominal Pt film thicknesses: 4, 8 and 16 nm were used. The ORR measurements were carried out in 0.5 M H_2SO_4 and 0.1 M KOH solutions.

6.1.1. SEM and XRD characterisation of PtNP/MWCNT samples

The freshly prepared PtNP/MWCNT catalysts were characterised by SEM and Fig. 1 shows typical examples of SEM micrographs of unmodified MWCNTs (Fig. 1a) and for as-prepared catalysts (Fig. 1b–d). The SEM images indicate a good dispersion of the Pt nanolayers throughout the surface of MWCNTs

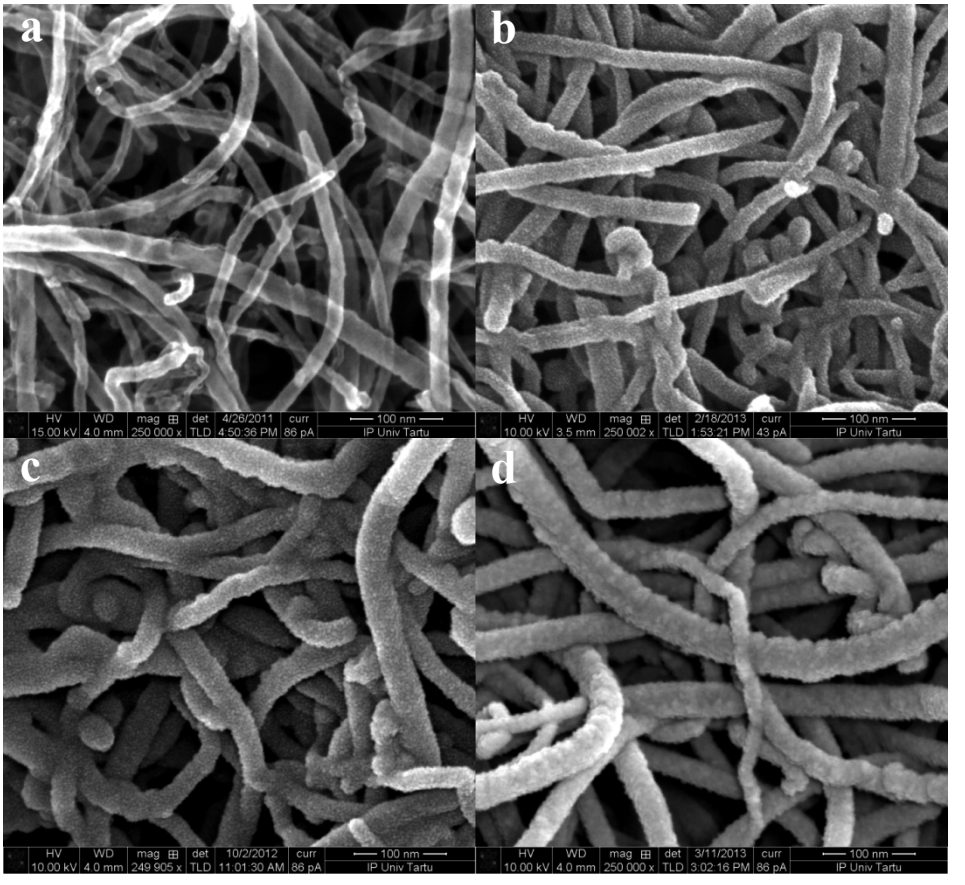

Figure 1. SEM images of (a) uncoated MWCNTs and (b–d) MWCNT support modified by Pt nanolayers with different film thicknesses: (b) 4, (c) 8 and (d) 16 nm.

support. SEM observations also show that the Pt nanolayers are located only on MWCNTs. Four images at the same magnifications show the morphological features of catalyst composite materials.

The presence of crystalline PtNPs was confirmed by XRD analysis (data not shown). The XRD peaks at 2θ = 39.7° and 46.1° and an ill-defined peak at 2θ = 67.2° can be assigned to the (111) and (220) planes of face-centred cubic Pt structure [37].

6.1.2. CO oxidation and cyclic voltammetry experiments

PtNP/MWCNT modified GC electrodes were cycled at 50 mV s^{-1} in Ar-saturated 0.5 M H_2SO_4 and 0.1 M KOH solutions in the potential range between 0.05 and 1.4 V. In order to improve the surface cleanliness, the CO-stripping experiments were performed following the operation conditions described elsewhere [47] and typical CO-stripping voltammograms in 0.5 M H_2SO_4 are presented in Fig. 2. The first cycle between 0.05 and 0.35 V vs. RHE indicates that Pt surface is completely blocked by adsorbed CO. CO-stripping technique is a surface sensitive probe [184]. Clearly distinguished anodic peak in the potential range between 0.8 and 0.9 V corresponds to CO oxidation and desorption from the Pt catalyst surface.

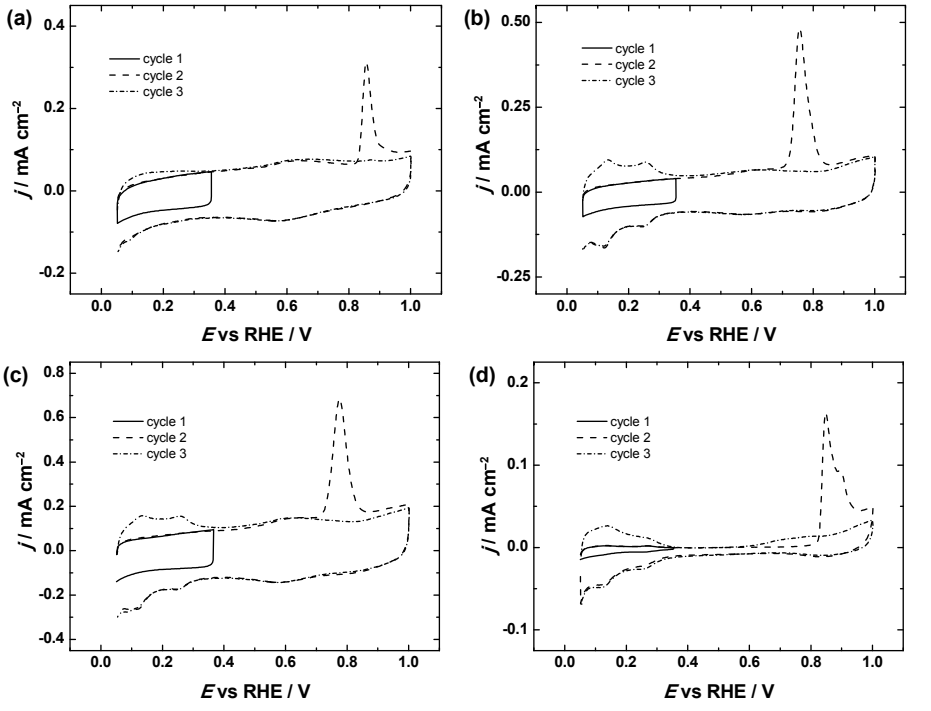

Figure 2. CO-stripping voltammograms for (a–c) 1-PtNP/MWCNT, 2-PtNP/MWCNT, 3-PtNP/MWCNT catalysts and (d) bulk Pt electrode in 0.5 M H_2SO_4. v = 20 mV s^{-1}. Current densities are normalised to the geometric surface area of GC substrate.

CO oxidation peaks are observed at different potentials for all catalysts in this study, namely at 0.90, 0.78, 0.80 and 0.85 V for 1-PtNP/MWCNT, 2-PtNP/MWCNT and 3-PtNP/MWCNT catalysts and bulk Pt, respectively. Cherstiouk et al. suggested that the positive shift of the CO oxidation onset is due to slow interaction of OH_{ads} and CO_{ads} on platinum surface [185]. Peak shoulders for 1-PtNP/MWCNT and 3-PtNP/MWCNT (Fig. 2a and c) indicate variations of surface sites present on Pt with different layer thicknesses. For bulk Pt electrode, multiple CO oxidation peak is observed, which indicates complex morphology of Pt surface. Similar behaviour was also evidenced in previous works [186, 187]. López-Cudero et al. showed that the increased agglomeration of Pt nanoparticles results in a development of a new peak at lower potentials [188]. Earlier developments have demonstrated that the CO oxidation peak location is strongly influenced by agglomeration and size of Pt nanoparticles supported on high-surface-area carbon [189, 190].

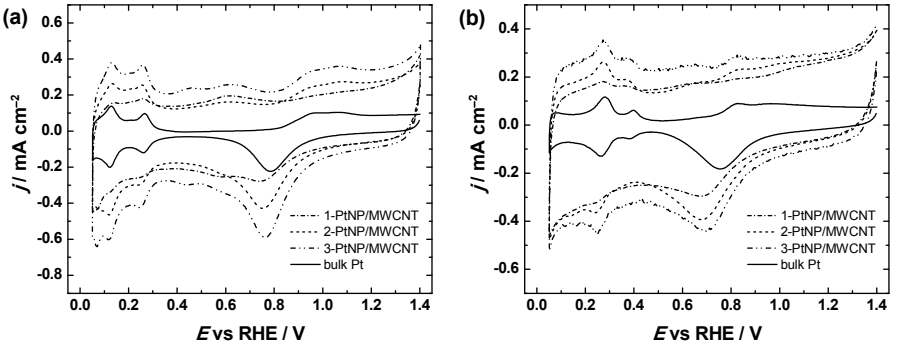

Figure 3. Cyclic voltammograms of PtNP/MWCNT catalysts and bulk Pt electrode in Ar-saturated solutions: (a) 0.5 M H_2SO_4, (b) 0.1 M KOH. v = 50 mV s^{-1}. Current densities are normalised to the geometric surface area of GC substrate.

The CV curves displayed in Fig. 3 were recorded in both acid and alkaline media after the electrochemical decontamination of the Pt surface. The cyclic voltammograms look similar to the CVs of the bulk Pt electrode presented in Fig. 3 for comparison purposes. The CVs show the presence of adsorption states associated with (110) and (100) sites at 0.12 and 0.27 V, respectively. Moreover, a shoulder around 0.35 V is apparent, being characteristic of small (100) terraces. The charge integrated under the hydrogen desorption peaks was used to calculate the electroactive Pt surface area of the electrodes, assuming that the charge required to oxidise a monolayer of adsorbed hydrogen on Pt is equal to 210 μC cm^{-2} [191]. As can be seen from Table 1 the 3-PtNP/MWCNT catalyst has larger real surface area than catalysts with thinner sputtered layers. For comparison reasons the A_r values were also obtained by integrating the charge under CO oxidation peak using the CO-stripping voltammetry data, taking into account that the charge required to oxidise on monolayer of CO adsorbed on a Pt surface as 420 μC cm^{-2} (equivalent to two electrons per CO molecule) [21, 192, 193]. The A_r values calculated from CO-stripping were slightly higher than

the electroactive areas determined from H_{UPD} (0.17, 0.29 and 0.42 cm^2 for 1-PtNP/MWCNT, 2-PtNP/MWCNT and 3-PtNP/MWCNT catalysts, respectively). Mezalira and Bron observed a similar tendency for Pt electrocatalyst supported on functionalised CNTs because of the easier and reliable baseline correction during the peak integration [194]. Analogous results were also presented by other groups [47, 195].

6.1.3. RDE studies of O_2 reduction

The RDE measurements were carried out in O_2-saturated 0.5 M H_2SO_4 and 0.1 M KOH solutions at different electrode rotation rates. The representative current–potential curves of the ORR for the 2-PtNP/MWCNT modified GC electrode in 0.5 M H_2SO_4 are shown in Fig. 4a. Only the negative-going potential scans are presented and further analysed. Single-wave polarisation curves with a well-defined current plateau were observed and a high electrocatalytic activity of the Pt nanoparticles towards the ORR is in evidence.

The RDE data were analysed using the Koutecky-Levich (K-L) equation [196]:

$$\frac{1}{j} = \frac{1}{j_k} + \frac{1}{j_d} = -\frac{1}{nFkC_{O_2}^b} - \frac{1}{0.62nFD_{O_2}^{2/3}\nu^{-1/6}C_{O_2}^b\omega^{1/2}} \quad (10)$$

where j is the measured current density, j_k and j_d are the kinetic and diffusion-limited current densities, respectively, n is the number of electrons transferred per O_2 molecule, k is the rate constant for oxygen reduction, F is the Faraday constant (96,485 C mol^{-1}), ω is the electrode rotation rate (rad s^{-1}), $C_{O_2}^b$ is the concentration of oxygen in the bulk (1.13×10^{-6} mol cm^{-3}) [197], D_{O_2} is the diffusion coefficient of oxygen (1.8×10^{-5} cm^2 s^{-1}) [197] and ν is the kinematic viscosity of the solution (0.01 cm^2 s^{-1}) [198]. The K–L plots were constructed (Fig. 4b) and the value of n was close to four for all the PtNP/MWCNT catalysts studied (see inset to Fig. 4b). This is an indication that the ORR predominantly follows a $4e^-$ pathway. The four-electron pathway of the ORR on Pt has been confirmed in many studies [199, 200], however, it is not possible to unambiguously establish whether the ORR proceeds through a "direct" $4e^-$ pathway or through H_2O_2 intermediate that is subsequently reduced. From the K–L plots it is obvious that the process of the ORR on PtNP/MWCNT is controlled by the diffusion of oxygen to the electrode surface in a large range of potentials.

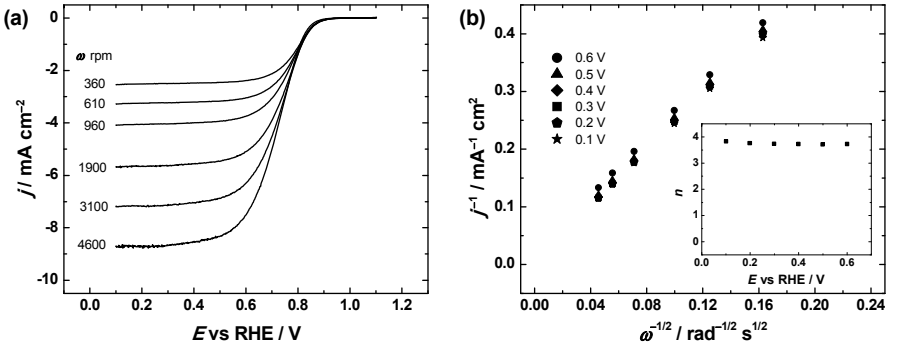

Figure 4. (a) RDE voltammetry curves for O_2 reduction on a 2-PtNP/MWCNT modified GC electrode in O_2-saturated 0.5 M H_2SO_4, v = 10 mV s^{-1}. (b) Koutecky–Levich plots for O_2 reduction on a 2-PtNP/MWCNT modified GC electrode in 0.5 M H_2SO_4. Inset shows the potential dependence of n. Current densities are normalised to the geometric surface area of GC substrate.

Fig. 5a presents the RDE behaviour of all the electrodes studied in the first phase of the work. For the sake of comparison a polarisation curve for acid-treated MWCNT modified GC electrode is also presented. The half-wave potential for oxygen reduction on the modified GC electrodes at 1900 rpm was determined to be 0.71, 0.75 and 0.76 V for 1-PtNP/MWCNT, 2-PtNP/MWCNT and 3-PtNP/MWCNT, respectively. This value is very similar to that of bulk Pt, which was determined to be 0.74 V. The value of $E_{1/2}$ for the ORR on commercial Pt/C modified GC electrode was 0.84 V which is in good agreement with previous studies [201]. Note that a remarkably positive shift of $E_{1/2}$ for Pt/C catalyst is largely due to the higher Pt area.

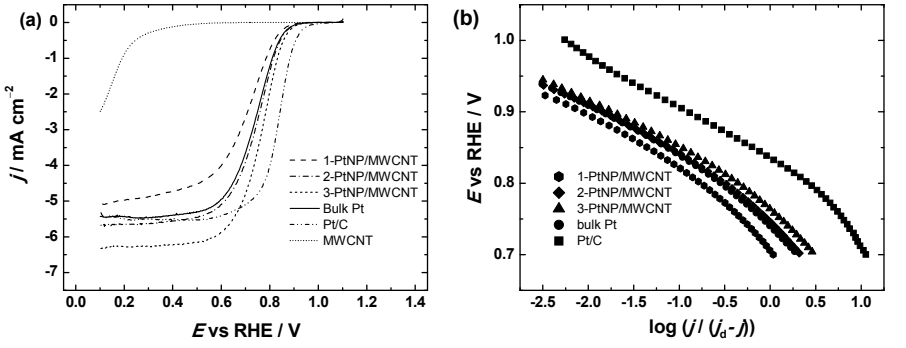

Figure 5. (a) Comparison of RDE results on oxygen reduction on PtNP/MWCNT catalysts, commercial Pt/C, acid-treated MWCNT modified GC and bulk Pt electrode in O_2-saturated 0.5 M H_2SO_4, v = 10 mV s^{-1}. (b) Mass-transfer corrected Tafel plots for O_2 reduction on PtNP/MWCNT catalysts, commercial Pt/C modified GC and bulk Pt electrodes in 0.5 M H_2SO_4. ω = 1900 rpm. Current densities are normalised to the geometric surface area of GC substrate.

The specific activity of O_2 reduction on PtNP/MWCNT, bulk Pt and Pt/C catalysts was calculated using the following equation:

$$SA = I_k / A_r \quad (11)$$

where I_k is the kinetic current at a given potential and A_r is the real surface area of platinum. The PtNPs deposited onto the MWCNT support show an enhanced ORR activity compared with the bulk Pt electrode. The SA values were close to 40 μA cm^{-2} for all the PtNP/MWCNT catalysts prepared in this study, which indicates that SA does not depend on the catalyst surface morphology for these composite materials. Strongly adsorbing (bi)sulphate anions block the active sites for oxygen reduction and as a result the electrocatalytic activity decreases [13, 14]. It has been shown, that the SA values of Pt catalyst strongly depend on the carbon support material structure [65]. In the previous study of our research group the SA values for Pt nanoparticles supported on SWCNTs were lower than that observed for PtNPs deposited on the surface of MWCNTs [47]. The SA value for PtNPs deposited onto TiO_2 functionalised graphene nanosheets was 69 μA cm^{-2} at 0.9 V vs. RHE [180]. Gasteiger et al. reviewed and compared the values of SA obtained by different research groups for Pt/C catalysts [202] and depending on the preparation method used the SA values varied between 36 and 470 μA cm^{-2}.

The mass activity values for the electrodes studied were calculated at 0.9 V using the following equation:

$$MA = I_k / m_{Pt} \quad (12)$$

taking into account Pt loading in PtNP/MWCNT catalyst materials. The MA values were 5, 4.7, 3.3 and 10.6 A g^{-1} for 1-PtNP/MWCNT, 2-PtNP/MWCNT and 3-PtNP/MWCNT catalysts and commercial Pt/C electrodes, respectively. The highest MA value was found for 1-PtNP/MWCNT modified electrode, which has lowest nominal Pt layer thickness. This is a reasonable result considering that for this PtNP/MWCNT catalyst the number of Pt atoms exposed to the solution and normalised to the weight is the largest of the three nanocomposites studied. The calculated MA values were relatively low compared with earlier studies of Pt/C catalysts in 0.5 M H_2SO_4, where MA values were 40 and 90 A g^{-1} (0.9 V vs. RHE) [203]. The reason for this difference in MA values can be explained by difference in Pt particle size. The MA values decrease when Pt particle size increases.

Tafel plots were constructed from the RDE data for the determination of kinetic parameters of O_2 reduction for all the electrodes studied. The Tafel behaviour of O_2 reduction on Pt-based catalysts in 0.5 M H_2SO_4 at a single electrode rotation rate (ω = 1900 rpm) is presented in Fig. 5b. Two Tafel regions with characteristic slopes close to −60 and −120 mV are clearly distinguished (Table 1). This indicates, that in both regions the charge transfer is the rate-determining step [51, 204] and the slope changes due to a significant change in

coverage of oxygen-containing species on the surface of Pt nanoparticles [199]. Tafel slopes were similar among all the electrodes studied, which indicates that the reaction mechanism is the same for all the electrocatalysts tested.

Table 1. Kinetic parameters for oxygen reduction on PtNP/MWCNT, commercial Pt/C and bulk Pt electrodes in 0.5 M H_2SO_4. ω = 1900 rpm.

Electrode	A_r (cm^2)	Tafel slope (mV) *Region I	Tafel slope (mV) *Region II	$E_{1/2}$ (V)	SA at 0.9 V (mA cm^{-2})	MA at 0.9 V (A g^{-1})
bulk Pt	0.44	–67	–119	0.74	0.033	n.a.
1-PtNP/ MWCNT	0.13	–66	–125	0.71	0.042	5.0
2-PtNP/ MWCNT	0.27	–64	–121	0.75	0.037	4.7
3-PtNP/ MWCNT	0.34	–65	–119	0.76	0.042	3.3
commercial Pt/C	4.33	–74	–84	0.84	0.020	10.6

*Region I corresponds to low current densities and region II to high current densities

The RDE experiments for the ORR were also carried out in 0.1 M KOH solution under otherwise identical conditions. Polarisation curves with well-defined diffusion-limited current plateaus were observed (Fig. 6a). The RDE data in alkaline solution were analysed using Eq. (10), where the values of O_2 solubility ($C_{O_2}^b$ = 1.2×10^{-6} mol cm^{-3}) [205] and diffusion coefficient (D_{O_2} = 1.9×10^{-5} cm^2 s^{-1}) [205] were used for 0.1 M KOH solution. The results of the K–L analysis are shown in Fig. 6b. Linear and parallel K–L plots were obtained

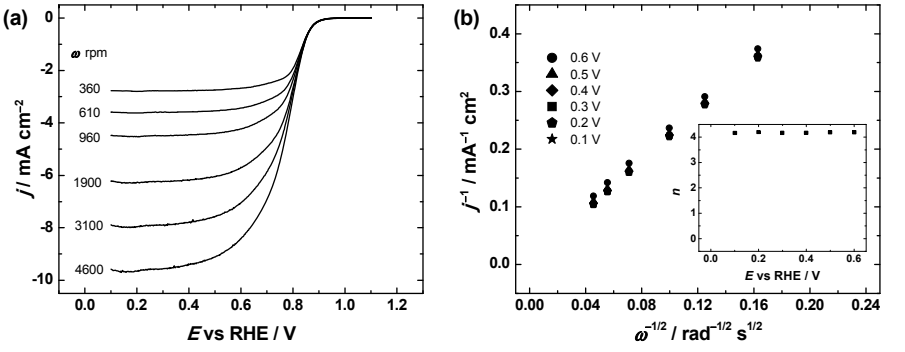

Figure 6. (a) RDE voltammetry curves for O_2 reduction on a 2-PtNP/MWCNT modified GC electrode in O_2-saturated 0.1 M KOH, v = 10 mV s^{-1}. (b) Koutecky–Levich plots for O_2 reduction on a 2-PtNP/MWCNT modified GC electrode in 0.1 M KOH. Inset shows the potential dependence of n. Current densities are normalised to the geometric surface area of GC substrate.

from the RDE data. The value of n was found from the K–L slopes, which was close to four for each electrode (see inset to Fig. 6b). The four-electron O_2 reduction pathway on Pt catalysts in alkaline media has been reported previously [206, 207]. Recently, Liu et al. performed systematic RRDE investigation on different functionalised Pt nanoparticles in 0.1 M NaOH and for all the catalyst in their study oxygen underwent 4-electron reduction to water [208].

The RDE results at a single electrode rotation rate are presented in Fig. 7a. As can be seen from Fig. 7a the limiting current densities are the same for MWCNT supported Pt catalysts and bulk Pt. The value of $E_{1/2}$ of the ORR on the PtNP/MWCNT catalysts was similar to that of bulk Pt (see Table 2). According to these $E_{1/2}$ values, the overall ORR activity of commercial Pt/C catalyst is higher than that of the PtNP/MWCNT nanocomposites in alkaline media. This is due to the lower density of active surface sites on the PtNP/MWCNT catalyst surface, which can also be reflected from the real electroactive surface area of Pt.

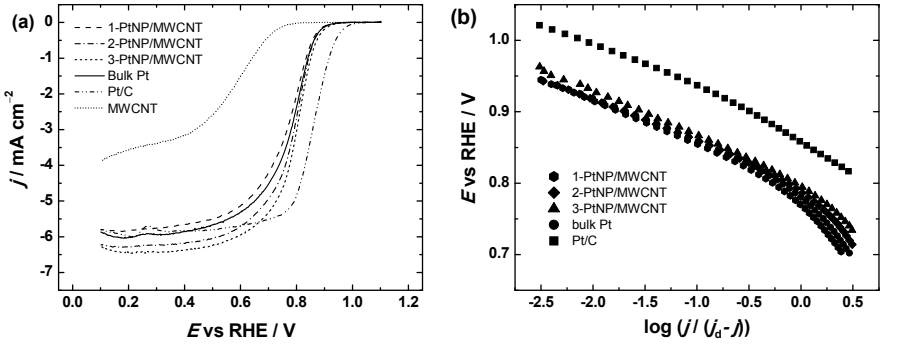

Figure 7. (a) Comparison of RDE results on oxygen reduction on PtNP/MWCNT catalysts, commercial Pt/C, acid-treated MWCNT modified GC and bulk Pt electrode in O_2-saturated 0.1 M KOH, v = 10 mV s^{-1}. (b) Mass-transfer corrected Tafel plots for O_2 reduction on PtNP/MWCNT catalysts, commercial Pt/C modified GC and bulk Pt electrodes in 0.1 M KOH. ω = 1900 rpm. Current densities are normalised to the geometric surface area of GC substrate.

Tafel plots of O_2 reduction were constructed and two regions of distinct slope are in evidence (Fig. 7b). The values of Tafel slopes are typical for polycrystalline and single-crystal Pt electrodes [8, 10, 209] and indicate that the mechanism of the ORR on PtNP/MWCNT catalysts is the same as for bulk Pt. Similar Tafel behaviour was also observed for carbon nanotube supported Pt nanoparticles in our previous work [47].

The SA and MA values for O_2 reduction on the PtNP/MWCNT catalysts in 0.1 M KOH solution were also determined at 0.9 V and are presented in Table 2. According to previous studies the specific ORR activity values should be higher in alkaline than in acid solution [8, 180]. This is the expected result due to the site-blocking effect of (bi)sulphate anions [210]. Hydroxide ions are not strongly adsorbed on Pt and therefore the inhibition of the kinetics of the ORR

is less pronounced in 0.1 M KOH than in 0.5 M H_2SO_4 solution. By comparison, the specific activities of the synthesised composite catalysts show slightly lower values than commercial Pt/C. The results obtained in 0.1 M KOH are in good agreement with previous reports on the kinetics of the ORR on Pt nanoparticles in alkaline solution [8].

Table 2. Kinetic parameters for oxygen reduction on PtNP/MWCNT, commercial Pt/C and bulk Pt electrodes in 0.1 M KOH. ω = 1900 rpm.

Electrode	A_r (cm^2)	Tafel slope (mV) *Region I	Tafel slope (mV) *Region II	$E_{1/2}$ (V)	SA at 0.9 V (mA cm^{-2})	MA at 0.9 V (A g^{-1})
bulk Pt	0.37	–54	–113	0.78	0.065	n.a.
1-PtNP/ MWCNT	0.13	–61	–149	0.77	0.101	12.1
2-PtNP/ MWCNT	0.26	–58	–145	0.79	0.061	7.2
3-PtNP/ MWCNT	0.34	–62	–141	0.79	0.071	5.6
commercial Pt/C	1.65	–57	–100	0.86	0.145	30.0

*Region I corresponds to low current densities and region II to high current densities

6.2. Oxygen reduction on Pt-TiO_2/MWCNT nanocomposites

In previous part, O_2 reduction studies were carried out on sputter-deposited Pt nanoparticles supported on multi-walled CNTs [I]. In this part of the study, a new approach for the preparation of Pt–TiO_2/MWCNT composite materials using chemical vapour deposition of MWCNTs, atomic layer deposition of TiO_2 and magnetron sputtering of Pt is explored [II]. Work is focused on the investigation of the electrocatalytic activity of Pt–TiO_2/MWCNT catalysts, with Pt layer thicknesses of 2, 4 and 8 nm for ORR in acid and alkaline solutions.

6.2.1. Physical characterisation of Pt–TiO_2/MWCNT catalysts

Fig. 8 shows SEM images of MWCNTs deposited on glassy carbon and Pt–TiO_2/MWCNT catalyst (Fig. 8a and b, respectively). As can be seen from Fig. 8, the overall surface morphology of carbon nanotubes is not affected by ALD of TiO_2. However, it is evident from Fig. 8b that the ALD treated nanotubes are slightly thicker. The same observation has been made by Lu et al. by depositing TiO_2 on the surface of aligned MWCNTs using the ALD method [211]. As can be seen from Fig. 8b, Pt nanoparticles were successfully deposited onto the TiO_2-coated MWCNT support, indicating that the presence of TiO_2 does not affect the homogeneity of sputter-deposited Pt nanoislands. Cross-

sectional SEM images of the structures (data not shown) reveal that near the GC substrate carbon nanotubes were vertically aligned, however, moving farther away, they became frizzled, which is a common feature of the catalytic CVD [212, 213] that was used in this work. According to SEM measurements, the typical thickness of the composite catalyst layer is of the order of μm.

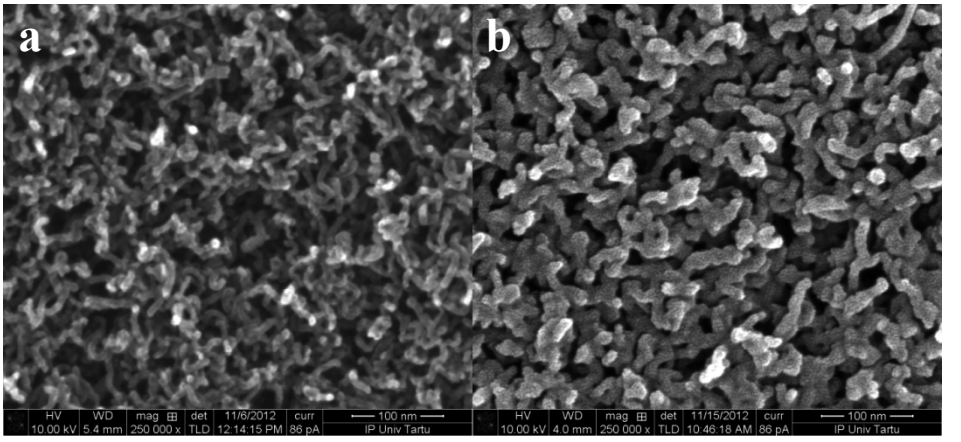

Figure 8. SEM images of (a) as-prepared MWCNTs and (b) Pt–TiO_2/MWCNT samples.

The XPS survey scan (data not shown) showed the presence of the following elements in the surface layer of the 3-Pt–TiO_2/MWCNT catalysts: C, O, Ti and Pt. Fig. 9a and b present the XPS core-level spectra in the Ti2p and Pt4f regions. As expected, all Ti is in an oxidised form (Ti^{4+}) that indicates the formation of TiO_2 by ALD. The XPS peak of $Ti2p_{3/2}$ is centred at 458.7 eV in agreement with previous study on Pt–TiO_2 catalysts [214]. High-resolution XPS spectrum in the Pt4f region shows that the sputter-deposited Pt was mainly in the zero valence (metallic) state (Fig. 9b). These Pt4f peaks appeared at the same binding energy values as those of bulk Pt (not shown).

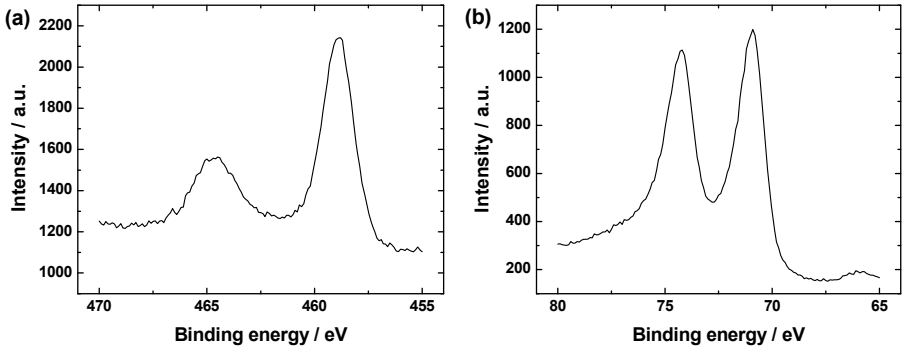

Figure 9. XPS core-level spectra of 3-Pt–TiO_2/MWCNT samples in (a) Ti2p and (b) Pt4f regions.

6.2.2. Cyclic voltammograms of Pt–TiO_2/MWCNT catalysts

The Pt–TiO_2/MWCNT modified GC and bulk Pt electrodes were cycled at 50 mV s^{-1} in Ar-saturated 0.5 M H_2SO_4 and 0.1 M KOH solutions in the potential range between 0.05 and 1.4 V vs. RHE. Each electrode was cycled 15 times in order to achieve a stable voltammogram. The CV curves presented in Fig. 10 show typical hydrogen adsorption–desorption peaks in the potential range of 0.05–0.35 V vs. RHE in 0.5 M H_2SO_4 (Fig. 10a) and between 0.1 and 0.4 V vs. RHE in 0.1 M KOH (Fig. 10b). In both acid and alkaline solutions the electrochemical fingerprints of Pt metal were clearly recognised. However, slight differences in the shape of the hydrogen adsorption–desorption peaks reveal different Pt crystallite orientation. The cyclic voltammograms obtained for Pt–TiO_2/MWCNT catalysts showed distinctly higher current density in the conventional double layer region compared to bulk Pt electrodes that is apparently caused by a higher surface area of the composite materials. Small peaks in this region could be related to quinone-type functionalities on the MWCNT surface exposed to solution. The regions of surface oxide formation and reduction typical for polycrystalline Pt in acid and alkaline electrolytes were observed. No additional peaks appeared, indicating that TiO_2 has sufficient electrochemical inertness and electrical conductivity [215]. As can be seen from the CV results presented, the platinum oxide reduction peak location was different for all the electrodes studied. This effect can be explained by the formation of Pt crystallites or agglomerates of different size during the magnetron sputtering procedure, when Pt layers of different thickness are deposited onto the TiO_2/MWCNT support. The reduction of oxide of smaller Pt particles needs more energy and therefore the oxide reduction peak shifts to more negative potentials. From this estimation we can assume, that the Pt crystallite size is larger for 3-Pt–TiO_2/MWCNT compared to 1-Pt–TiO_2/MWCNT and 2-Pt–TiO_2/MWCNT catalysts.

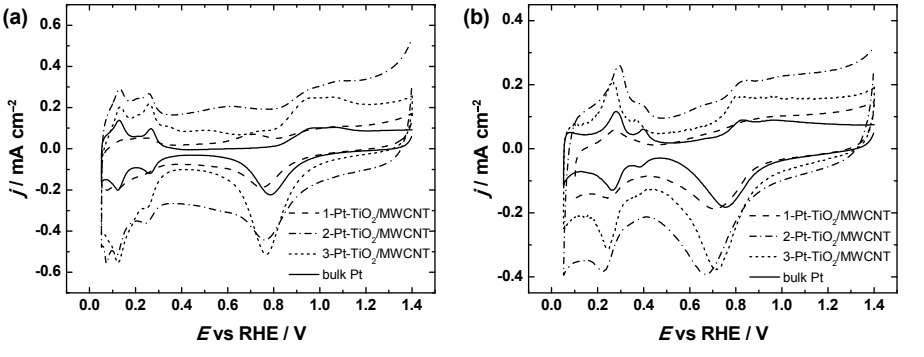

Figure 10. Cyclic voltammograms of 1-Pt–TiO_2/MWCNT, 2-Pt–TiO_2/MWCNT and 3-Pt–TiO_2/MWCNT modified GC and bulk Pt electrodes in Ar-saturated solutions: (a) 0.5 M H_2SO_4 and (b) 0.1 M KOH. v = 50 mV s^{-1}. Current densities are normalised to the geometric surface area of GC substrate.

In order to calculate the electroactive Pt surface area for all the electrodes studied, the integrated charge under the hydrogen desorption peak was used. It can be seen from Tables 3 and 4 that the electroactive Pt surface area of the commercial Pt/C catalyst is significantly higher than that of the prepared catalyst materials. However, it needs to be mentioned that the determination of real surface area of metal-oxide supported Pt catalysts is not straightforward, because of the difficulties in baseline correction [216].

6.2.3. Oxygen reduction on Pt–TiO_2/MWCNT catalysts

The RDE measurements were carried out in O_2-saturated 0.5 M H_2SO_4 and 0.1 M KOH solutions at different electrode rotation rates. The representative current–potential curves of the ORR for Pt–TiO_2/MWCNT modified GC electrodes in acid media are shown in Fig. 11a–c. Fig. 11d shows the comparison of the ORR activity for Pt–TiO_2/MWCNT catalysts, unmodified MWCNTs,

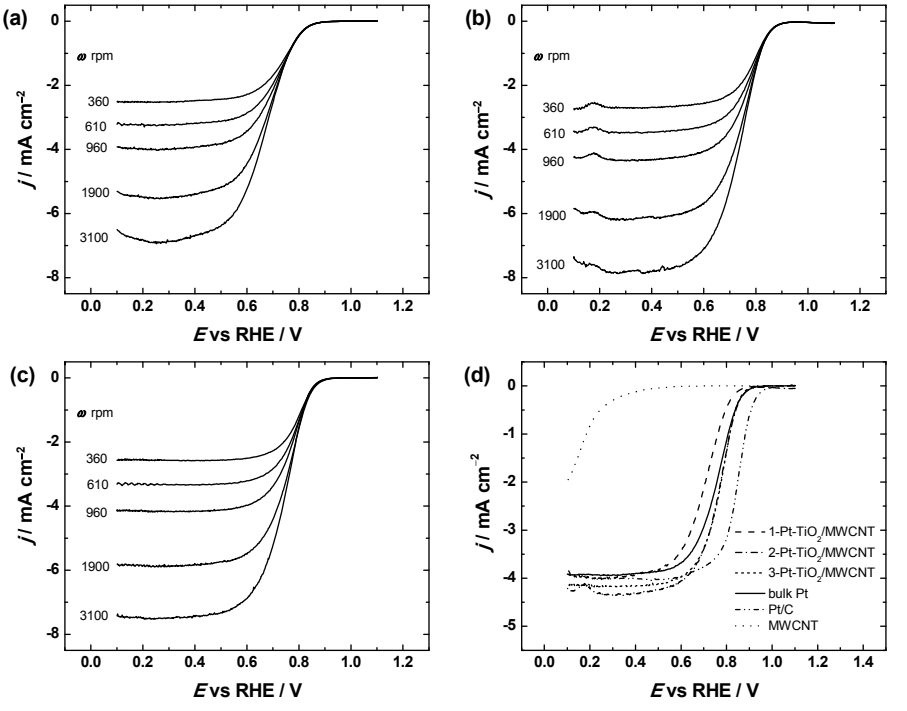

Figure 11. RDE voltammetry curves for oxygen reduction on (a) 1-Pt–TiO_2/MWCNT, (b) 2-Pt–TiO_2/MWCNT and (c) 3-Pt–TiO_2/MWCNT modified GC electrodes in O_2-saturated 0.5 M H_2SO_4, v = 10 mV s^{-1}. (d) Comparison of RDE results on oxygen reduction on Pt–TiO_2/MWCNT, MWCNT and commercial Pt/C modified GC and bulk Pt electrode in 0.5 M H_2SO_4 at 960 rpm. Current densities are normalised to the geometric surface area of GC substrate.

commercial Pt/C modified GC and bulk Pt electrodes in O_2-saturated 0.5 M H_2SO_4 at 960 rpm. The oxygen reduction studies in 0.5 M H_2SO_4 showed that the commercial Pt/C catalyst exhibited the best ORR performance due to its remarkably higher electroactive surface area (Fig. 11d). Half-wave potential values for the prepared 3-Pt–TiO_2/MWCNT catalysts shifted negative by 80 mV compared with commercial Pt/C. Due to different electroactive area, which depends on the Pt loading and nanoparticle size, a shift of RDE voltammetry curves and a slight variation of limiting current is an expected result [212]. The value of $E_{1/2}$ for ORR on commercial Pt/C modified GC electrode was 0.85 V which is in good agreement with previous studies [I]. The $E_{1/2}$ value for un-modified MWCNTs is significantly lower in acid media, consistent with our early work [177, 217].

The K–L plots were constructed (Fig. 12a–c) and the *n* value was found to be close to four for all catalysts in this study (see insets in Fig. 12a–c). This indicates that the process of O_2 reduction follows predominantly a $4e^-$ pathway on Pt–TiO_2/MWCNT catalysts.

To calculate the specific activity of oxygen reduction for Pt–TiO_2/MWCNT and commercial Pt/C catalysts the reduction current at 0.9 V was used (Table 3). The SA of Pt–TiO_2/MWCNT catalysts shows a slight enhancement compared to the commercial Pt/C catalyst. An increase in SA could be explained by the modification of electronic properties of Pt by the metal oxide. However, lower SA of Pt/C might arise from the reduced intrinsic activity of Pt particles of smaller size. Gasteiger et al. studied Pt particle size effect on the ORR kinetics in non-adsorbing 0.1 M $HClO_4$ solution and showed that the Pt oxide reduction peak shifted to more negative potentials for smaller Pt particles [202]. This research group proposed that this effect occurred due to increasing adsorption strength of OH_{ads} species with their negative impact on the ORR with decreasing Pt particle size. Similar trends were shown by Hayden group for Pt particle size effect at Pt layer thicknesses smaller than 1 nm on TiO_x and carbon supports [218]. Mayrhofer et al. examined this effect on Pt particles sized 1–30 nm and observed the same trend [20].

For better overview of kinetics results, the mass-transfer corrected Tafel plots for O_2 reduction on Pt–TiO_2/MWCNT, commercial Pt/C modified GC and bulk Pt electrodes were constructed from the RDE data obtained at 960 rpm and shown in Fig. 12d. Similar Tafel slope for all the electrodes compared was also observed in earlier studies, indicating that the ORR mechanism does not change after incorporation of TiO_2 into the catalyst structure [219, 220].

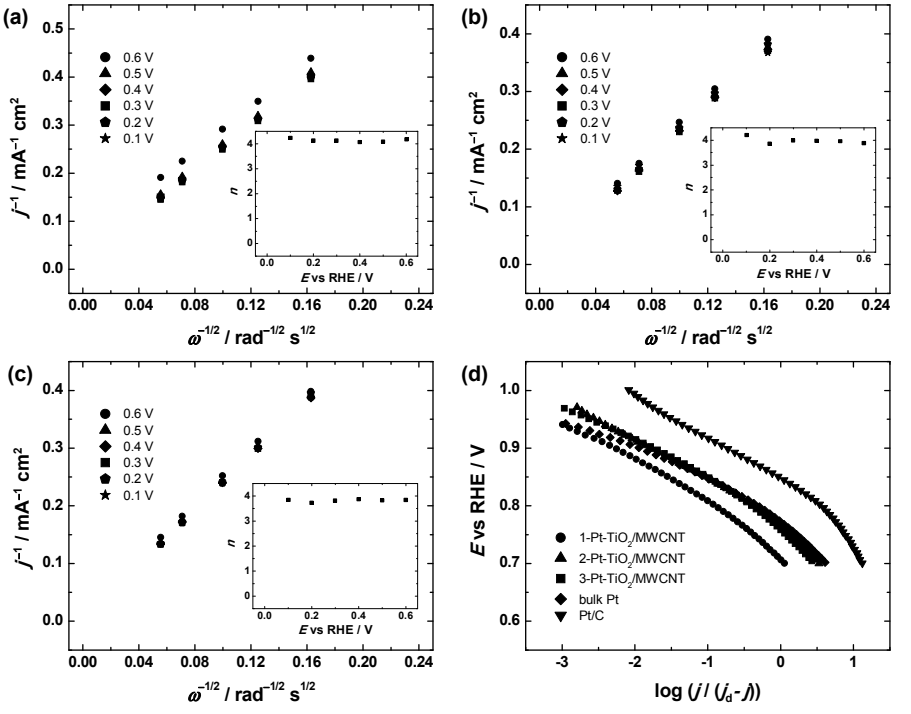

Figure 12. Koutecky–Levich plots for O_2 reduction on (a) 1-Pt–TiO_2/MWCNT, (b) 2-Pt–TiO_2/MWCNT and (c) 3-Pt–TiO_2/MWCNT modified GC electrode in 0.5 M H_2SO_4. Insets show the potential dependence of *n*. (d) Mass-transfer corrected Tafel plots for O_2 reduction on Pt–TiO_2/MWCNT, commercial Pt/C modified GC and bulk Pt electrodes in 0.5 M H_2SO_4. ω = 960 rpm. Data derived from Fig. 11. Current densities are normalised to the geometric surface area of GC substrate.

Table 3. Kinetic parameters for oxygen reduction on Pt-TiO_2/MWCNT, commercial Pt/C and bulk Pt electrodes in 0.5 M H_2SO_4. ω = 960 rpm.

Electrode	A_r (cm^2)	Tafel slope (mV) *Region I	Tafel slope (mV) *Region II	$E_{1/2}$ (V)	SA at 0.9 V (mA cm^{-2})	MA at 0.9 V (A g^{-1})
1-Pt-TiO_2/ MWCNT	0.16 ± 0.03	–67 ± 3	–105 ± 8	0.71 ± 0.01	0.025 ± 0.002	5.7 ± 0.7
2-Pt-TiO_2/ MWCNT	0.36 ± 0.04	–73 ± 3	–112 ± 13	0.77 ± 0.02	0.032 ± 0.002	3.6 ± 0.5
3-Pt-TiO_2/ MWCNT	0.39 ± 0.02	–55 ± 2	–107 ± 11	0.77 ± 0.02	0.024 ± 0.003	2.9 ± 0.4
comm. Pt/C	4.33 ± 0.16	–71 ± 5	–131 ± 16	0.85 ± 0.01	0.021 ± 0.002	11.3 ± 1.2
bulk Pt	0.44 ± 0.03	–65 ± 3	–117 ± 6	0.76 ± 0.01	0.031 ± 0.005	n.a.

*Region I corresponds to low current densities and region II to high current densities

The calculated MA values at 0.9 V vs. RHE for 1-Pt–TiO_2/MWCNT were two-fold smaller than that of the commercial Pt/C catalyst in acid solution. The obvious reason might be a smaller size of Pt particles of the Pt/C catalyst [202]. Very recently Ruiz-Camacho et al. proposed that the TiO_2 loading on carbon material is an essential parameter that should be taken into account [221]. In their study Pt–TiO_2–C samples prepared with TiO_2 loading of 5 wt% resulted in homogeneous oxide dispersion with an enhanced metal-oxide interaction, compared to 15 wt% Pt–TiO_2–C catalyst, which had lower electronic transfer to carry out the electrocatalysis of the ORR.

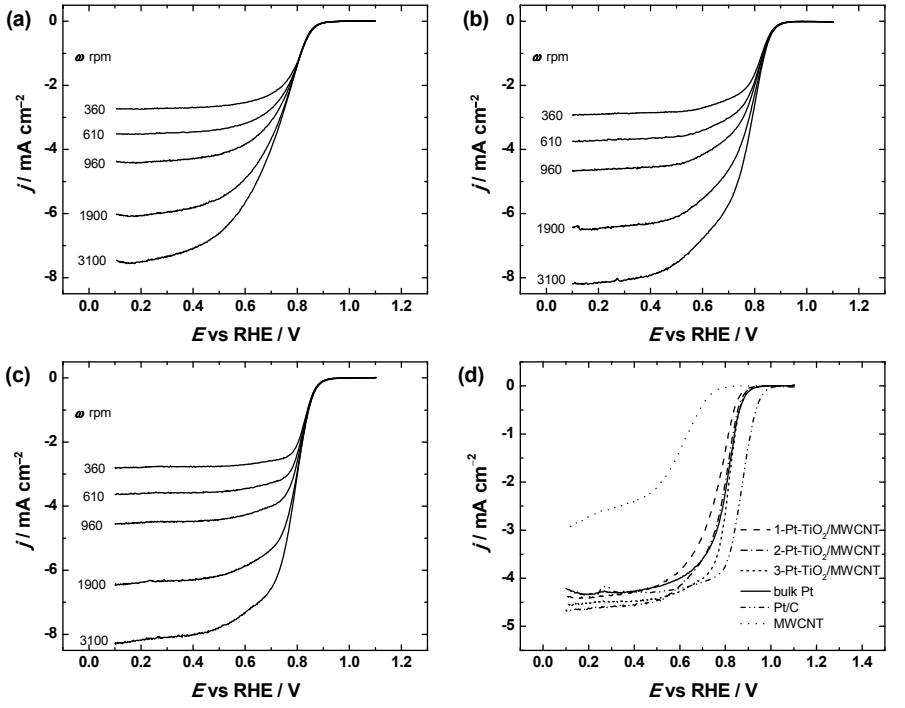

Figure 13. RDE voltammograms for oxygen reduction on (a) 1-Pt–TiO_2/MWCNT, (b) 2-Pt–TiO_2/MWCNT and (c) 3-Pt–TiO_2/MWCNT modified GC electrode in O_2-saturated 0.1 M KOH, v = 10 mV s^{-1}. (d) Comparison of RDE results on oxygen reduction on Pt–TiO_2/MWCNT, MWCNT and commercial Pt/C modified GC and bulk Pt electrodes in 0.1 M KOH at 960 rpm. Current densities are normalised to the geometric surface area of GC substrate.

Using identical RDE operation conditions the ORR experiments were also carried out in O_2-saturated 0.1 M KOH solution. Similarly to the RDE results obtained in 0.5 M H_2SO_4 the ORR polarisation curves with well-defined diffusion-limited current plateaus were observed (Fig. 13a–c). As can be seen from Fig. 13d, commercial Pt/C catalyst demonstrated highest ORR activity, while all the Pt–TiO_2/MWCNT catalysts showed the ORR performance similar to that of bulk Pt. The $E_{1/2}$ value for unmodified MWCNTs in 0.1 M KOH is considerably

lower than that of Pt-based catalysts, in agreement with our previous reports [222, 223]. The results of the K–L analysis are shown in Fig. 14a–c. Linear K–L plots were obtained from the RDE data. The value of *n* was found from the K–L slopes, which was close to four for each electrode (inset in Fig. 14a–c). The $4e^-$ ORR pathway on Pt catalyst in alkaline media has been reported previously [47, 180, 206, 207, 224].

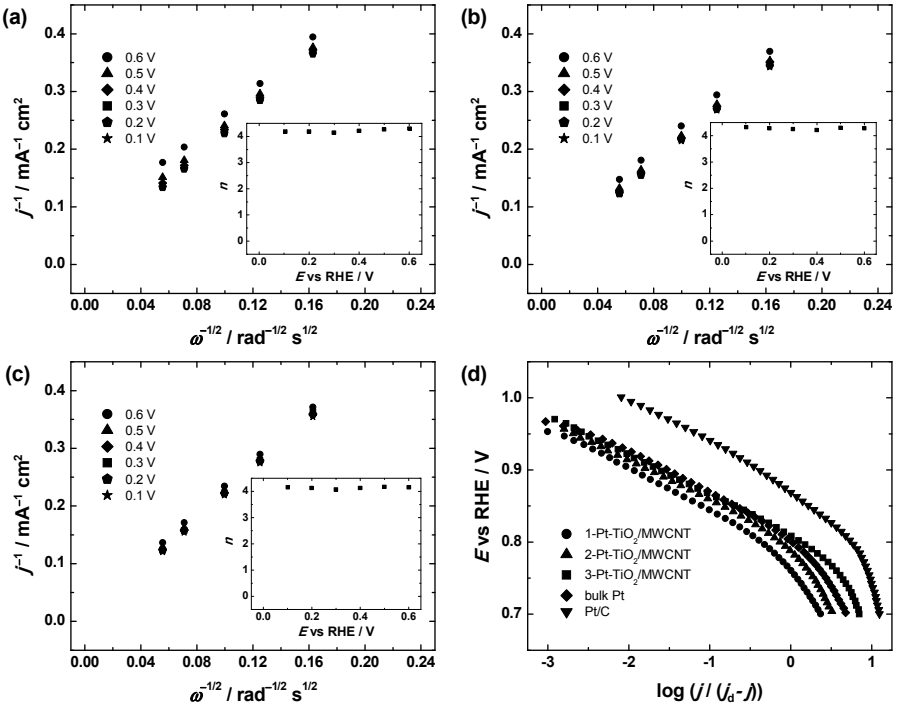

Figure 14. Koutecky–Levich plots for O_2 reduction on (a) 1-Pt–TiO_2/MWCNT, (b) 2-Pt–TiO_2/MWCNT and (c) 3-Pt–TiO_2/MWCNT modified GC electrode in 0.1 M KOH. Insets show the potential dependence of *n*. (d) Mass-transfer corrected Tafel plots for O_2 reduction on Pt–TiO_2/MWCNT and commercial Pt/C modified GC and bulk Pt electrodes in 0.1 M KOH. ω = 960 rpm. Data derived from Fig. 13. Current densities are normalised to the geometric surface area of GC substrate.

For all the Pt–TiO_2/MWCNT electrocatalysts prepared the decrease in kinetic performance was evident in alkaline electrolyte. The SA values obtained for these catalysts are lower than those determined for bulk Pt and commercial Pt/C catalyst, indeed the value of $E_{1/2}$ obtained for Pt–TiO_2/MWCNT is comparable to that obtained for bulk Pt electrode. It turns out that O_2 reduction in 0.1 M KOH is more favourable for the commercial Pt/C catalyst.

In both acid and alkaline solutions a slight increase in Tafel slope was observed for 1-Pt−TiO_2/MWCNT catalyst. Two regions of distinct Tafel slope were evident from Fig. 14d and a higher slope value than –120 mV at higher current densities is in accordance with literature results for Pt catalysts in

alkaline media [225]. Due to variation in catalyst structure and morphology, enhanced interactions between Pt and TiO_2 should result in faster ORR kinetics. Gustavsson et al. showed that the presence of TiO_2 can either increase or decrease the ORR performance of Pt catalyst, depending on deposition order of the thin films [226]. According to their model, electrocatalytic performance is greater when TiO_2 is placed in between Pt and Nafion, while a decreased performance was observed when TiO_2 was placed in between Pt and the carbon conductor.

Table 4. Kinetic parameters for oxygen reduction on Pt-TiO_2/MWCNT, commercial Pt/C and bulk Pt electrodes in 0.1 M KOH. ω = 960 rpm.

Electrode	A_r (cm^2)	Tafel slope (mV) *Region I	Tafel slope (mV) *Region II	$E_{1/2}$ (V)	SA at 0.9 V (mA cm^{-2})	MA at 0.9 V (A g^{-1})
1-Pt-TiO_2/ MWCNT	0.28 ± 0.02	–59 ± 2	–138 ± 14	0.76 ± 0.01	0.034 ± 0.003	13.0 ± 0.5
2-Pt-TiO_2/ MWCNT	0.50 ± 0.04	–57 ± 3	–156 ± 19	0.79 ± 0.02	0.035 ± 0.004	9.8 ± 0.6
3-Pt-TiO_2/ MWCNT	0.57 ± 0.03	–55 ± 2	–136 ± 15	0.81 ± 0.01	0.037 ± 0.003	6.5 ± 0.4
comm. Pt/C	1.65 ± 0.13	–65 ± 6	–166 ± 22	0.87 ± 0.01	0.133 ± 0.011	27.4 ± 2.0
bulk Pt	0.37 ± 0.04	–57 ± 3	–150 ± 9	0.80 ± 0.01	0.067 ± 0.007	n.a.

*Region I corresponds to low current densities and region II to high current densities

The stability of Pt–TiO_2/MWCNT and commercial Pt/C catalysts was tested using repetitive potential cycling in 0.5 M H_2SO_4 between 0.05 and 1.2 V for a total of 1000 scans (Fig. 15a) and obvious changes in the amount of charge under the H_{UPD} peak were observed (Fig. 15b). The formation of quinone-type groups on the surface of MWCNTs is also evident by repeat cycling and a pair of peaks appears at ca 0.6 V. The electrochemically accessible surface area of Pt–TiO_2/MWCNT decreased to 41% and only 25% of Pt electroactive area was left on commercial Pt/C after long-term durability tests under identical conditions.

The advantages of TiO_2-carbon composites as catalyst support materials have been recently highlighted in a review by Alonso-Vante and co-workers [227]. It was reported that up to 20 wt% TiO_2/C the resistance does not increase as compared to Vulcan carbon. The incorporation of TiO_2 into the composite decreases the contact between Pt and carbon and therefore increases the stability of the electrocatalyst. Pt catalysts supported on TiO_2/C showed an improved ORR activity by a factor of 2–3 and increased stability under potential cycling [228]. The enhanced activity was explained by alloying of Pt with Ti that alters the electronic properties of Pt. Sakai et al. annealed the Pt–TiO_x/C catalysts

prepared from reversed micelles [229]. It was found that the reduced state of TiO_2 was essential for high ORR activity to be observed. The reason for increased activity was the formation of Ti^{3+} species that leads to oxygen defect-Pt or Ti^{3+}–Pt interactions. The heat-treated Pt–TiO_x/C samples showed also an excellent stability. Bauer et al. investigated the ORR performance and durability of Pt nanoparticles supported on Nb–TiO_2–carbon composite prepared by electrospinning [230]. The Pt/Nb–TiO_2–carbon catalyst showed a comparable ORR activity and better stability than commercial Pt/C catalyst. Pt/Nb–TiO_2–carbon was used as a cathode material in low-temperature fuel cell and a good fuel cell performance was observed (peak power density 0.34 W cm^{-2}). In a further development, non-carbon ceramic Nb-doped TiO_2 nanofibers were used as Pt catalyst support [231]. This Pt/Nb–TiO_2 material retained a significantly higher ECSA during repetitive potential cycling than Pt deposited on carbon nanofibers. This was explained by an enhanced corrosion resistance of TiO_2-based support. Huang et al. explored the electrocatalysis of the ORR on electrodeposited Pt catalysts on mesoporous TiO_2 film [232]. The ORR mass-activity decreased with increasing electrodeposition time, which is concomitant with a decrease in specific surface area. The increased stability of the Pt/TiO_2 catalysts as compared to commercial Pt/C was attributed to the interaction between Pt particles and TiO_2 support as confirmed by XPS. This finding is in good agreement with that of a previous study [233]. Recently, sputter-deposition was employed for the preparation of Pt/titanium dioxide nanotubes showing a great promise of this method for the development of cathode catalysts for low-temperature fuel cells [234].

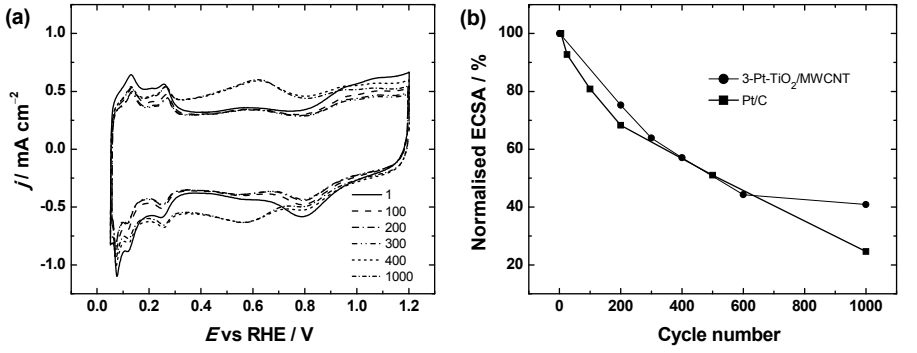

Figure 15. (a) Repetitive cyclic voltammograms of 3-Pt–TiO_2/MWCNT modified GC electrodes. Cycle numbers are indicated in legend. Test solution: Ar-saturated 0.5 M H_2SO_4. $v = 50$ mV s^{-1}. (b) Comparison of ECSA value loss for the 3-Pt–TiO_2/MWCNT and commercial Pt/C catalysts during repetitive potential cycles. Current densities are normalised to the geometric surface area of GC substrate.

6.3. Oxygen reduction on N-doped graphene-nanosheet supported PtNPs

Platinum nanoparticles supported on N-doped graphene sheets are studied as electrocatalysts for ORR [III]. As-prepared Pt/NG catalysts are physically characterised by transmission electron microscopy and X-ray photoelectron spectroscopy. The electrochemical properties of the Pt/NG materials are studied in acid and alkaline solutions using cyclic voltammetry and the RDE method.

6.3.1. Surface characterisation of Pt/NG catalysts

The surface morphology of the Pt/NG catalysts was examined by TEM. Figure 16a and 16d provide an overview of the Pt distribution in the 40-Pt/NG_{BH} and 20-Pt/NG_{EG} nanomaterials, respectively. In both samples, creasing of the graphene sheet is clearly visible and is manifested by an excess of PtNPs in this area. In the 40-Pt/NG_{BH} sample, the nanoparticles appear to be less densely dispersed compared to the 20-Pt/NG_{BH} as expected from the quantity of Pt loading in the two samples. Moreover, the size of the nanoparticles in the 40-Pt/NG_{BH} sample is larger and less uniformly shaped compared to 20-Pt/NG_{BH}. It can be seen that smaller nanoparticles were formed when ethylene glycol was used as reducing agent.

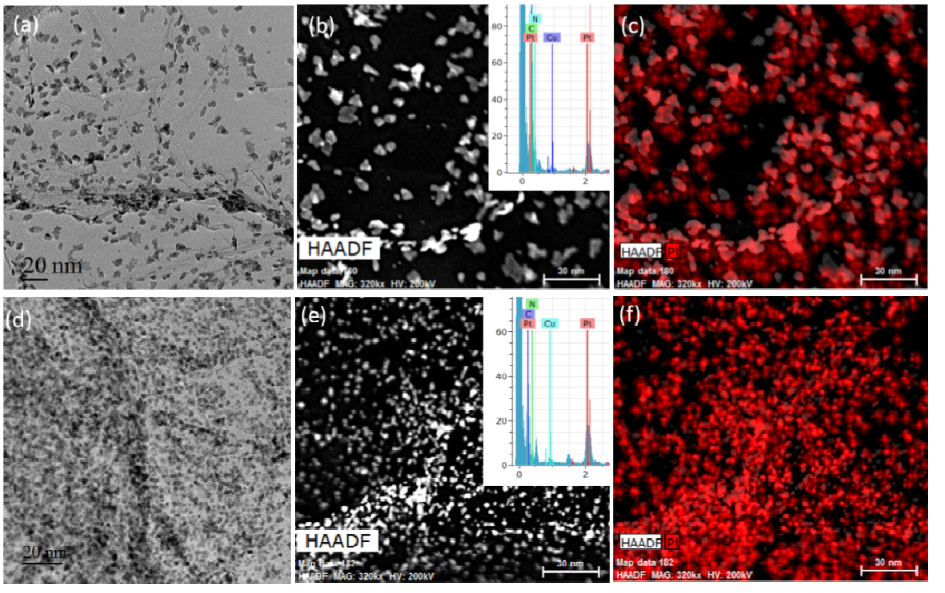

Figure 16. TEM micrographs for (a) 40-Pt/NG_{BH} and (d) 20-Pt/NG_{EG} nanomaterials. The HAADF-STEM images of (b) 40-Pt/NG_{BH} and (e) 20- Pt/NG_{EG} samples. The insets in (b) and (e) are the EDX spectra of the various elements acquired from areas shown in (b) and (e). EDX maps of Pt in (c) 40-Pt/NG_{BH} and (f) 20-Pt/NG_{EG} samples.

In Fig. 16b,e, HAADF-STEM images have been acquired from the 40-Pt/NG_{BH} and 20-Pt/NG_{EG} samples, respectively. EDX spectra shown in the insets of these images were acquired from the zones indicated in the images. The spectra confirm the presence of all elements such as N, Pt and C. Cu present in the spectra originates from the carbon-coated Cu grid used for TEM analysis. For the 40-Pt/NG_{BH} sample we observe in Fig. 16b that along with larger particles of ~10 nm, smaller nanoparticles of ~2 nm are also visible. Figure 16c, f is the EDX Pt elemental mapping confirming the distribution of the Pt nanoparticles in the graphene sheet. Similar TEM images were also obtained for the 20-Pt/NG_{BH} and 40-Pt/NG_{EG} samples (Fig. 17). Uniform distribution of PtNPs is clearly observed in both samples. However, a denser Pt distribution along with a larger Pt nanoparticle size distribution is observed for the 20-Pt/NG_{BH} sample (Fig. 17a) compared to the 40-Pt/NG_{EG} sample (Fig. 17c). The corresponding diffraction patterns for both samples 20-Pt/NG_{BH} and 40-Pt/NG_{EG} are also provided in subpanels b and d of Fig. 17, respectively. In both cases, the graphene sheets are oriented along the (0001) zone axis. However, small amount of rotation of graphene sheets/flakes with respect to each other is also visible as indicated by the smudging of the diffraction spots of graphene. For all four samples, the average particle size for Pt/NG catalysts has been calculated by measuring 100 isolated particles. The average particle sizes were found to be 4, 6.9, 2.2 and 2.9 nm for 20-Pt/NG_{BH}, 40-Pt/NG_{BH}, 20-Pt/NG_{EG} and 40-Pt/NG_{EG}, respectively.

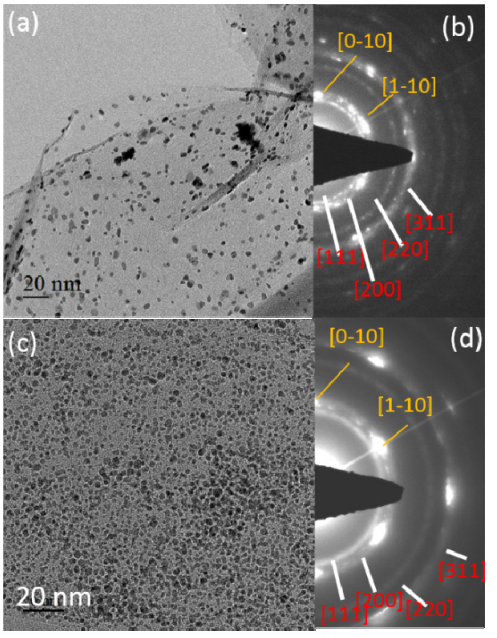

Figure 17. TEM micrographs for (a) 20-Pt/NG_{BH} and (c) 40-Pt/NG_{EG} nanomaterials. Electron diffraction patterns showing the crystal structure of pure Pt indexed in red and graphene sheet indexed in yellow for (b) 20-Pt/NG_{BH} and (d) 40-Pt/NG_{EG}.

XPS was employed to analyse the surface composition of the catalysts and identify the chemical states of the elements present. The XPS survey spectra (Fig. 18) showed O1s, N1s, C1s, Pt4d and Pt4f peaks for all the Pt/NG samples. The main peak of C1s can be seen at 284.5 eV, which corresponds to sp^2 carbon. As suggested in previous studies, the smaller peaks at 285.6 and 287.2 eV correspond to the formation of N-sp^2 C and N-sp^3 C bonds [235, 236] and these can be also due to the formation of carbon oxygen (mostly C–OH and C=O) surface groups [178]. The high-resolution XPS spectra in the N1s region are shown in the insets of Fig. 18a–d. The N1s spectrum can be deconvoluted into four peaks at 398, 400, 401 and 403 eV that correspond to pyridinic N, pyrrolic N, graphitic N and pyridine-N-oxide, respectively [235]. The overall nitrogen content in the Pt/NG samples was calculated from the XPS data, and it was found to be between 6 and 7 at.% for NG-supported Pt catalysts. The XPS results confirmed that the incorporation of nitrogen into the graphene structure was successful.

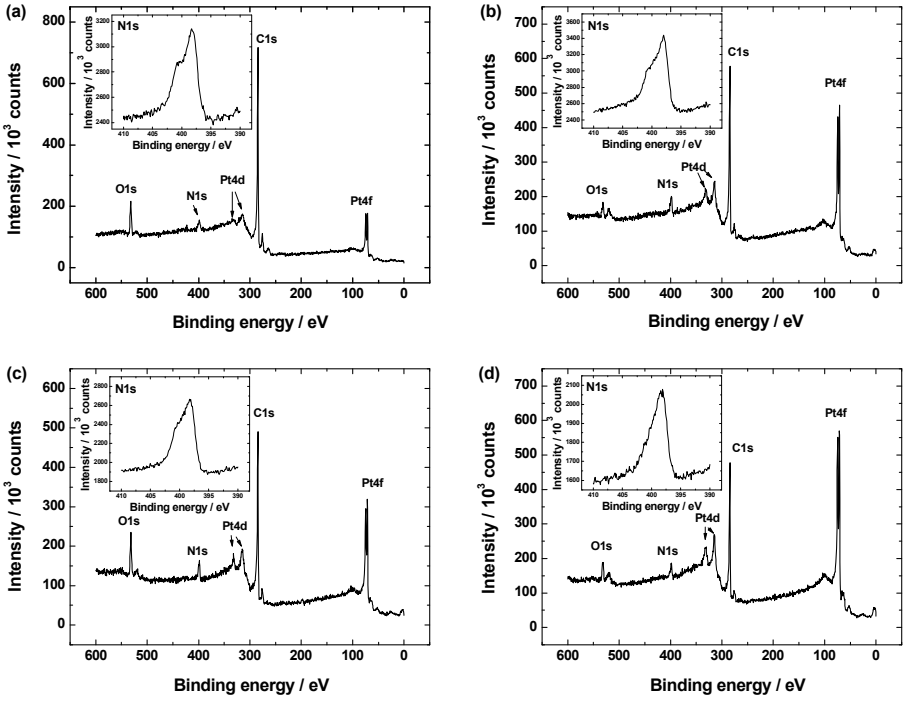

Figure 18. The XPS survey spectra of Pt/NG samples: (a) 20-Pt/NG_{BH}, (b) 40-Pt/NG_{BH}, (c) 20-Pt/NG_{EG} and (d) 40-Pt/NG_{EG}. Insets: High-resolution XPS spectra in the N1s regions for a (a) 20-Pt/NG_{BH}, (b) 40-Pt/NG_{BH}, (c) 20-Pt/NG_{EG} and (d) 40-Pt/NG_{EG} samples.

It has been found that the type of nitrogen plays a critical role in determining the ORR performance, but it is still under debate, which of the N-functionalities are responsible for high O_2 reduction activity. It has been suggested that pyridinic and/or graphitic N are actually responsible for the high ORR performance of N-doped carbon materials [139, 237, 238]. Kim et al. performed density functional calculations on nitrogen-doped graphene nanoribbons and suggested that the edge structure and doped-N near the edge enhanced the oxygen adsorption, first electron transfer and also the selectivity towards four-electron rather than two-electron O_2 reduction pathway [139]. According to this, high nitrogen contents are expected to be favourable for enhanced ORR activity; however, too high N content might be disadvantageous for ORR because of the interruption of the π–π electron conjugation thus leading to low electronic conductivity [90]. The Pt4f peaks confirm the presence of metallic Pt, since the binding energy of the main spin-orbit is split into doublet at about 71.1 and 74.6 eV, which correspond to $Pt4f_{7/2}$ and $Pt4f_{5/2}$, respectively [239]. As found by XPS, the electronic structure of Pt is similar for all four catalysts in this study.

6.3.2. Cyclic voltammetry and CO oxidation

Electro-oxidation of pre-adsorbed carbon monoxide can be used to clean PtNPs without their distortion and also for their characterisation [240]. In Fig. 19, the CO-stripping voltammograms in acid media are presented. It can be observed that initially the surface of Pt is completely blocked as there are no distinguishable hydrogen adsorption/desorption peaks observed (cycle 1), CO is completely oxidised by the first scan to 0.9 V (cycle 2) and the last cycle corresponds to clean platinum surface (cycle 3).

The oxidation of adsorbed CO on Pt surface yields a sharp peak centred at 0.83 V in 0.5 M H_2SO_4 and at 0.67 V in 0.1 M KOH (data not shown). It can be seen that there is a pre-wave of the CO oxidation peak for Pt/NG_{BH} catalysts (Fig. 19a, b) in acidic media. The different CO oxidation profiles for Pt/NG_{BH} and Pt/NG_{EG} in 0.5 M H_2SO_4 solution could be attributed to the modifications in the number and nature of active sites present on the surface of the PtNPs. The pre-peak may also appear because of some agglomeration of Pt nanoparticles, especially with the PtNPs prepared by borohydride reduction as can be seen from TEM images (Figs. 16a and 17a). In addition, Urchaga et al. have suggested that the pre-wave is characteristic to atomically ordered domains containing surface defects and they have also found that the origin of pre-wave comes from different CO oxidation mechanism [241, 242]. In alkaline solution, the pre-wave in the CO oxidation peak is evident for all the Pt/NG catalysts studied.

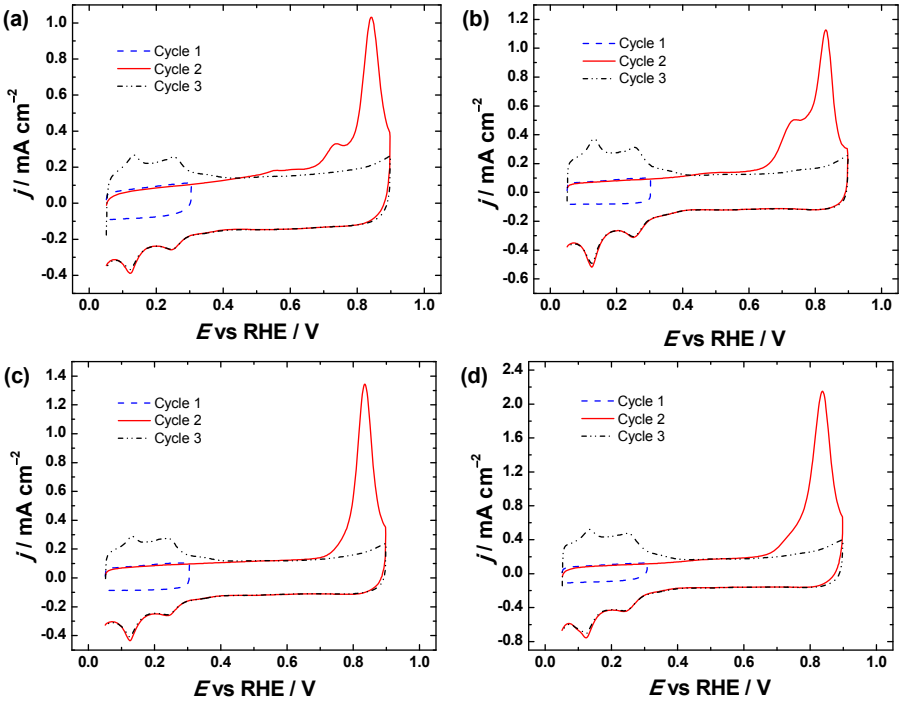

Figure 19. Electro-oxidation of pre-adsorbed CO on Pt/NG catalysts: (a) 20-Pt/NG_{BH}, (b) 40-Pt/NG_{BH}, (c) 20-Pt/NG_{EG} and (d) 40-Pt/NG_{EG} in 0.5 M H_2SO_4 solution (v = 20 mV s^{-1}). Current densities are normalised to the geometric electrode area.

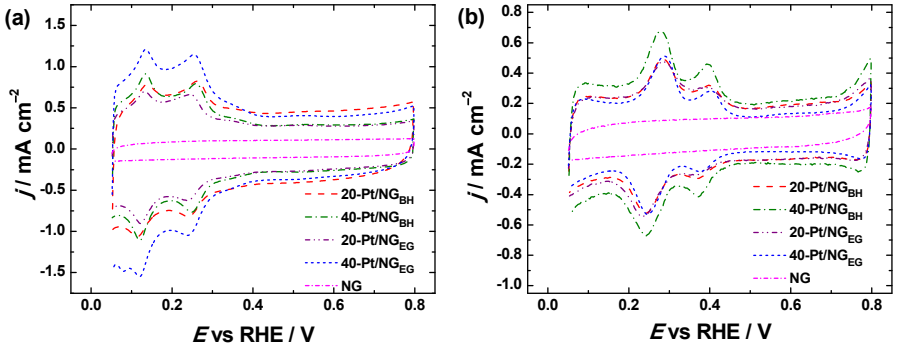

Figure 20. Cyclic voltammograms of Pt/NG catalysts and NG modified GC electrodes in Ar-saturated (a) 0.5 M H_2SO_4 and (b) 0.1 M KOH solutions (v = 50 mV s^{-1}). Current densities are normalised to the geometric electrode area.

Stable cyclic voltammograms displayed in Fig. 20 are recorded in acid and alkaline solutions after the electro-oxidation of carbon monoxide. In 0.5 M H_2SO_4, characteristic peaks of platinum low-index planes (110) and (100) can be observed at 0.13 and 0.26 V, respectively [243]. A shoulder apparent at

0.35 V can be associated with small (100) terraces. In alkaline media, typical peaks of adsorption/desorption of underpotential deposited hydrogen on Pt surface in the potential range of 0.05–0.45 V were observed. The electrochemically accessible surface area of Pt catalysts was evaluated by charge integration under the hydrogen desorption peaks. The obtained values of A_r are presented in Table 5 for acid and in Table 6 for alkaline media.

6.3.3. Oxygen reduction on Pt/NG materials in acid media

The RDE measurements were carried out in 0.5 M H_2SO_4 solution at different electrode rotation rates to access to the kinetics data from the Koutecky-Levich equation. The representative polarisation curves of O_2 reduction on the 20-Pt/NG_{EG}-modified GC electrode are presented in Fig. 21a. Only the cathodic sweeps are shown and further analysed. For all the Pt/NG catalysts, single-waved polarisation curves with well-defined diffusion-limited current plateaus were observed.

From the K-L plots (Fig. 21b), it was determined that the reduction of oxygen proceeds mainly via four-electron pathway yielding water, which is in accordance with our previous studies [I, 47, 180, 199].

Figure 21c presents the comparison of the electrochemical oxygen reduction behaviour of Pt/NG, NG and Pt/C catalyst materials at 1900 rpm. The half-wave potentials of O_2 reduction were found to be 0.80, 0.78, 0.74 and 0.79 V for 20-Pt/NG_{BH}, 40-Pt/NG_{BH}, 20-Pt/NG_{EG} and 40-Pt/NG_{EG} catalysts, respectively. These values remain a little bit lower than that of the commercial Pt/C catalyst ($E_{1/2}$ = 0.82 V). Slightly lower $E_{1/2}$ values for Pt/NG catalysts might be due to the differences in the crystallographic structure of Pt nanoparticles.

Tafel behaviour of oxygen reduction on Pt/NG and Pt/C catalysts in 0.5 M H_2SO_4 at a single electrode rotation rate (ω = 1900 rpm) is shown in Fig. 21d. Two Tafel regions with distinct slopes can be clearly distinguished (Table 5). In the low overpotential region, the slope was close to −60 mV and the rds of oxygen reduction on Pt-based catalysts is the transfer of the first electron to O_2 molecule. As suggested previously, the change of the slope is not related to a change of the reaction mechanism, but it has been attributed to the potential-dependent coverage of surface oxides that inhibit the adsorption of O_2 and reaction intermediates [1, 8, 9, 73]. Tafel slopes were similar for all the electrodes studied, which indicate that the reaction mechanism is the same for all the Pt-based electrocatalysts tested.

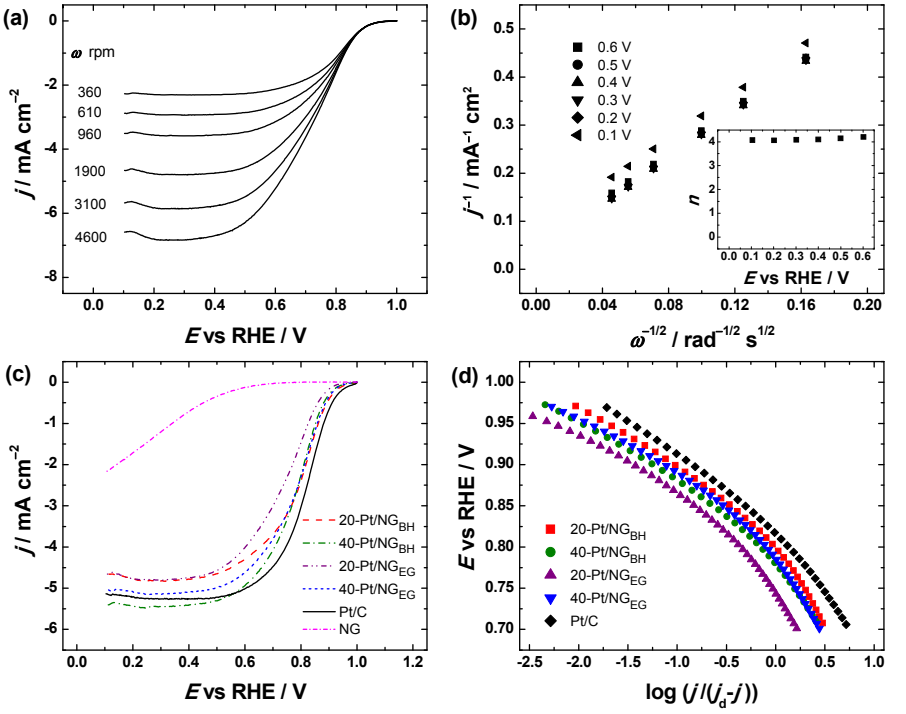

Figure 21. (a) ORR polarisation curves for 20-Pt/NG_{EG} in O_2-saturated 0.5 M H_2SO_4 (v = 10 mV s^{-1}). (b) Koutecky-Levich plots for ORR (inset shows the potential dependence of n). (c) Comparison of the RDE results for O_2 reduction on Pt/NG, NG and Pt/C catalysts (v = 10 mV s^{-1}, ω = 1900 rpm). (d) Tafel plots for ORR in 0.5 M H_2SO_4 (ω = 1900 rpm), data derived from Fig. 21c. Current densities are normalised to the geometric electrode area.

The specific activities for oxygen reduction on Pt/NG catalysts at 0.9 V are given in Table 5. 20-Pt/NG_{BH} electrocatalyst showed the highest specific activity (0.059 mA cm^{-2}) from the Pt/NG materials studied, and the value of SA was comparable with that found for commercial Pt/C catalyst (0.062 mA cm^{-2}). It can be seen that the SA values in H_2SO_4 are not dependent on the Pt particle size. It might be due to the different adsorption behaviour of (bi)sulphate anions on the surface of PtNPs that inhibits the ORR and lowers the specific activity. This remarkable improvement in the ORR performance for 20-Pt/NG_{BH} catalyst can also be attributed to higher utilisation of PtNPs on N-doped graphene nanosheets and the modified electronic structure of PtNPs by nitrogen functionalities present on the NG support, which enhances their intrinsic ORR activity. It is believed that the electronic interactions between PtNPs and N-doped carbon support would drastically affect the electronic structures of the surface Pt atoms, thus the adsorption/desorption of oxygen species on Pt nanocrystal surface [244]. This contributes to the improvement of stability and electro-catalytic activity of Pt/NG materials.

Table 5. Kinetic parameters for oxygen reduction on Pt/NG modified GC electrodes and Pt/C catalyst in O_2-saturated 0.5 M H_2SO_4. ω = 1900 rpm.

Electrode	A_r (cm^2)	Tafel slope (V) I region*	Tafel slope (V) II region*	$E_{1/2}$ (V)	SA at 0.9 V ($mA\ cm^{-2}$)
20-Pt/NG_{BH}	0.520	–0.072	–0.177	0.80	0.059
40-Pt/NG_{BH}	0.671	–0.072	–0.152	0.78	0.032
20-Pt/NG_{EG}	0.499	–0.062	–0.161	0.74	0.024
40-Pt/NG_{EG}	1.079	–0.069	–0.171	0.79	0.025
Pt/C	0.880	–0.079	–0.156	0.82	0.061

* Region I corresponds to low current densities and Region II to high current densities.

6.3.4. Oxygen reduction on Pt/NG materials in alkaline media

The ORR electrocatalytic activity of the Pt/NG catalysts prepared in this study along with commercial Pt/C is also tested in 0.1 M KOH solution. Figure 22a presents the RDE data of 20-Pt/NG_{BH}; all catalysts showed similar O_2 reduction behaviour being single-waved with distinct diffusion-limiting current plateaus.

The ORR polarisation curves recorded in alkaline solution were analysed using Eq. (10). Linear and parallel K-L plots (Fig. 22b) were obtained from the RDE data, indicating the first-order reaction kinetics towards the concentration of dissolved O_2 and similar electron transfer numbers at different electrode potentials. The value of n was calculated from the slope of the K-L plots, which was close to 4 for each electrode (inset to Fig. 22b). The four-electron O_2 reduction pathway on Pt catalysts in alkaline media has been reported previously [I, 93]; however, it has been proposed that on Pt-group metals, this reaction proceeds at least partly via peroxide intermediate [106].

Figure 22c presents the RDE results at a single electrode rotation rate (ω = 1900 rpm). The values of $E_{1/2}$ of oxygen reduction for Pt/NG catalysts in alkaline media are similar to that of commercial Pt/C. Only 20-Pt/NG_{EG} nano-material showed slightly lower half-wave potential value than the other Pt/NG electrocatalysts studied. The differences in the $E_{1/2}$ value might be caused by the differences in the crystallographic structure of the Pt nanoparticles. The kinetic current densities of the prepared catalyst are higher than that of commercial Pt/C, highlighting the improved ORR activities of N-doped graphene-supported Pt catalysts.

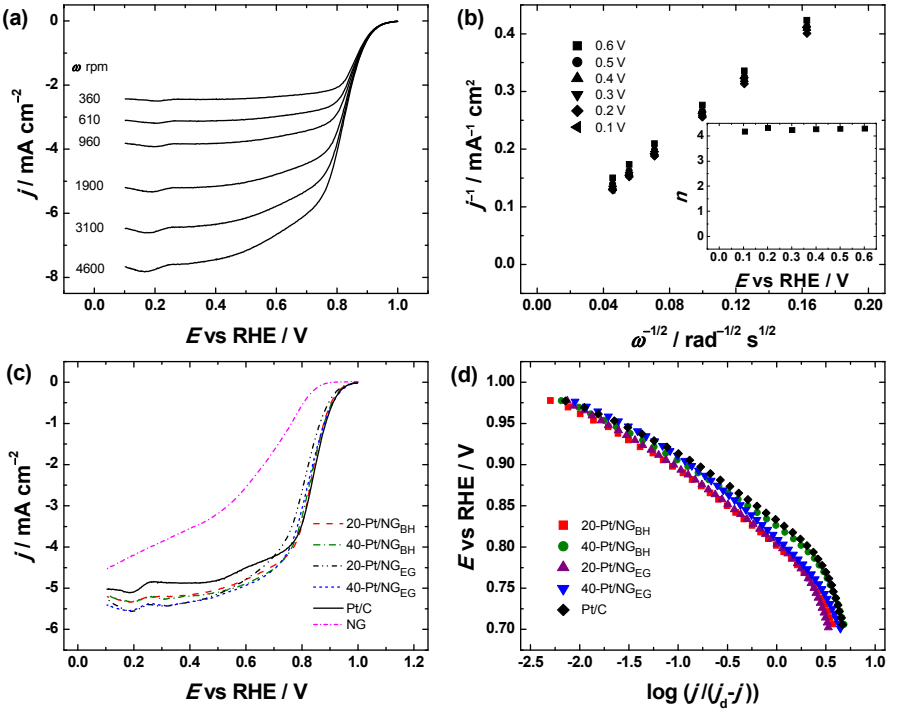

Figure 22. (a) ORR polarisation curves for 20-Pt/NG_{BH} in O_2-saturated 0.1 M KOH (v = 10 mV s^{-1}). (b) Koutecky-Levich plots for ORR (inset shows the potential dependence of n). (c) Comparison of the RDE results for O_2 reduction on Pt/NG, NG and Pt/C catalysts (v = 10 mV s^{-1}, ω = 1900 rpm). (d) Tafel plots for ORR in 0.1 M KOH (ω = 1900 rpm), data derived from Fig. 22c. Current densities are normalised to the geometric electrode area.

Tafel plots for O_2 reduction on Pt/NG and Pt/C catalysts in 0.1 M KOH solution are shown in Fig. 22d. Two regions with different Tafel slopes were determined. In the low current density region, the slope values for Pt nanocatalysts were slightly higher than −60 mV and at high current densities the slope value is higher than −150 mV. Similar Tafel slopes have been found on stepped Pt surfaces [209] and also in our previous works [I, 47, 206, 207].

The SA values for oxygen reduction on the Pt/NG catalysts in alkaline media were also determined at 0.9 V and are presented in Table 6. In 0.1 M KOH solution, all the Pt/NG catalysts showed higher SA values than that of commercial Pt/C. The highest value of SA was found for the 40-Pt/NG_{EG} nanomaterial. It is known that the specific activity depends on the particle size, but in the case of Pt/NG catalysts, no effect of the variation of Pt particle size on the value of SA could be seen. Similar observations have been reported elsewhere [86, 245]. An enhanced electrochemical performance may be attributed to the synergetic effect of the nitrogen incorporated into the graphene structure and Pt particles. Difference in the SA values most likely arises from the electronic modification of Pt generated by the substrate effect.

Table 6. Kinetic parameters for oxygen reduction on Pt/NG modified GC electrodes and Pt/C catalyst in O_2-saturated 0.1 M KOH. ω = 1900 rpm.

Electrode	A_r (cm^2)	Tafel slope (V) I region*	Tafel slope (V) II region*	$E_{1/2}$ (V)	SA at 0.9 V (mA cm^{-2})
20-Pt/NG_{BH}	0.409	–0.070	–0.173	0.83	0.102
40-Pt/NG_{BH}	0.499	–0.066	–0.208	0.82	0.095
20-Pt/NG_{EG}	0.320	–0.073	–0.194	0.80	0.102
40-Pt/NG_{EG}	0.422	–0.072	–0.182	0.81	0.121
Pt/C	0.582	–0.063	–0.245	0.83	0.092

* Region I corresponds to low current densities and Region II to high current densities.

It has been noted that the introduction of nitrogen into carbon structure increases the ORR activity due to the improved catalyst support binding and increased electrical conductivity [79, 80, 246]. The improved activity of Pt supported on N-doped carbon materials has been also ascribed to the specific interaction between N-doped carbon and the overlaying Pt catalyst, which could result in modifications to the electronic structure of the overlaying PtNPs that in turn can change their catalytic activity [82]. The electron transfer from the N-doped carbon support to the Pt catalyst is suggested to occur through the nitrogen group, thus leading to a higher electron density of PtNPs and therefore increase the electrocatalytic activity. According to theoretical considerations, the changes in the electronic structure are more evident as the functional groups and nitrogen are more electronegative [247]. Higher ORR activity on N-doped carbon-supported platinum is directly related to changes in the O_2 adsorption energy on catalyst surface. It was shown that atomic oxygen adsorption is weaker for the N-doped substrates, O-O distance is elongated and O_2 dissociation barriers are lower, which explains the increased electrocatalytic activity of Pt/NG towards the ORR.

As mentioned, smaller PtNPs and narrower size distribution have been consistently reported on N-doped carbon materials, even at relatively high metal loading, suggesting that these surfaces are capable of nucleating PtNPs more uniformly [78, 193, 248]. It has also been found that the Pt particle size decreases when the amount of nitrogen increases [81]. The better dispersion can be attributed to the higher number of structural defects on the surface.

NG-supported Pt catalysts in this study showed remarkable stability during experimental testing. The cycling procedure had no obvious influence on the diffusion-limited current for all four Pt/NG catalysts tested. Due to anti-corrosion properties of graphene and improved adhesion between Pt nano-particles and N-doped graphene, major aggregation, dissolution and detaching of PtNPs from support material can be avoided.

6.4. Oxygen reduction on carbon-supported Pt nanocubes

The loading effect of Vulcan XC-72R carbon-supported Pt nanocubes on the ORR kinetics in alkaline and acid solutions has been systematically investigated using a rotating disk electrode [IV]. Pt/C catalysts were characterised by transmission electron microscopy, the real Pt loading was found by thermogravimetric analysis and for electrochemical characterisation CO-stripping and cyclic voltammetry experiments were performed.

6.4.1. TEM and TG characterisation of Pt/C samples

Figure 23 shows the representative TEM images for all the catalysts prepared in this part of the work. Well-defined cubic-shaped Pt nanoparticles can be observed. From Figures 23b-f, it can be seen that platinum nanocubes are evenly distributed on the high-area carbon support and by increasing the amount of Pt more agglomerates are formed. For lower Pt content the nanoparticles are better separated from each other. Even though the Pt nanocubes come from the same synthesis batch, the determination of their mean particle size was done for each sample by measuring about 150–200 isolated particles. The mean particle sizes obtained were 9.25 ± 1.24, 9.56 ± 1.16, 9.63 ± 1.11, 9.71 ± 1.31, 9.44 ± 1.16 and 9.29 ± 0.9 nm corresponding to the unsupported Pt nanocubes and carbon-supported nanocubes with a nominal loading of 10, 20, 30, 40 and 50 wt%, respectively. As expected, within experimental error, the Pt nanocubes have the same mean particle size.

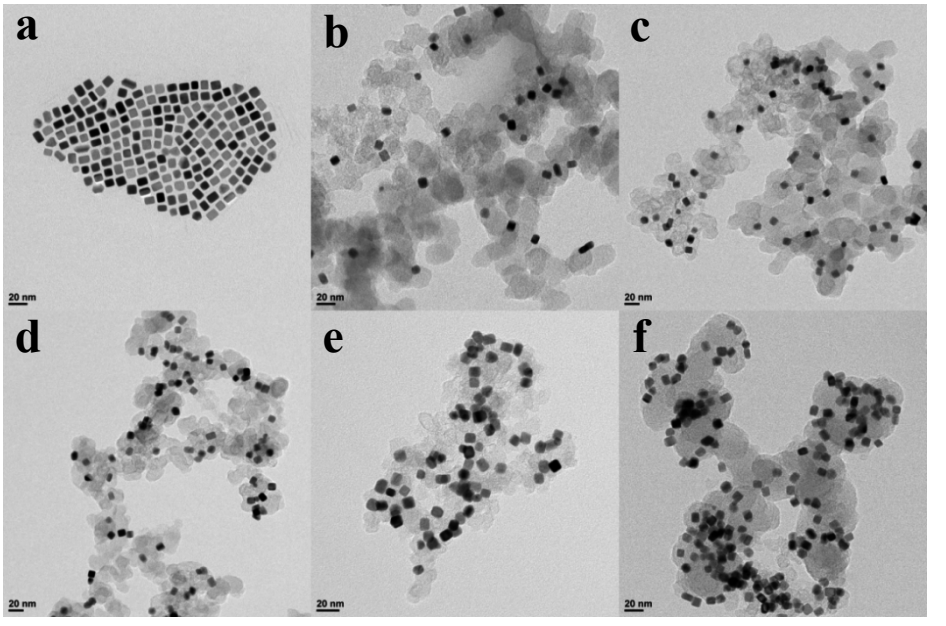

Figure 23. TEM micrographs of (a) unsupported Pt nanocubes, and carbon-supported cubic Pt nanoparticles: (b) 10, (c) 20, (d) 30, (e) 40 and (f) 50 wt% Pt/C catalysts.

Thermogravimetric analyses were also carried out to obtain the information about the real Pt content. The Pt content in carbon-supported catalysts was found to be 9, 19, 28, 35 and 47 wt% for nominal 10, 20, 30, 40 and 50 wt% Pt/C catalysts, respectively. The TGA results showed good correlations with the expected values from the experimental synthesis.

6.4.2. Surface structure characterisation by voltammetric measurements

It is well-recognised that, for Pt surfaces including massive and nanoparticulate electrodes, the cyclic voltammetric response in Ar-saturated 0.5 M H_2SO_4 and particularly the so-called hydrogen adsorption/desorption region can be used as fingerprint of the surface structure of the Pt electrode under study [249]. The voltammetric profiles of the samples here obtained are reported in Fig. 24. As expected, the voltammetric profiles are essentially similar regardless of the different electric double layer contribution. Figure 24a shows the response obtained with the unsupported PtNPs where the voltammetric features at about 0.12, 0.27 and 0.37 V vs. RHE characteristic of the presence of (110) sites, (100) steps and terrace borders and (100) terraces, respectively, are clearly observed. Similar voltammetric responses have been obtained with analogous cubic Pt nanoparticles prepared using other synthetic approaches [182, 249, 250] and denote the presence of a (100) preferential surface structure. Figure 24b reports the voltammetric responses of the samples having different metal loading. For samples with lower Pt loadings (10 and 20 wt%), the electric double layer contribution is well-marked as a consequence of the presence of the carbon support. Interestingly and regardless of the metal loading, the voltammetric profiles of the different samples are essentially identical. However, it is worth noting that, in comparison with the unsupported samples (Fig. 24a), all voltammetric features and particularly the feature at 0.37 V vs RHE characteristic to the presence of (100) terraces, are less defined/marked. This fact can be attributed to the Nafion used during the preparation of the inks [251], which is missing in the case of the pure (unsupported) Pt nanocubes which are simply dispersed in ultrapure water.

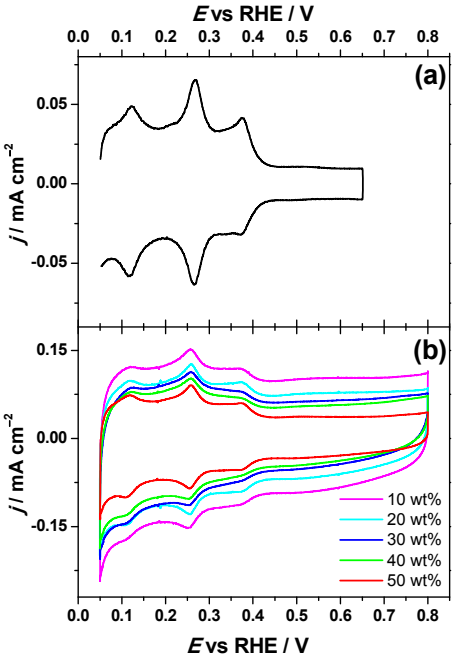

Figure 24. Cyclic voltammograms corresponding to (a) unsupported Pt nanoparticles and (b) carbon-supported cubic Pt nanoparticles with 10, 20, 30, 40 and 50 wt% Pt loading. Test solution: Ar-saturated 0.5 M H_2SO_4, v = 50 mV s^{-1}. Current densities are normalised to the electroactive surface area of Pt.

On the other hand, and taking into consideration that i) all Pt/C inks were prepared using the same total amount of catalyst (5 mg) and ii) the catalyst-modified GC electrodes were prepared by depositing the same volume of different inks (3 μL), the correct proportionality of the Pt electroactive surface area of the Pt nanoparticles is warranted, particularly for high metal loading where an evident agglomeration of the PtNPs takes place (see Fig. 23f). As described in previous contributions [188, 250], to estimate if the agglomeration of PtNPs induces a loss of the electroactive surface area, two analyses can be carried out, a) plotting the estimated electroactive surface area versus the corresponding metal loading (experimentally measured by TGA) and b) measuring the ratio between the currents at 0.27 and 0.44 V vs. RHE both without any double layer correction and plotting this ratio versus the corresponding Pt loading. In both cases, as discussed in previous works [188, 250], a linear relationship should be observed. Figures 25a and 25b show the results obtained, respectively, and a good linear relationship is found in both cases, thus pointing out that the carbon-supported cubic Pt nanoparticles were electrochemically accessible independently of the particular metal loading and allowing the effect of the metal loading towards the ORR to be properly studied both in acidic and alkaline solutions.

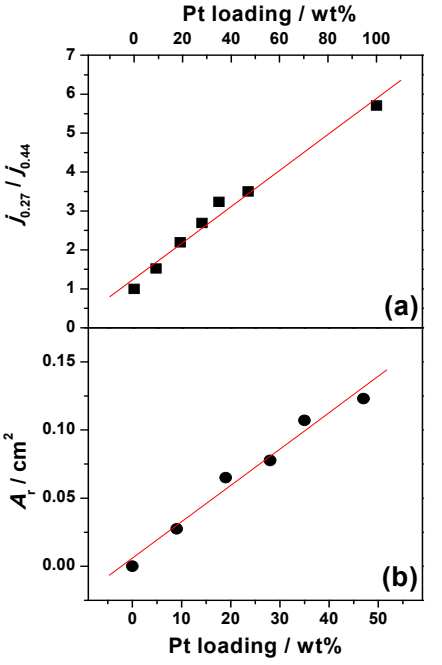

Figure 25. (a) Ratio between current densities at 0.27 V and 0.44 V vs. RHE for each sample vs the Pt loading. (b) Real electroactive surface area vs Pt loading. The linear fit is also presented in both cases. Test solution: Ar-saturated 0.5 M H_2SO_4, v = 50 mV s^{-1}.

To evaluate the ECSA of the samples their electroactive surface area was normalised to the corresponding mass of platinum. The Pt mass of each sample was calculated from the total mass of sample used in the experiment (3 μL of a 1 mg mL^{-1} suspension) and its particular metal loading. The value of ECSA was found to be constant for all the catalysts studied, which confirms that all the Pt nanocubes supported on Vulcan carbon are fully accessible as independent particles also in the agglomerates that were formed when the Pt content increased.

6.4.3. Oxygen reduction in 0.1 M $HClO_4$ and 0.1 KOH solutions

The electroreduction of O_2 was first studied in acidic media (0.1 M $HClO_4$). Figures 26a and 26b show the voltammetric response of the different samples in Ar-saturated 0.1 M $HClO_4$ solution. Similarly to the results obtained in 0.5 M H_2SO_4, the voltammetric profiles of the carbon supported nanocube samples (Fig. 26b) are similar to that obtained with the pure Pt nanocubes (Fig. 26a). As discussed in a previous work [252], the voltammetric profile displays characteristic peaks between 0.3–0.5 V, related to the OH adsorption on the (100) well-ordered domains whereas, the contributions in the range between 0.09–0.22 V can be attributed to (110) sites. In addition, as shown in

Fig. 26c, a linear relationship is again found between the electroactive surface area and the specific metal loading of the samples.

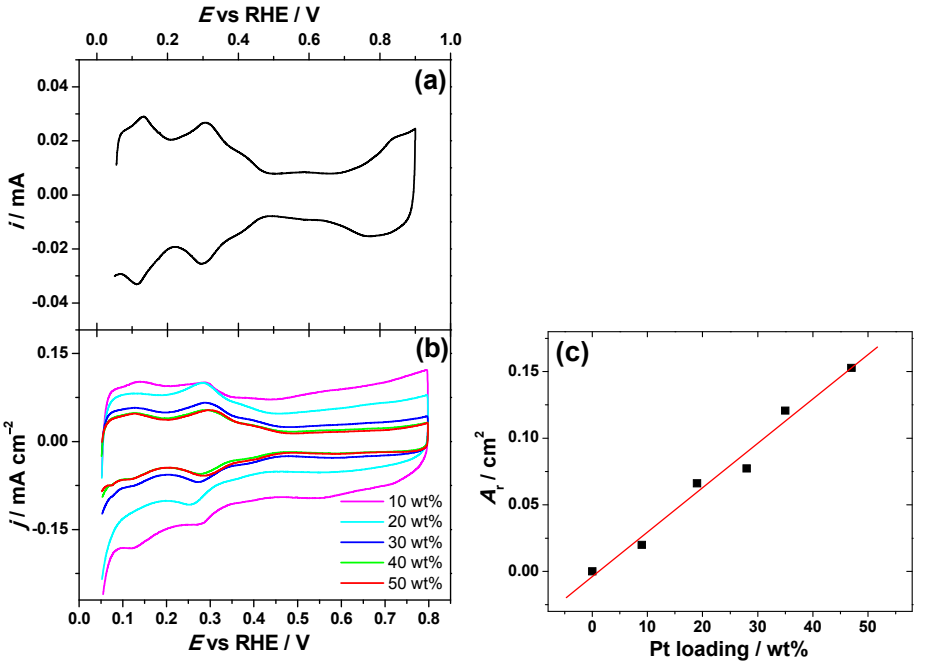

Figure 26. Cyclic voltammograms corresponding to (a) unsupported Pt nanoparticles and (b) carbon-supported cubic Pt nanoparticles with 10, 20, 30, 40 and 50 wt% Pt loading. Test solution: Ar-saturated 0.1 M $HClO_4$, v = 50 mV s^{-1}. (c) Real electroactive surface area vs Pt loading. The linear fit is also presented.

The positive-going sweeps at different rotation speeds of the ORR polarisation curves for 30% Pt/C catalyst are presented in Fig. 27a. For all electrode rotation rates, single-waved current density-potential (*j*-*E*) curves with well-defined diffusion-limited current plateaus were observed.

The obtained RDE data were analysed using Eq. (10), where the values of O_2 solubility ($C_{O_2}^b$ = 1.26×10^{-6} mol cm^{-3}) [253] and the diffusion coefficient (D_{O_2} = 1.93×10^{-5} cm^2 s^{-1}) [253] were used for 0.1 M $HClO_4$ solution. Linear K-L plots are shown in Fig. 27b. The K-L analysis revealed that the electron transfer number was close to 4 for all the catalyst materials tested (inset to Fig. 27b). Similar n values have been found for different Pt-based catalysts in the literature [199, 254–258].

Figure 27c shows the anodic sweeps of the oxygen reduction polarisation curves for the different Pt/C catalysts in O_2-saturated 0.1 M $HClO_4$ solution recorded at a rotation speed of 1900 rpm. It can be observed that with increasing Pt loading, the ORR onset potential (E_{onset}) and half-wave potential shift towards positive values. The E_{onset} is 0.93 and 0.99 V for 10% Pt/C and 50% Pt/C catalysts, respectively. The $E_{1/2}$ value for 10% Pt/C is 0.74 V and it

increases to 0.85 V for 50% Pt/C catalyst. Similar tendency has been also found by Fabbri et al. [259, 260]. The $E_{1/2}$ values for all the catalysts are given in Table 7. Similar E_{onset} and $E_{1/2}$ values have been also reported by Kim et al., who studied oxygen reduction on PtNPs supported on ordered mesoporous carbon [261].

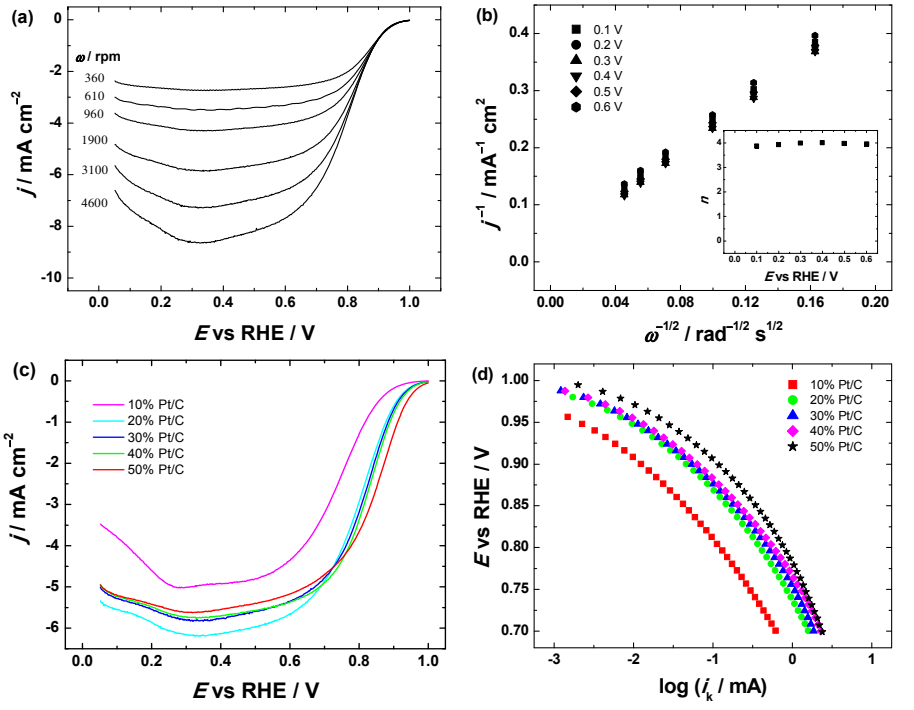

Figure 27. (a) RDE voltammetry curves for O_2 reduction on 30% Pt/C catalyst in O_2-saturated 0.1 M $HClO_4$ at different rotation rates (v = 10 mV s^{-1}), (b) the corresponding K-L plots in 0.1 M $HClO_4$ (inset shows n dependence on potential), (c) comparison of the RDE results of Pt/C modified GC electrodes in O_2-saturated 0.1 M $HClO_4$ at 1900 rpm (v = 10 mV s^{-1}), (d) Tafel plots for O_2 reduction in 0.1 M $HClO_4$ (ω = 1900 rpm). Current densities are normalised to the geometric area of GC.

Tafel plots for O_2 reduction shown in Fig. 27d were constructed from the RDE data at 1900 rpm. Two specific Tafel regions with distinct slopes were found. At low overpotentials the slope was close to –60 mV and at high overpotentials it increased to –120 mV. Similar Tafel behaviour for O_2 reduction in perchloric acid has been reported in earlier works [29, 199, 255].

Specific activities for O_2 reduction on Pt/C catalysts were calculated at 0.9 V. As can be seen from Fig. 28a, the value of SA is almost constant for all the catalysts studied (0.73±0.06 mA cm^{-2}), which is in accordance with our assumptions that the reaction kinetics are identical and does not depend on the Pt loading. The SA value is slightly higher for the 10% Pt/C catalyst

(1.17±0.03 mA cm^{-2}), which is most likely due to the complexity of determination of the real electroactive surface area. Compared to some other studies [22, 256, 262], the SA values found in this work are approximately two to three times higher, but the differences may arise from the Pt particle size, as described in the respective literature, the SA value increases with increasing the particle size.

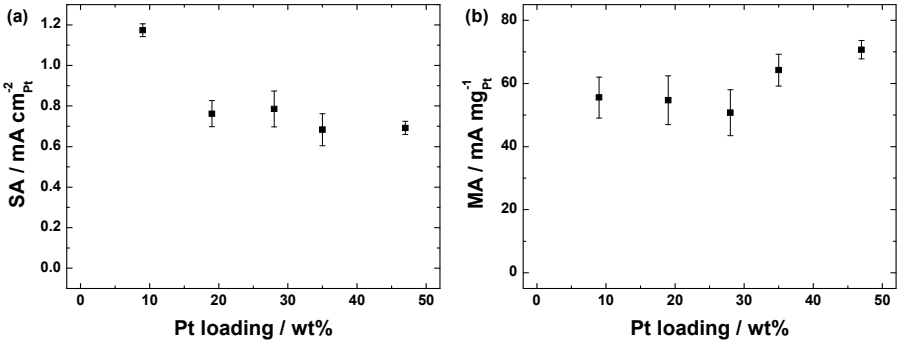

Figure 28. The dependence of (a) specific activity and (b) mass activity for O_2 reduction on the Pt loading in O_2-saturated 0.1 M $HClO_4$ solution at 0.9 V.

Mass activity for O_2 reduction of each electrode was calculated using Eq. (12), where the mass of Pt was calculated using the concentration of the catalyst ink (1 mg mL^{-1}), volume deposited onto the GC electrode (3 μL) and Pt loading determined by TGA. The mass activities vs. Pt loading are shown in Fig. 28b. The average MA at 0.9 V was found to be 59.2±5.9 mA mg^{-1}. Almost constant MA value for all the catalysts studied is indicating that the mass activity does not depend on the loading of Pt nanocubes. The observed MA values are somewhat smaller than that found for smaller Pt particles in the literature [22, 23, 263, 264]. It has been suggested in earlier studies that PtNPs in the size range of 3.3–3.5 nm show the highest MA values [16, 265, 266]. Comparable mass activities for O_2 reduction have been found by Kim et al. for PtNPs supported on ordered mesoporous carbons [261] and by Angelopoulos and co-workers on clustered and single crystal Pt nanoparticles [267].

Table 7. Kinetic parameters for oxygen reduction on Pt/C modified GC electrodes in O_2-saturated 0.1 M $HClO_4$ and 0.1 M KOH solutions (v = 10 mV s^{-1}, ω = 1900 rpm).

Electrode	A_r (cm^2)	Tafel slope (V) I region*	Tafel slope (V) II region*	$E_{1/2}$ (V)	A_r (cm^2)	Tafel slope (V) I region*	Tafel slope (V) II region*	$E_{1/2}$ (V)
	0.1 M $HClO_4$				0.1 M KOH			
10% Pt/C	0.020	–0.064	–0.122	0.74	0.019	–0.061	–0.114	0.79
20% Pt/C	0.066	–0.064	–0.126	0.79	0.061	–0.064	–0.127	0.80
30% Pt/C	0.077	–0.065	–0.128	0.81	0.075	–0.063	–0.128	0.82
40% Pt/C	0.121	–0.063	–0.126	0.82	0.119	–0.062	–0.128	0.84
50% Pt/C	0.153	–0.063	–0.125	0.85	0.156	–0.064	–0.134	0.85

* Region I corresponds to low current densities and Region II to high current densities.

The oxygen reduction studies were also carried out in O_2-saturated 0.1 M KOH solution. Figure 29a reports the voltammetric response of the different samples in Ar-saturated 0.1 M KOH solution. As expected, the voltammetric profile of the samples shows different contributions which are well-established to be associated with a (100) preferential surface structure [252]. In alkaline solution, the calculation of the electroactive surface area is not as well-defined as in acidic solution (H_2SO_4 and $HClO_4$). In this regard, in a previous contribution, a reference value of 390 μC cm^{-2} for the total charge measured between 0.06 and 0.90 V (without any double-layer correction) was proposed [252]. Unfortunately, this calculation is only valid for pure Pt nanoparticles but not for carbon-supported Pt nanoparticles due to the important contribution of the carbon substrate to the double layer region. In this work, we proposed a different approach which involves the calculation of the charge between 0.05 and 0.65 V after double-layer correction as visually described in Fig. 29b. The double layer contribution is estimated from the current at 0.65 V and a charge density value of 187 μC cm^{-2} is used. This charge density value is an average value deduced from the charge density values of 282, 164 and 114 μC cm^{-2} corresponding to Pt(100), Pt(110) and Pt(111) single crystal electrodes, respectively [268]. Interestingly, the calculated surface areas are essentially similar to those obtained in 0.1 M $HClO_4$ (Table 7) and also show a linear relationship with the Pt loading (Fig. 29c). These facts further confirm the validity of our approach.

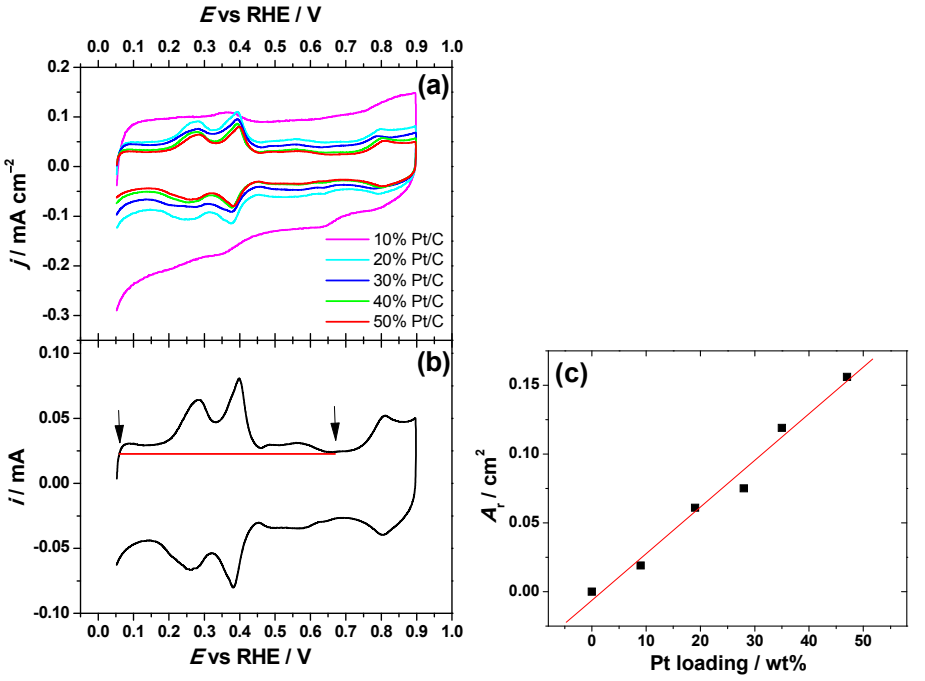

Figure 29. (a) Cyclic voltammograms corresponding to carbon-supported cubic Pt nanoparticles with 10, 20, 30, 40 and 50 wt% Pt loading. (b) Region used for the calculation of the electroactive surface area. Test solution: Ar-saturated 0.1 M KOH, $v = 50$ mV s^{-1} (c) Real electroactive surface area vs Pt loading. The linear fit is also presented.

Figure 30a represents the positive-going ORR polarisation curves for 30% Pt/C catalyst. The *j*-*E* curves for all the electrodes tested in alkaline media were also single-waved with well-defined diffusion-limited current plateaus as observed in acidic electrolyte. The obtained K–L plots (Fig. 30b) were linear and parallel, indicating the first order reaction kinetics towards the concentration of dissolved O_2 and similar electron transfer numbers at different electrode potentials. From the slope of the K–L plots the value of *n* was found to be close to four for each electrode (inset to Fig. 30b). The four-electron O_2 reduction pathway on Pt-based catalysts in alkaline media has been reported previously [I, III, 47, 207, 257, 269].

Figure 30c displays the comparison of the RDE results at a single electrode rotation rate (ω = 1900 rpm). As in acidic media, the values of E_{onset} and $E_{1/2}$ for O_2 electroreduction on Pt/C catalysts in alkaline media are more positive when the amount of Pt in the catalysts increases. The E_{onset} for 50% Pt/C is 0.99 V and it decreases to 0.94 V for 10% Pt/C. The $E_{1/2}$ values for all the Pt/C catalysts studied are listed in Table 7. The highest $E_{1/2}$ value of 0.85 V was found for 50% Pt/C. It has been reported by Markovic et al. that Pt(100) single-crystal electrode shows higher electrocatalytic activity for ORR in 0.1 M $HClO_4$ solution as compared to 0.1 M KOH [8]. In our work, the activity of oxygen electroreduction is enhanced in alkaline media, the reason of which needs further investigation.

Tafel plots for O_2 reduction on Pt/C catalysts in 0.1 M KOH solution are shown in Fig. 30d. Two regions of different Tafel slope were found. In the low current density region, the slope values for Pt nanocatalysts were around –60 mV and at high current densities the slope values were close to –120 mV [I, III, 47, 269]. The change in the Tafel slope is related to the potential-dependent coverage of oxygenated species on the surface of Pt catalysts. These slope values indicate that the rds is the transfer of the first electron to the O_2 molecule.

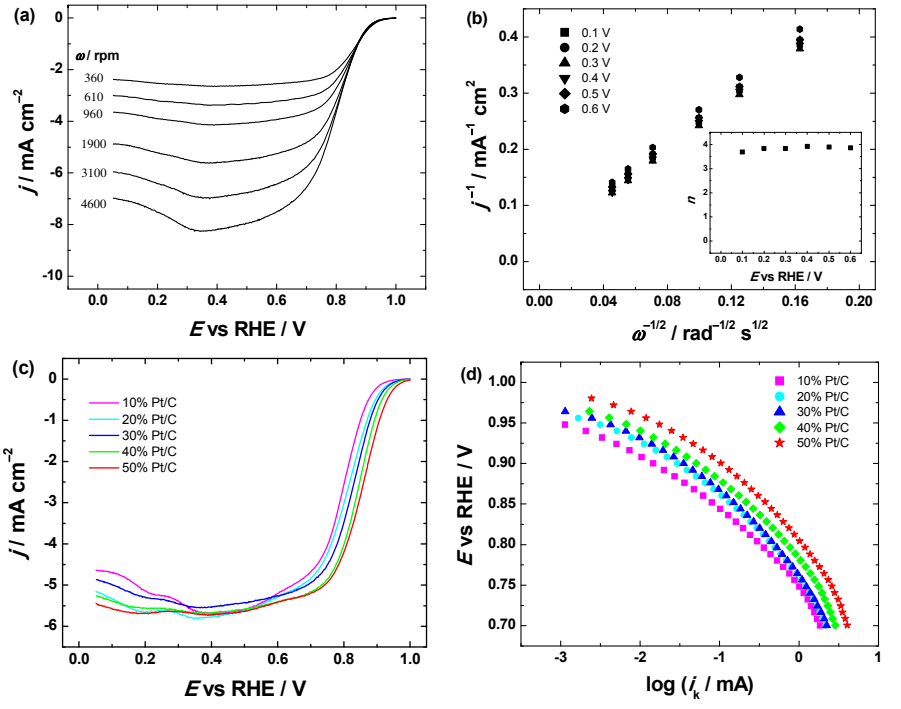

Figure 30. (a) RDE voltammetry curves for O_2 reduction on 30% Pt/C catalyst in O_2-saturated 0.1 M KOH at different rotation rates (v = 10 mV s^{-1}), (b) the corresponding K-L plots in 0.1 M KOH (inset shows the dependence of n on potential), (c) comparison of the RDE results of Pt/C modified GC electrodes in O_2-saturated 0.1 M KOH at 1900 rpm (v = 10 mV s^{-1}), (d) Tafel plots for O_2 reduction in 0.1 M KOH (ω = 1900 rpm). Current densities are normalised to the geometric area of GC.

The SA values for O_2 reduction on the Pt/C catalysts in alkaline media were also determined at 0.9 V and are presented in Fig. 31a. In 0.1 M KOH solution all the Pt/C catalysts showed almost constant SA. The average value of SA was around 0.57±0.04 mA cm^{-2}. As in acidic media, the SA value for 10% Pt/C catalyst was slightly higher than that of other Pt loadings. This observation might arise also from the errors in calculating the electroactive area of Pt by charge integration under the hydrogen desorption peaks. The SA values in both solutions were rather similar, which may be due to a relatively weak adsorption

of spectator species in these electrolytes ($HClO_4$ and KOH). It is obvious that the ORR kinetics is mainly influenced by adsorbed OH coverage on Pt in these electrolytes, which inhibits the ORR rate.

The mass activity in 0.1 M KOH solution showed almost constant values for O_2 reduction on all the catalysts studied (Fig. 31b). The mean value of MA for the carbon-supported Pt/C nanomaterials was 53.1±3.4 mA mg^{-1} at 0.9 V, which is slightly lower than that found in acidic media.

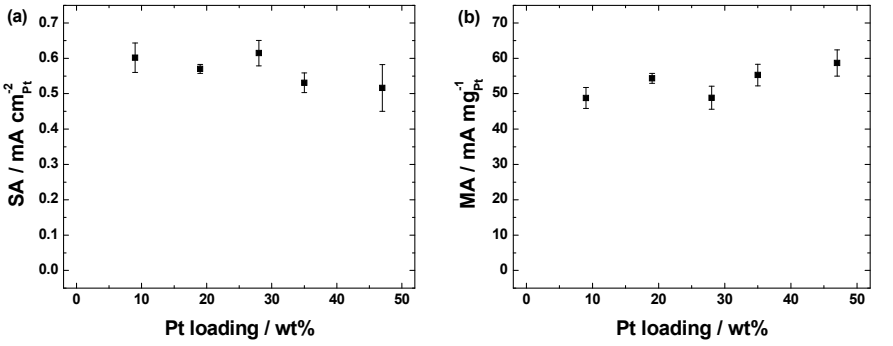

Figure 31. The dependence of (A) specific activity and (B) mass activity for O_2 reduction on the Pt loading in O_2-saturated 0.1 M KOH solution at 0.9 V.

The effect of Pt particle size in ORR electrocatalysis has been a matter of controversy [245]. According to several previous studies the size effect of Pt particles on the ORR kinetics has been reported for smaller nanoparticles than 6–7 nm [28]. Above this particle diameter the SA is virtually constant. The investigation of Pt particle size effect in different electrolytes did not yield the expected results on the basis of model predictions of cubo-octahedral Pt particles [270]. The size of Pt nanocubes studied in the present work is above the size range for which the change in the SA value is expected. Also, there have been variations regarding the ORR activity trend of shape-controlled PtNPs, which might arise from imperfect particle shapes. Even though the overall quality of particle shape could be perfect in some studies on the basis of HR-TEM images, there is still a high likelihood that Pt surface atoms of lower coordination number exist and this could lead to scatter in the data and differences in the electrocatalytic ORR behaviour.

6.5. Oxygen reduction on magnetron sputtered PdNP/MWCNT

The electroreduction of oxygen was studied on magnetron sputtered Pd nanoparticles supported on multi-walled carbon nanotubes [V]. The nominal Pd-film thicknesses were 5, 10 and 15 nm. The ORR activities were compared with that of the bulk Pd electrode.

6.5.1. Physical and electrochemical characterisation of the PdNP/MWCNT catalysts

Fig. 32 presents typical micrographs of uncoated and Pd-coated MWCNTs on GC substrates. HR-SEM images showed that the sputtered Pd was uniformly distributed on the surface of MWCNTs for all the composite catalysts studied.

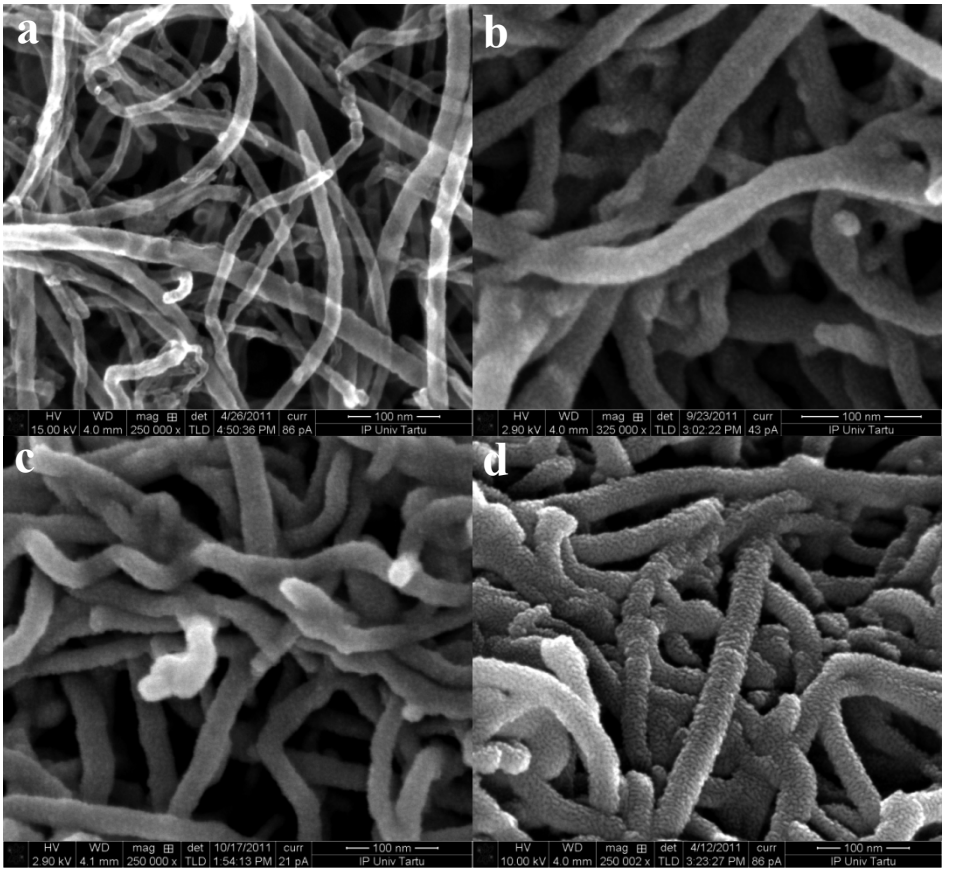

Figure 32. SEM images of uncoated (a) and Pd-coated (b-d) MWCNTs on GC electrodes. Nominal Pd film thickness: (b) 5, (c) 10 and (d) 15 nm (calculated per geometric area of GC).

The cyclic voltammetry experiments were performed to clean and characterise the surface of sputtered PdNPs on MWCNTs. Shown in Fig. 33 are stable CV curves of PdNP/MWCNT-modified GC electrodes recorded in Ar-saturated 0.5 M H_2SO_4 and 0.1 M KOH solutions at 50 mV s^{-1}. The anodic peaks at $E > 0.8$ V and the cathodic peak at ca. 0.6–0.7 V correspond to the formation of Pd surface oxides and to their reduction, respectively. Characteristic peaks of adsorption/desorption of underpotential deposited hydrogen are in evidence in the potential range of 0.1–0.3 V. By integrating the charge under the Pd oxide reduction peak, the A_r value of Pd catalysts was estimated, assuming the value

of 424 μC cm^{-2} as the charge density for the reduction of Pd oxides [271]. The real area of Pt catalyst was evaluated by charge integration under the hydrogen desorption peak, assuming 210 μC cm^{-2} for a monolayer of H_{UPD} [47]. The values of A_r of palladium and platinum catalysts are presented in Table 8 and 9.

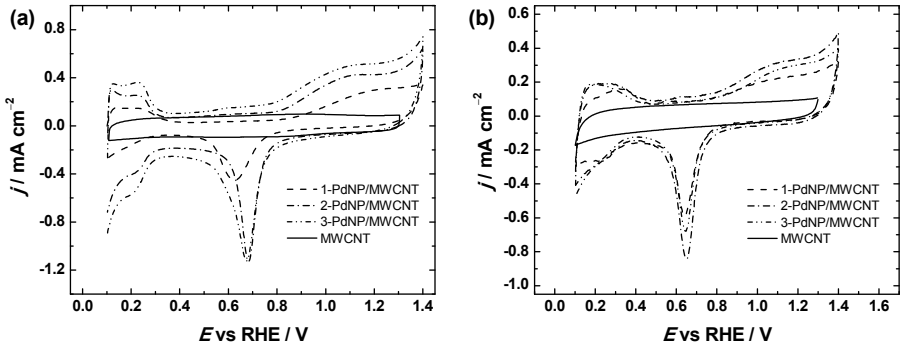

Figure 33. Representative cyclic voltammograms of PdNP/MWCNT/GC electrodes in Ar-saturated (a) 0.5 M H_2SO_4 and (b) 0.1 M KOH. $v = 50$ mV s^{-1}. The CV of MWCNT/GC is also shown. Current densities are normalised to geometric area of the GC electrode.

6.5.2. Oxygen reduction on PdNP/MWCNT catalysts in acidic media

First, the RDE experiments of oxygen reduction were performed in O_2-saturated 0.5 M H_2SO_4 solution. A set of polarisation curves of the ORR on a 3-PdNP/MWCNT catalyst is shown in Fig. 34a. Only the cathodic sweeps are given and further analysed.

Fig. 34b presents the K-L plots for O_2 reduction on a 3-PdNP/MWCNT modified electrode. Linear K-L plots were observed for all the catalysts studied. From the slope of the K-L lines the value of n was calculated, which was found to be close to 4 over the whole range of potentials for all the Pd catalysts studied (see inset to Fig. 34b).

For better comparison of the RDE results the $j-E$ curves for O_2 reduction recorded at a single rotation rate are presented in Fig. 34c. The values of half-wave potential of oxygen reduction for PdNP/MWCNT catalysts were lower than that of bulk Pd and Pt/C catalysts.

From the RDE data of the ORR the Tafel plots were constructed (Fig. 34d). Two Tafel regions with different slope values can be distinguished. At low overpotentials the Tafel slope is close to −60 mV and at higher current densities the slope is approximately −100 mV. Similar slope values have been reported earlier for ORR on nanoparticulate and bulk Pd in acid media [116]. The kinetic parameters for oxygen reduction in 0.5 M H_2SO_4 are listed in Table 8.

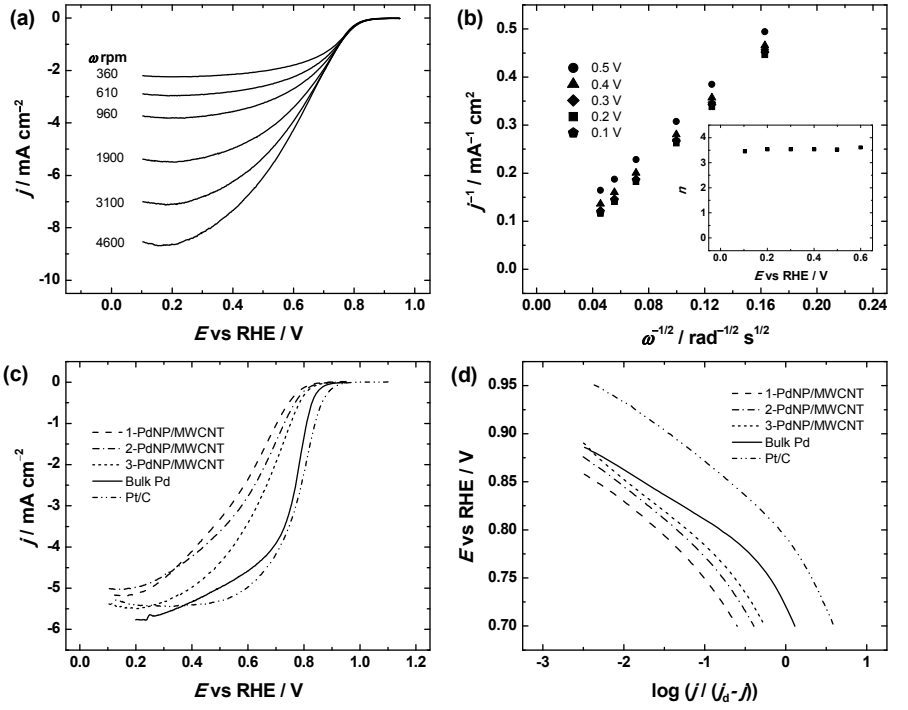

Figure 34. (a) RDE voltammetry curves for oxygen reduction on a 3-PdNP/MWCNT/GC electrode in O_2-saturated 0.5 M H_2SO_4 (v = 10 mV s^{-1}), (b) K–L plots for ORR in 0.5 M H_2SO_4 (inset shows the potential dependence of n), (c) comparison of the RDE results for the ORR (ω = 1900 rpm, v = 10 mV s^{-1}) and (d) mass-transfer corrected Tafel plots for oxygen reduction on PdNP/MWCNT, bulk Pd and commercial Pt/C catalysts in 0.5 M H_2SO_4. Current densities are normalised to geometric area of the GC electrode.

Table 8. Kinetic parameters for oxygen reduction on PdNP/MWCNT, bulk Pd and commercial Pt/C catalysts in 0.5 M H_2SO_4.

Electrode	A_r (cm^2)	Tafel slope (V) *Region I	Tafel slope (V) *Region II	$E_{1/2}$ (V)	SA at 0.85 V (mA cm^{-2})
1-PdNP/MWCNT	0.30	–0.066	–0.103	0.58	0.009
2-PdNP/MWCNT	0.48	–0.060	–0.107	0.64	0.013
3-PdNP/MWCNT	0.71	–0.066	–0.104	0.65	0.010
Bulk Pd	0.69	–0.052	–0.111	0.72	0.024
Pt/C	1.64	–0.061	–0.096	0.78	0.058

* Region I corresponds to low current densities and Region II to high current densities.

The specific activities of O_2 reduction for the PtNP/MWCNT modified GC electrodes were calculated at 0.9 V vs. RHE using Eq. (11). The SA values of PdNP/MWCNT catalysts remained lower than that of bulk Pd. The reason for that may come from crystallographic differences, it is difficult to precisely control the size and the shape of sputter-deposited Pd catalysts. It is well-known that the electrocatalytic activity for ORR depends on the size and shape of PdNPs. Shao et al. found that octahedral Pd particles showed about 10 times lower ORR activity than Pd nanocubes [101]. The SA value of Pt/C is higher than that of Pd-based catalysts and this is the expected result in H_2SO_4 solution [47].

6.5.3. Oxygen reduction on PdNP/MWCNT catalysts in alkaline electrolyte

The RDE experiments of O_2 reduction were also carried out in 0.1 M KOH solution. The ORR polarisation curves with well-defined diffusion-limited current plateaus were observed (Fig. 35a). It should be noted that unmodified multi-walled carbon nanotubes are active catalysts for oxygen reduction in alkaline media according to our previous reports [222, 223, 272]. However, a substantial positive shift of the onset potential for O_2 reduction is evident upon depositing Pd catalyst on the surface of MWCNTs. Therefore, the reduction current at low overpotentials is caused by PdNPs only and these data suggest that the kinetics of the ORR is determined entirely by the Pd catalyst at low overpotentials. In acid electrolyte much lower electrocatalytic activity of PdNP/MWCNT composites was in evidence (Fig. 34a). The reason for this can be strong adsorption of (bi)sulphate anions on the PdNP surface.

Linear K-L plots were obtained from the RDE data. The value of n was calculated from the K-L slopes, which was close to four for each electrode (see inset to Fig. 35b). For better comparison of the RDE results the j−E curves for O_2 reduction recorded at ω = 1900 rpm are shown in Fig. 35c. The values of $E_{1/2}$ for O_2 reduction for PdNP/MWCNT catalysts and bulk Pd were similar. Note that the electroactive surface area of Pt catalyst was also higher. The RDE data presented in Fig. 35c were used for the construction of Tafel plots for oxygen reduction in 0.1 M KOH (Fig. 35d). At low current densities the Tafel slope was close to −60 mV, which is in agreement with previous observations [116]. The slope increased at higher overpotentials. Erikson et al. reported a similar Tafel behaviour of oxygen reduction on electrodeposited Pd coatings on GC [124]. In 0.1 M KOH solution the specific activities of O_2 reduction were also determined (Table 9).

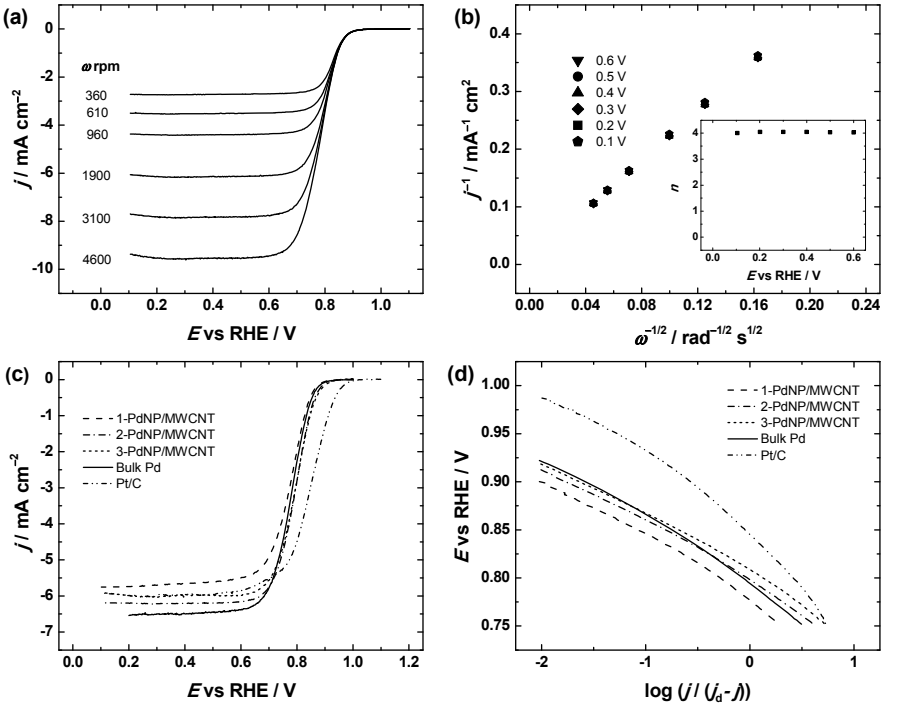

Figure 35. (a) RDE voltammetry curves for oxygen reduction on a 2-PdNP/MWCNT/ GC electrode in O_2-saturated 0.1 M KOH (v = 10 mV s^{-1}), (b) K–L plots for ORR in 0.1 M KOH (inset shows the potential dependence of n), (c) comparison of the RDE results for the ORR (ω = 1900 rpm, v = 10 mV s^{-1}) and (d) mass-transfer corrected Tafel plots for oxygen reduction on PdNP/MWCNT, bulk Pd and commercial Pt/C catalysts in 0.1 M KOH. Current densities are normalised to geometric area of the GC electrode.

Table 9. Kinetic parameters for oxygen reduction on PdNP/MWCNT, bulk Pd and commercial Pt/C catalysts in 0.1 M KOH.

Electrode	A_r (cm^2)	Tafel slope (V) *Region I	Tafel slope (V) *Region II	$E_{1/2}$ (V)	SA at 0.85 V (mA cm^{-2})
1-PdNP/MWCNT	0.32	–0.057	–0.086	0.78	0.091
2-PdNP/MWCNT	0.48	–0.057	–0.076	0.80	0.187
3-PdNP/MWCNT	0.36	–0.058	–0.085	0.81	0.176
Bulk Pd	0.64	–0.066	–0.085	0.79	0.126
Pt/C	1.90	–0.058	–0.102	0.85	0.351

* Region I corresponds to low current densities and Region II to high current densities.

The SA values were comparable for PdNP/MWCNT catalysts and bulk Pd. Similar values of SA for nanoparticulate Pd catalysts were reported in our earlier work [177]. Higher SA values for O_2 reduction in alkaline solution than in acid electrolyte have been also found for the electrodeposited Pd/GC electrodes [124]. The SA of Pt/C catalyst is higher by a factor of two compared with PdNP/MWCNT (Table 9). This indicates that the electrocatalytic activity of carbon nanotube supported Pd nanoparticles towards the ORR is only slightly inferior than that of Pt/C in alkaline media. The ORR results obtained in this work with the PdNP/MWCNT composites show a great promise of these materials as an alternative cathode catalyst for alkaline membrane fuel cells (AMFCs). Recently, there has been an enormous progress in the preparation of anion exchange membranes and ionomers for AMFCs. A significant break-through in the fabrication of this type of fuel cells is expected in the near future. Our preliminary work has shown a good fuel cell performance of non-platinum cathode catalysts in AMFCs [273]. Recently, a similar electrocatalyst was proposed as a cathode material for AMFCs [129].

6.6. Electroreduction of oxygen on heat-treated sputtered PdNP/MWCNT catalysts

In continuation of previous work [V], where sputter-deposition was used to prepare PdNP/MWCNT catalyst materials for ORR, similar composite material to 3-PdNP/MWCNT nanocatalyst, with Pt nanolayer thickness 15 nm, is annealed at three different temperatures (300 – 500 °C) to investigate the influence of the heat-treatment on the electrocatalytic activity towards the ORR [VI].

6.6.1. Surface characterisation of PdNP/MWCNT composites

Figure 36a shows typical image of PdNP/MWCNT fixed onto the GC substrate surface by depositing 15 nm thick palladium layer onto the nanotubes by magnetron sputtering. It can be seen that the carbon nanotubes are covered with a continuous Pd nanolayer, the fine grains of which are clearly visible. Pd layer is applied uniformly onto the surface of MWCNTs. Figure 36b–d shows the SEM micrographs of PdNP/MWCNT samples after heat treatment. No visible changes were observed in catalyst surface morphology by annealing the PdNP/MWCNT samples at 300 °C for 30 min (Fig. 36b). Annealing at higher temperature (400 °C, 30 min) resulted in the formation of even surface (Fig. 36c). The Pd particles of different morphology appeared after annealing at 500 °C (Fig. 36d). In addition to well-distributed small rounded particles, a number of large agglomerates can be seen. Their size increases even to ~60 nm. In comparison to the sample annealed at 300 °C, in this case, the surface of

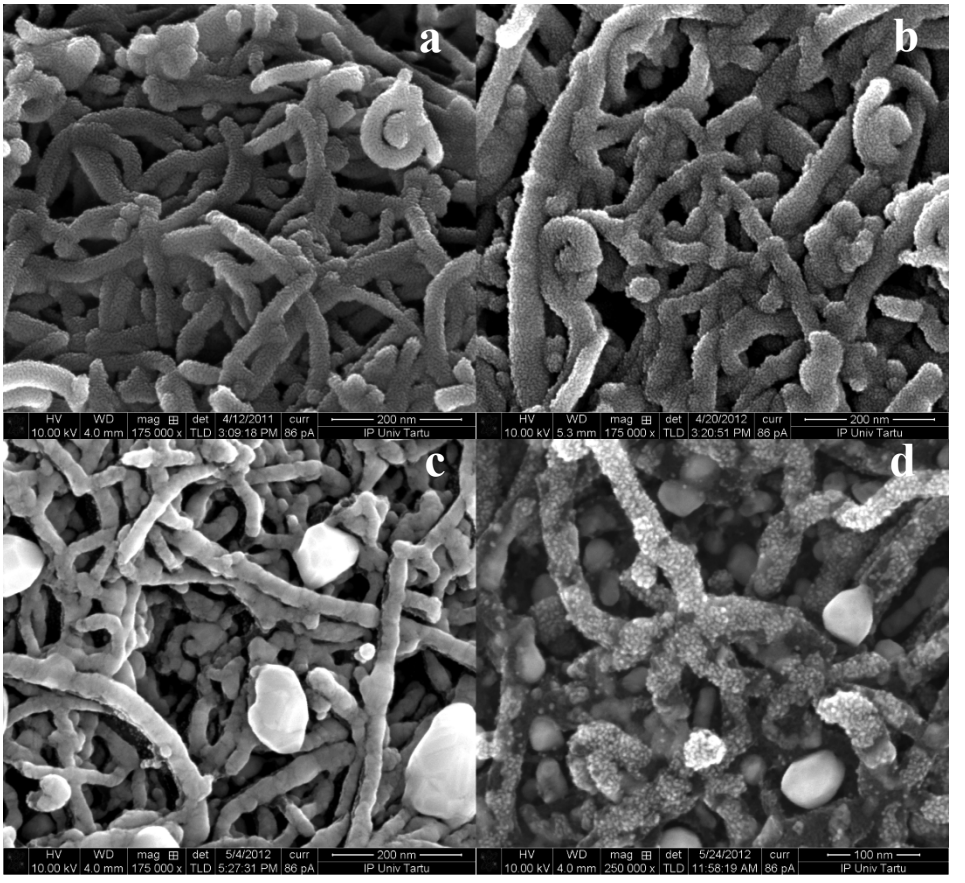

Figure 36. HR-SEM images of PdNP/MWCNT samples: (a) before annealing and after annealing at (b) 300 °C, (c) 400 °C and (d) 500 °C for 30 min.

MWCNTs is less uniformly covered with palladium, and as a result, more uncoated nanotube area can be observed. Instead of uniform metal film, regularly shaped rounded Pd particles are seen. Particle diameter varies from 1.9 to 12.5 nm, their average diameter was ca. 4.5±1.7 nm, measured over 100 particles.

The structural characterisation of PdNP/MWCNT catalysts was carried out by X-ray diffraction. Glassy carbon plate substrate was used for the XRD analysis. Figure 37 shows typical XRD pattern of PdNP/MWCNT catalyst fixed onto a GC substrate after annealing at 500 °C for 30 min. Magnified selected region of Pd (111) peak is presented in inset. The XRD peak at 40.1° which corresponds to (111) reflection demonstrates the presence of crystalline Pd. The signals which correspond to Pd features are rather small which might be caused by the low amount of Pd deposited on the surface of MWCNTs. Pd particles of different morphology appeared only after annealing at 500 °C. For other composite catalysts only residual XRD peaks were observed due to rather small particle size or amorphous Pd layer.

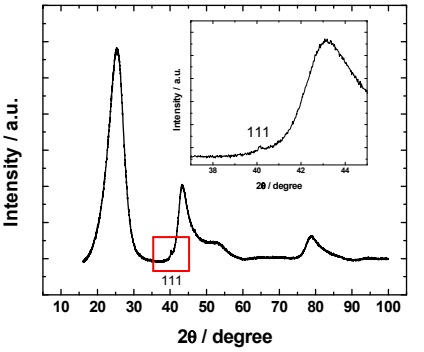

Figure 37. X-ray diffraction pattern of PdNP/MWCNT catalyst after annealing at 500 °C for 30 min. Inset: magnified selected region of Pd(111) peak.

6.6.2. Electrochemical characterisation of the PdNP/MWCNT-modified electrodes

PdNP/MWCNT-modified GC electrodes were first cycled three times in Ar-saturated 0.1 M KOH solution in the range of potentials from 0.1 to 1.4 V using a potential sweep rate of 50 mV s^{-1} (Fig. 38). It is suggested that the growth of the Pd(II)oxide is completed at 1.1–1.3 V vs. RHE in basic electrolytes [271]. Cathodic reduction of PdO was used to determine the real surface area of Pd electrodes, assuming a charge density of 424 μC cm^{-2} for oxide monolayer [271].

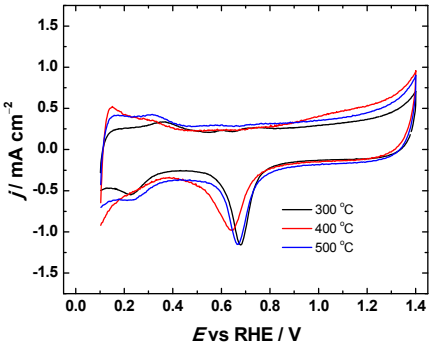

Figure 38. Cyclic voltammograms for PdNP/MWCNT-modified GC electrodes in Ar-saturated 0.1 M KOH. v = 50 mVs^{-1}. Current densities are calculated per geometric surface area of GC.

The O_2 reduction was studied on PdNP/MWCNT-modified GC electrodes using the RDE technique. The RDE experiments were performed in O_2-saturated 0.1 M KOH solution at various rotation rates from 360 to 4600 rpm and at a scan rate of 10 mV s^{-1}. The polarisation curves for O_2 reduction on the heat-treated PdNP/MWCNT catalysts in alkaline solution are shown in Fig. 39a–c.

The RDE results for all the composites studied and bulk Pd at a single rotation rate (ω = 1900 rpm) are also presented for comparison purposes (Fig. 39d). Only the negative-going potential scans are presented and further analysed. The ORR onset potential in 0.1 M KOH was 0.94, 0.92, 0.96, and 0.95 V for PdNP/MWCNT catalysts annealed at 300 °C, 400 °C, 500 °C and bulk Pd, respectively. The half-wave potentials for O_2 reduction were determined at 1900 rpm and are given for all the studied catalysts in Table 10.

The K-L plots were constructed (insets of Fig. 39) and the number of electrons transferred per O_2 molecule was calculated from Eq. (10). On PdNP/MWCNT catalysts and on bulk Pd electrode, the value of n was 4 in the whole range of potentials studied. The $4e^-$ oxygen reduction pathway on Pd catalysts in alkaline solution has been also reported in previous studies [71, 115, 274]. For PdNP/MWCNT catalysts annealed at 300 °C and 400 °C, the O_2 reduction current densities are slightly lower than theoretically calculated j_d values. It appears that the loading of Pd applied (18 μg cm^{-2} calculated per geometric area of GC electrode substrate) for this particular 3D catalyst structure is not sufficient to achieve limiting current densities for a 4-electron reduction of oxygen.

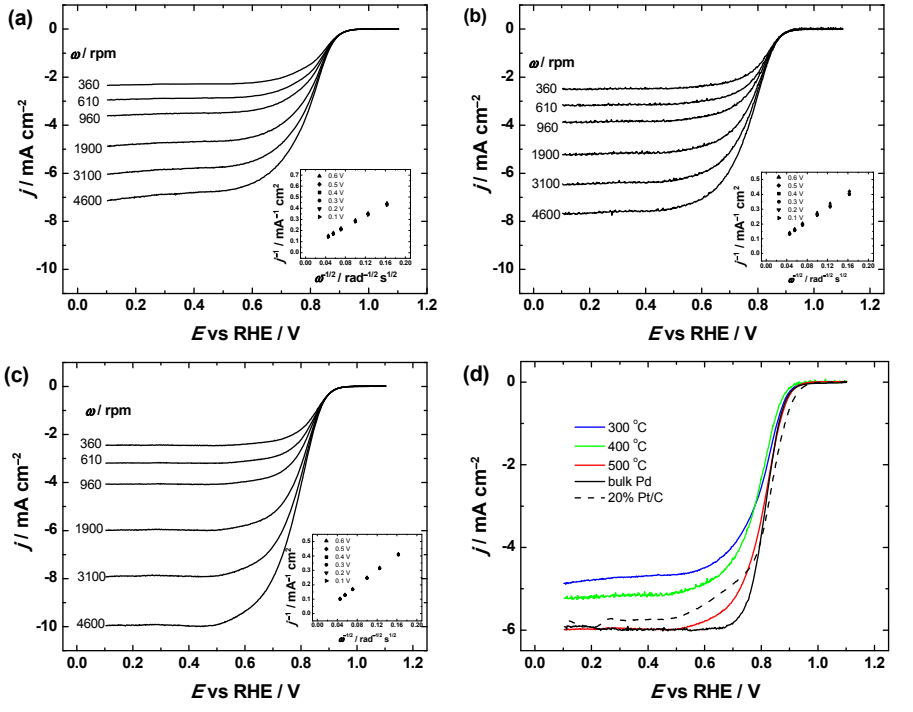

Figure 39. RDE voltammetry curves for O_2 reduction on annealed PdNP/MWCNT modified GC electrodes in O_2-saturated 0.1 M KOH at various electrode rotation rates. PdNP/MWCNT catalysts were heat-treated at: (a) 300, (b) 400 and (c) 500 °C, respectively. Insets: K-L plots for oxygen reduction at different potentials. (d) A comparison of RDE results on PdNP/MWCNT modified GC electrodes, bulk Pd and Pt/C catalyst. ω = 1900 rpm, v = 10 mV s^{-1}.

As can be seen from the comparison of the RDE results presented in Fig. 39d, the PdNP/MWCNT catalyst annealed at 500 °C shows the best performance. Both the ORR onset potential and half-wave potential are higher for this particular electrode. The ORR activity of Pt/C catalyst is slightly higher than that of PdNP/MWCNT composites and bulk Pd (Fig. 39d).

The ORR on Pd is a structure-sensitive reaction and changing the morphology and shape of Pd nanoparticles by different heat-treatment procedures leads to altered electrocatalytic activity. Therefore, it is expected that the Pd-based catalysts having a large fraction of (100) surface sites can act as more active O_2 reduction electrocatalysts as compared to untreated nanoparticles. In addition, recent investigations have shown that in alkaline solution, the specific activity of Pd particles towards the ORR decreases with decreasing the particle size [115]. This has been attributed to the stronger adsorption of OH on smaller particles that block the active sites for ORR. From the CV curves presented in Fig. 38, it is seen that the peak potential of the reduction of Pd surface oxides shifts negative as the Pd particle size decreases. It has been pointed out that the electrocatalytic activity of Pd for ORR depends on the coverage of surface oxides, which in turn is highly dependent on the conditions of the experiment, such as on the start potential if the potential is scanned to the negative direction.

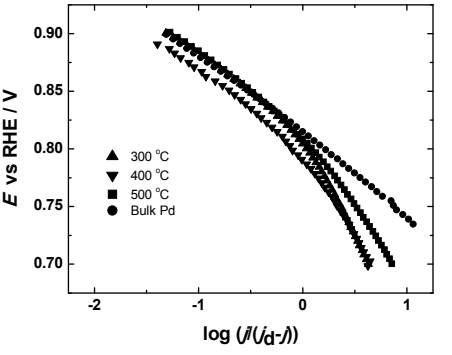

Figure 40. Mass-transfer corrected Tafel plots for oxygen reduction on PdNP/MWCNT-modified GC electrodes and bulk Pd in 0.1 M KOH.

The Tafel plots shown in Fig. 40 were constructed from the RDE data on O_2 reduction at 1900 rpm. Two Tafel regions of different slope can be distinguished. At low current densities, the Tafel slope of heat-treated PdNP/MWCNT catalysts is near −70 mV and in the second region the slope value is higher than −130 mV. The Tafel analysis shows that the kinetics of the ORR is affected by Pd surface oxides; however, the mechanism remains the same. The Tafel slopes on all the PdNP/MWCNT catalysts studied continuously change to a higher value when the potential is more negative than 0.8 V (the high overpotential region). This Tafel behaviour is in agreement with previous report of O_2 reduction on Pd catalysts in alkaline solution [106]. SA values were determined at 0.85 V (Table 10). The highest value of SA was found for the PdNP/MWCNT catalyst annealed at 500 °C.

Table 10. Kinetic parameters for oxygen reduction on Pd/MWCNT modified GC electrodes and bulk Pd in O_2-saturated 0.1 M KOH. ω = 1900 rpm.

Electrode	A_r (cm^2)	Tafel slope (mV) I region*	Tafel slope (mV) II region*	$E_{1/2}$ (mV)	SA at 0.85 V (mA cm^{-2})
Pd/MWCNT (300 ºC)	0.40	–73	–171	804	0.18
Pd/MWCNT (400 ºC)	0.36	–67	–135	791	0.15
Pd/MWCNT (500 ºC)	0.32	–74	–130	809	0.26
Bulk Pd	0.68	–65	–79	815	0.20

* Region I corresponds to low current densities and Region II to high current densities.

6.7. Electroreduction of oxygen on PdNPs supported on N-doped graphene

Nitrogen-doped graphene nanosheets were used as support materials also for Pd nanoparticles that were prepared by borohydride reduction [VII]. Pd/NG composites were used as electrocatalysts for oxygen reduction and their ORR performance was evaluated in acidic and alkaline media.

6.7.1. Surface characterisation of Pd/NG samples

Graphene-based materials are interesting supports for electrocatalysis because of their high surface area and high conductivity. However, graphene is susceptible for stacking induced by π-π interactions between the nanosheets and this reduces surface area and may even prevent mass transfer of reactants to the active sites on the catalyst surface. TEM measurements were performed in order to obtain information about the surface morphology of the prepared Pd/NG catalysts. Transparent corrugated flake-shaped sheets characteristic for few-layered graphene are observed revealing a high exfoliation degree. No evidence of agglomeration of NG flakes is observed. Pd nanoparticles deposited on the micron-sized NG support are visible in Fig. 41a. The TEM images show a good dispersion of Pd nanoparticles on the support surface and the average size of the PdNPs is 2.6 ± 0.7 nm (Fig. 41b) indicating successful synthesis. To determine the particle size, 250 isolated particles were measured.

XPS was used to identify chemical state of nitrogen species. The XPS survey spectrum showed O1, N1s, C1s and Pd3d peaks for Pd/NG sample (Fig. 41c). Fig. 41c shows the main peak of C1s at 284.5 eV, which corresponds to sp^2 carbon. As suggested in previous studies, the smaller peaks that appear at 285.6 and 287.2 eV correspond to the formation of N-sp^2 C and N-sp^3 C bonds [236] or be due to the formation of C-OH and C = O bonds [178]. Four different types of nitrogen species can be seen in inset N1s spectra. Namely, pyridinic-N at

binding energy of 397.8 eV prevails on the surface, peak shoulder between 399 and 400 eV corresponds to pyrrolic-N and graphitic-N [178] and smaller peak at ca. 402.5 eV is due to the presence of pyridine-N-oxide functionalities on the surface [275]. The overall nitrogen content in the sample was calculated from the XPS data and it was ca. 9 at.%. It is still under debate, which type of nitrogen functionalities is responsible for high ORR activity [139, 275]. According to our previous investigations on N-doped carbons, we assume that the main reason for enhanced electrocatalytic activity is the presence of pyridinic nitrogen groups in nanocarbons [178, 213]. In the inset of Fig. 41c Pd3d peaks confirm the presence of metallic Pd, since the binding energy of the main spin-orbit is split into doublet at about 336.9 and 340.6 eV, which correspond to $Pd3d_{5/2}$ and $Pd3d_{3/2}$, respectively [276].

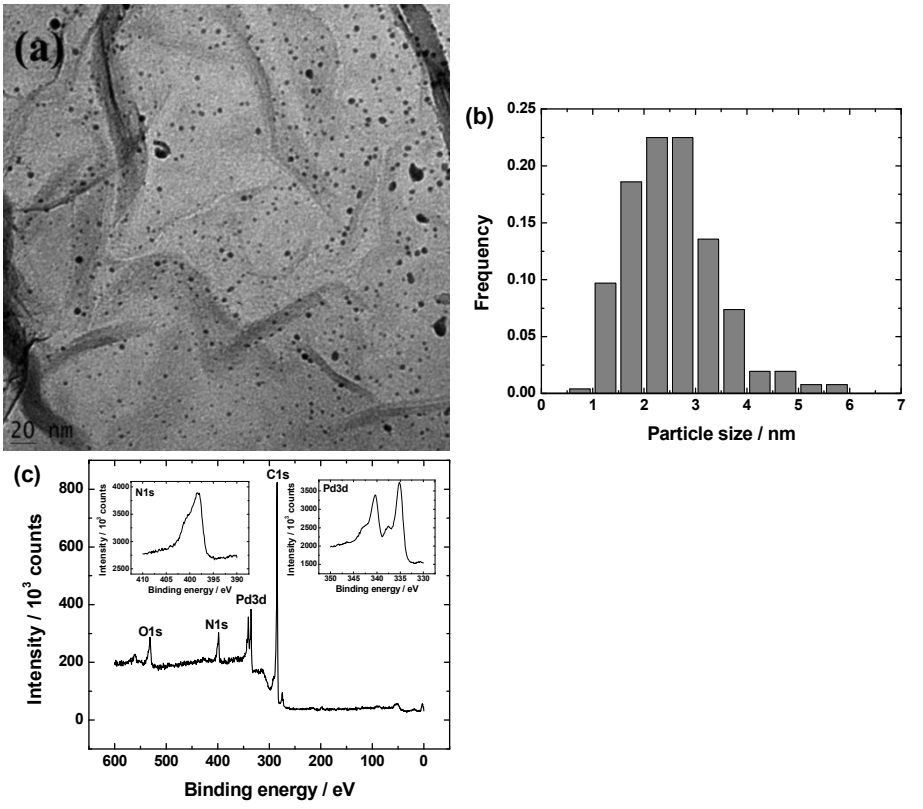

Figure 41. (a) TEM image, (b) particle size distribution and (c) XPS survey spectrum of Pd/NG sample. Insets to Fig. 41c: N1s and Pd3d core-level spectra.

6.7.2. Electrochemical characterisation of Pd/NG catalysts

Shown in Fig. 42 are stable CV curves of Pd/NG modified GC electrodes recorded in O_2-free 0.5 M H_2SO_4 and 0.1 M KOH at a scan rate of 50 mV s^{-1}. In both solutions, the CV profiles of Pd/NG samples are similar to those observed for a bare polycrystalline Pd, but the charging current in double-layer region is much higher due to the contribution of the high surface area NG support. The anodic peaks at $E > 0.8$ V and the cathodic peak at ca. 0.6–0.7 V correspond to the formation of Pd surface oxides and to their reduction, respectively [V, 117]. Typical peaks of adsorption/desorption of underpotential deposited hydrogen in the potential range of 0.1–0.3 V were also observed. The A_r values were of the same order for different batch of Pd/NG catalysts, therefore showing a good batch-to-batch reproducibility.

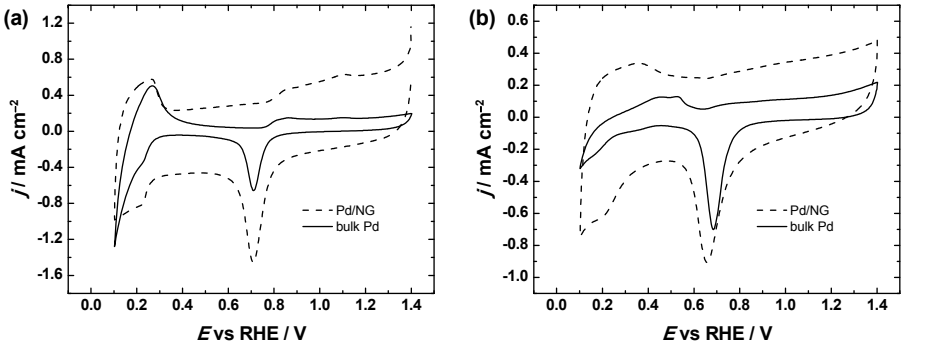

Figure 42. Cyclic voltammograms of Pd/NG modified GC and bulk Pd electrodes in Ar-saturated solutions: (a) 0.5 M H_2SO_4 and (b) 0.1 M KOH. v = 50 mV s^{-1}. Current densities are normalised to the geometric GC electrode area.

The RDE results obtained at different rotation rates for Pd/NG modified GC and bulk Pd electrodes in acid and alkaline electrolytes are shown in Figs. 43a and 44a, respectively. Only the cathodic sweeps are shown in the Figures and are further analysed. In acid electrolyte, the ORR polarisation curves with well-defined limiting current plateaus are observed only at low rotation rates (Fig. 43a). At high rotation speed the reduction current gradually increases reaching a diffusion-limited value at high overpotentials. This indicates sluggish kinetics of O_2 reduction on Pd catalysts in H_2SO_4 and is in accordance with previous observation [117].

Koutecky–Levich plots for oxygen reduction were constructed for both solutions (Fig. 43b and 44b) and the n value was calculated from Eq. (10). Linear K-L plots were obtained from the RDE data. The value of n was close to four (see insets in Fig. 43b and 44b), which indicates that the process of O_2 reduction follows predominantly a $4e^-$ pathway on Pd/NG catalysts in acid and alkaline solutions. The $4e^-$ ORR pathway on Pd catalyst in alkaline media has been reported previously [117].

The comparison of j–E curves of O_2 reduction recorded at a single rotation rate (ω = 1900 rpm) are presented in Fig. 43c and 44c. Compared with bulk Pd the onset potential of O_2 reduction on Pd/NG shifted slightly positive in acid media and in 0.1 M KOH the onset potential is ∼100 mV higher, showing remarkably higher ORR activity in alkaline media.

In both acid and alkaline media the values of $E_{1/2}$ of O_2 reduction for Pd/NG catalyst were higher than that of bulk Pd. Tafel plots were constructed from the RDE data of the ORR and are presented in Fig. 43d and 44d. Two Tafel regions with distinct slope were observed and this behaviour is in agreement with the results of our earlier studies of O_2 reduction on Pd nanocatalysts [V, VI, 98, 102, 103, 117, 124].

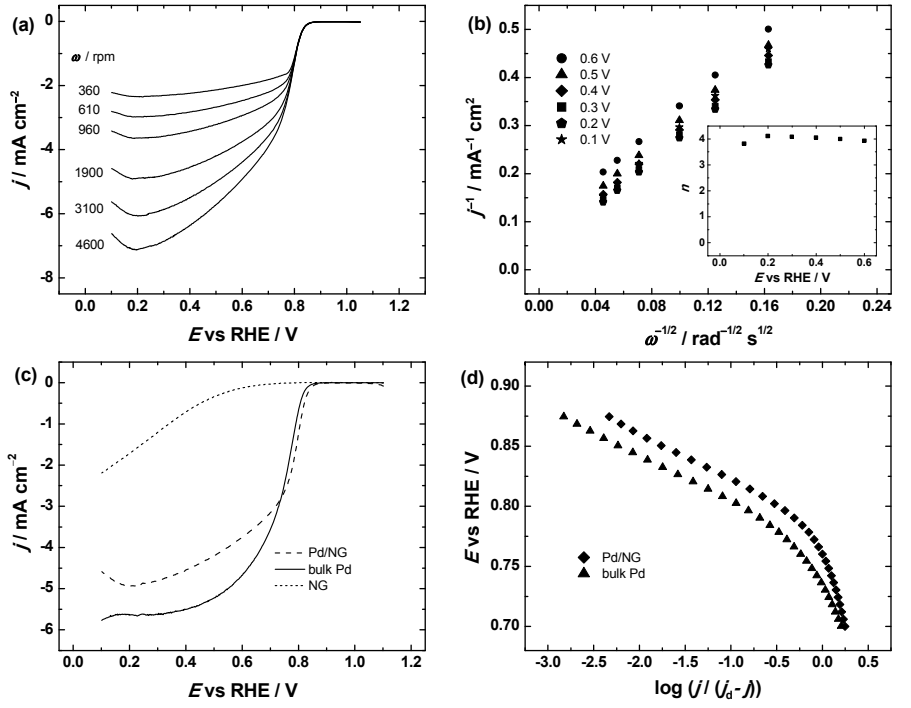

Figure 43. (a) RDE voltammetry curves for oxygen reduction on a Pd/NG modified GC electrode in O_2-saturated 0.5 M H_2SO_4 solution at different rotation rates, v = 10 mV s^{-1}. (b) K–L plots for O_2 reduction on a Pd/NG modified GC electrode in 0.5 M H_2SO_4. Inset shows the potential dependence of n. (c) Comparison of RDE results on O_2 reduction on Pd/NG modified GC and bulk Pd electrodes in O_2-saturated 0.5 M H_2SO_4 solution at ω = 1900 rpm. (d) Mass-transfer corrected Tafel plots for O_2 reduction on Pd/NG modified GC and bulk Pd electrodes in acid electrolyte.

Previous studies confirm that N-doped carbon nanomaterial itself is a good electrocatalyst for ORR [178, 213, 277, 278]. It was reported that N-doped graphene has low efficiency in catalysing the ORR in acid solution [279], however it greatly improves the electrocatalytic performance of Pd nanoparticles when utilised as a support material. A better ORR performance is caused by the improved adhesion between graphene and metal catalyst, which enhances the stability of catalyst nanoparticles dispersed over the substrate surface. The enhanced performance can be attributed to the stronger carbon–catalyst binding and increased electrical conductivity caused by nitrogen doping [91].

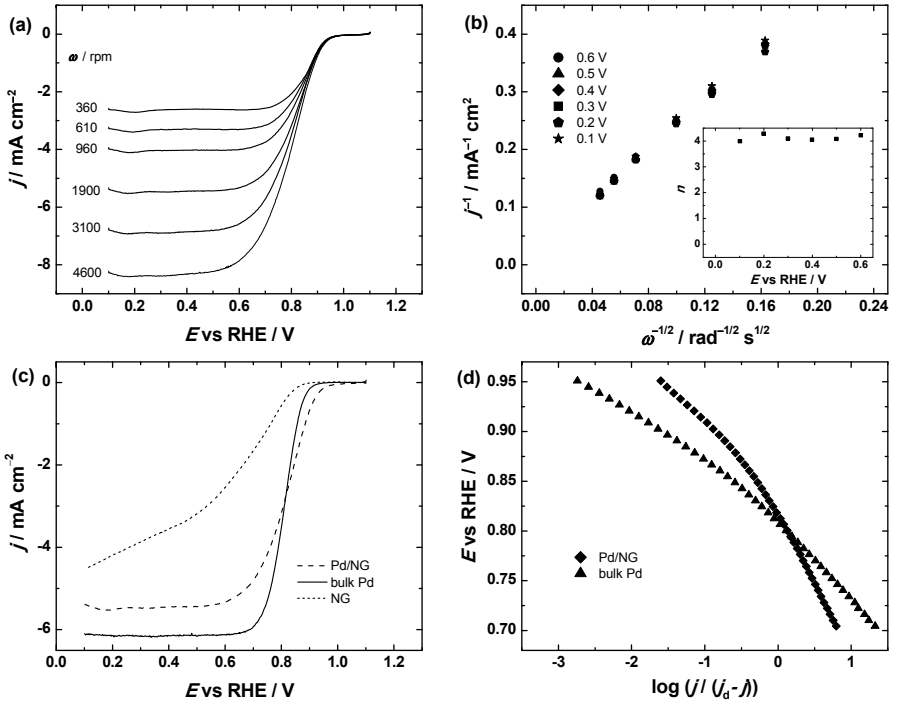

Figure 44. (a) RDE voltammetry curves for oxygen reduction on a Pd/NG modified GC electrode in O_2-saturated 0.1 M KOH solution at different rotation rates, v = 10 mV s^{-1}. (b) K–L plots for O_2 reduction on a Pd/NG modified GC electrode in 0.1 M KOH. Inset shows the potential dependence of n. (c) Comparison of RDE results on O_2 reduction on Pd/NG modified GC and bulk Pd electrodes in O_2-saturated 0.1 M KOH solution at ω = 1900 rpm; (d) Mass-transfer corrected Tafel plots for O_2 reduction on Pd/NG modified GC and bulk Pd electrodes in alkaline electrolyte.

Table 11. Kinetic parameters for oxygen reduction on Pd/NG and bulk Pd in O_2-saturated 0.5 M H_2SO_4 and 0.1 M KOH solutions. ω = 1900 rpm.

Electrode	A_r (cm^2)	Tafel slope (mV) I region*	Tafel slope (mV) II region*	$E_{1/2}$ (V)	SA at 0.85 V (mA cm^{-2})
0.5 M H_2SO_4					
Pd/NG	0.69	–45	–141	0.76	0.015
Bulk Pd	0.54	–40	–124	0.73	0.009
0.1 M KOH					
Pd/NG	0.55	–67	–129	0.82	0.55
Bulk Pd	0.59	–48	–77	0.81	0.52

*Region I corresponds to low current densities and Region II to high current densities.

Table 11 summarises the main kinetic parameters obtained for oxygen reduction in this part of the work. The specific activities for O_2 reduction were calculated at 0.85 V vs RHE. The specific activity of the prepared Pd/NG catalyst was 0.015 mA cm^{-2} in acid media, which is almost twice that observed for poly-crystalline Pd (0.009 mA cm^{-2}). In alkaline electrolyte, the value of SA of Pd/NG was significantly higher than that observed in acid solution. This is due to the inhibiting effect of (bi)sulphate anions on the kinetics of the ORR in H_2SO_4 solution. The superior ORR activity of Pd/NG as compared to other Pd-based catalysts in alkaline media is in evidence, indicating that the Pd/NG catalysts studied could be successfully employed in alkaline membrane fuel cell and other electrochemical applications.

It has been clearly shown, that N-doped carbon materials have a great potential in fuel cell application as highly active and stable electrocatalyst supports. Up to now nitrogen-doped nanocarbons have been primarily employed as supports for nanoparticulate Pt catalysts. Huang et al. used NG-vanadium carbide hybrids as Pt catalyst support for ORR in alkaline media. After annealing at 1000 ºC the catalyst showed higher MA than commercial Pt/C (0.210 vs. 0.200 mA g_{Pt}^{-1} at $E_{1/2}$) under the same conditions [280]. Four times higher power density was achieved for Pt_2Co alloy supported on N-doped carbon as compared to commercial Pt/C [239]. Electrochemical experiments showed that Pt nanoparticles supported on N-doped carbon show higher ORR activity and much better stability [83, 92, 235, 281, 282]. The enhanced properties are generally considered to occur due to: controlled and optimised Pt particle size and distribution on N-doped carbon materials [79–82, 84, 85, 193, 283, 284]; the increase in electrical conductivity [248]; and the action of doped N as catalyst stabilising agent with enhanced activity for ORR [40, 285–287]. Strong interaction between catalyst and support is attributed to a larger N-content and smaller Pt particle size [78, 288, 289]. Gracia-Espino et al. confirmed that N-doped graphene has a significant effect in reducing the energy barrier for O_2

dissociation and decrease the energetic stability of $HO^{\bullet}$ intermediates resulting in enhanced ORR activity [89].

A thorough electrocatalytic study performed in this work confirms that the proposed simple procedure for the preparation of highly dispersed Pd nanoparticles over nitrogen-doped graphene results in cathode catalyst with good electrocatalytic properties for ORR. This investigation shows that the attachment of Pd nanoparticles into the catalyst matrix increases its electrocatalytic activity in both acid and alkaline media.

6.8. Oxygen reduction on cubic PdPt nanoalloys

The reduction of oxygen on palladium-platinum alloy nanocubes synthesised in the presence of PVP was investigated using a rotating disc electrode [VIII, IX]. Different Pd-to-Pt ratios were used and the electrocatalytic activity of PdPt catalysts for ORR was compared with that of cubic Pd and Pt nanoparticles.

6.8.1. TEM/EDX characterisation of PdPt catalysts

TEM analysis was carried out to obtain knowledge about the particle size and morphology of PdPt alloy nanoparticles. Figures 45a-c show PdPt nanoparticles with preferential cubic particle shape. Most of the PdPt nanoparticles were cubic-shaped, but there were also observed some truncated particles. To determine the particle size of PdPt nanocubes, 200 isolated particles were measured. The mean particle sizes were 8.6 ± 0.9, 9.4 ± 1.4 and 10.4 ± 1.2 nm for $Pd_{34}Pt_{66}$, $Pd_{50}Pt_{50}$ and $Pd_{66}Pt_{34}$ samples, respectively. Particle size distributions for all the alloyed catalysts are shown in Fig. 45. The average particle sizes of Pd and Pt nanocubes were about 10 nm.

The composition of the prepared PdPt alloy nanocubes was analysed by energy dispersive X-ray spectroscopy. The EDX analyses displayed that the atomic compositions were close to the nominal values and the Pd-to-Pt ratios of 36:64, 54:46 and 72:28 were determined.

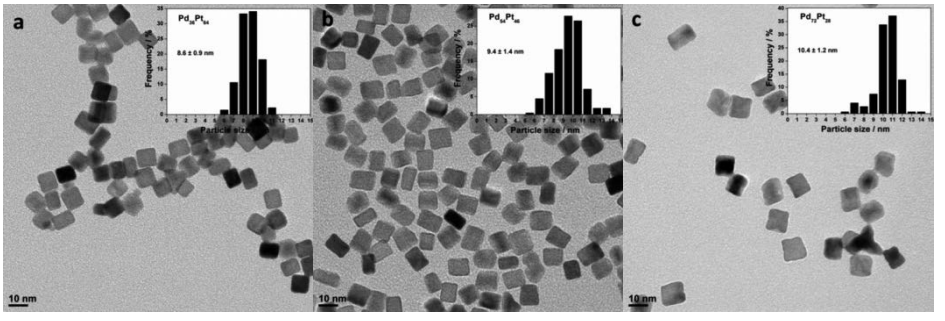

Figure 45. TEM images of PdPt catalysts: (a) $Pd_{36}Pt_{64}$, (b) $Pd_{54}Pt_{46}$ and (c) $Pd_{72}Pt_{28}$ and their corresponding particles size histogram.

6.8.2. CO stripping and CV experiments

Typical CO-stripping behaviour of PdPt catalysts in 0.5 M H_2SO_4, 0.1 M $HClO_4$ and 0.1 M KOH solutions are shown in Figs. 46a–c. In all the solutions, it can be seen that there is a positive potential shift in the position of the CO oxidation peak of PdPt alloys with rising the amount of Pd. It has been proposed to be related to a gradual Pd surface enrichment for increasing Pd content [191].

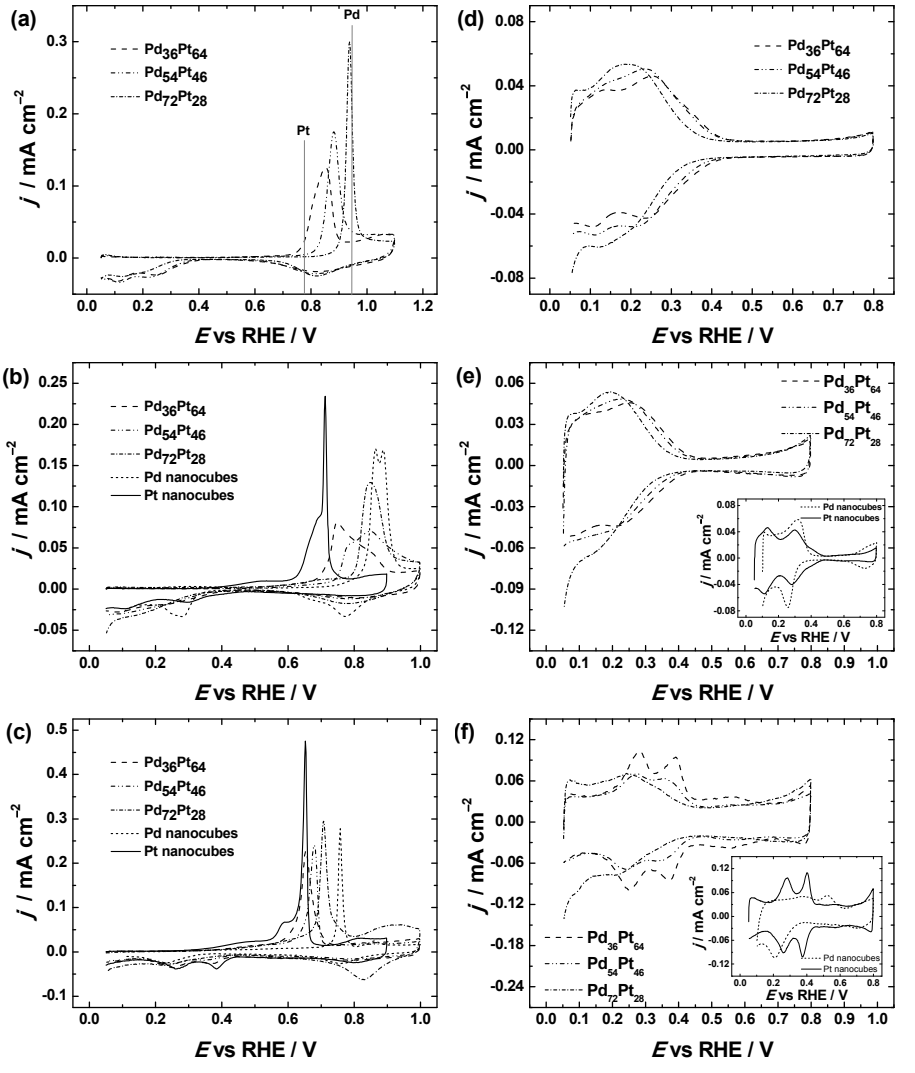

Figure 46. Electro-oxidation of pre-adsorbed CO on PdPt catalysts, Pd and Pt nanocubes in Ar-saturated (a) 0.5 M H_2SO_4, (b) 0.1 M $HClO_4$ and (c) 0.1 M KOH solutions (v = 20 mV s^{-1}). Cyclic voltammograms after CO oxidation on PdPt catalysts, Pd and Pt nanocubes in Ar-saturated (d) 0.5 M H_2SO_4, (e) 0.1 M $HClO_4$ and (f) 0.1 M KOH solutions (v = 50 mV s^{-1}). Current densities are normalised to the real surface area of electrocatalysts.

Representative CVs recorded after the CO-stripping experiments are shown in Fig. 46d–f. The CV responses showed improvement in surface cleanness compared with those initially measured. Better defined peaks in the hydrogen adsorption/desorption region are in evidence. The real surface areas of the PdPt electrocatalysts were determined by charge integration under the hydrogen desorption peaks (see Tables 12–14).

6.8.3. Oxygen reduction on PdPt catalysts

The electroreduction of oxygen on PdPt alloy nanocubes was firstly studied in O_2-saturated 0.5 M H_2SO_4 solution using the RDE method. The representative ORR polarisation curves for the $Pd_{54}Pt_{46}$-catalyst modified GC electrode are shown in Fig. 47a. Only the positive-going potential scans are presented and further analysed. For all the PdPt catalysts the ORR polarisation curves were single-waved and well-defined diffusion-limited current plateaus were observed.

Figure 47b presents the K–L plots for $Pd_{54}Pt_{46}$-catalyst. The value of n was close to four for all the PdPt catalysts studied (inset of Fig. 47b). This is in agreement with previous studies of O_2 reduction on Pd and Pt catalysts in acid media [I, 103, 116, 117, 148].

For better comparison of the RDE results the j-E curves of ORR recorded at 1900 rpm are shown in Fig. 47c. Half-wave potentials of oxygen reduction for all the alloyed catalysts were higher than that of Pd nanocubes and were comparable to that of cubic PtNPs (Table 12). The onset potential for $Pd_{36}Pt_{64}$ was the highest.

Tafel plots were constructed from the RDE data on O_2 reduction at 1900 rpm as shown in Fig. 47d. Two regions with distinct slope values were observed (Table 12). In the low overpotential region the slope was close to −60 mV and the rate-determining step of oxygen reduction on oxide-covered PdPt alloys is the first electron transfer. At high overpotentials the Tafel slope value was over −130 mV, which is slightly higher than that reported for Pd and Pt electrodes in early work [9, 116]. Similar slope values have been found for different Pd- and Pt-based catalysts [I, V, 102, 103, 117].

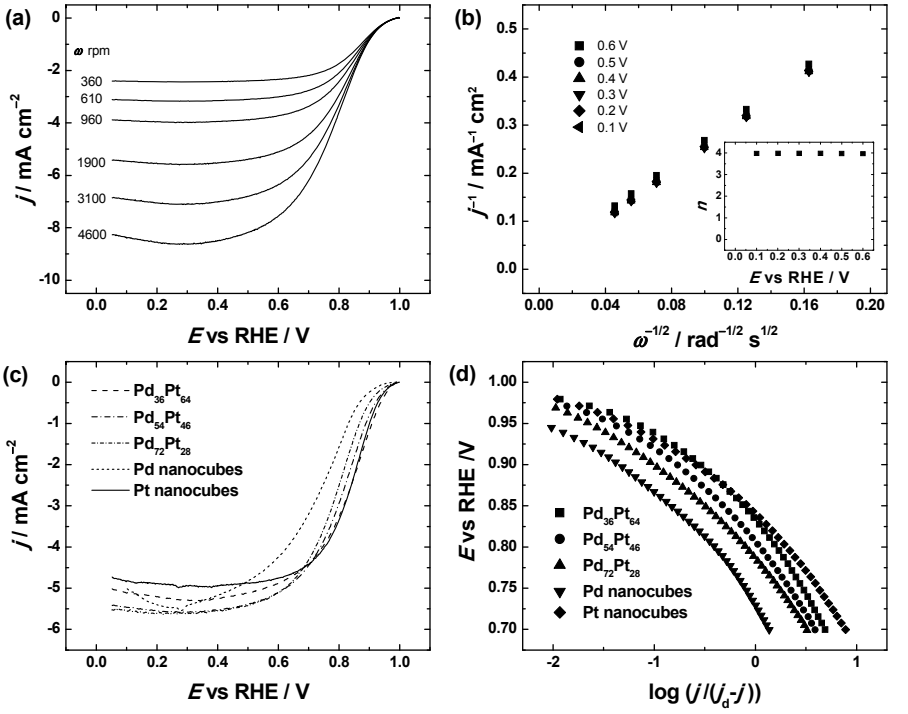

Figure 47. (a) RDE voltammetry curves for O_2 reduction on $Pd_{54}Pt_{46}$ alloy nanocubes in O_2-saturated 0.5 M H_2SO_4 (v = 10 mV s^{-1}), (b) K–L plots for ORR in 0.5 M H_2SO_4 (inset shows the potential dependence of n), (c) comparison of the RDE results for the ORR (v = 10 mV s^{-1}, ω = 1900 rpm) and (d) Tafel plots for ORR in 0.5 M H_2SO_4 (ω = 1900 rpm). Current densities are normalised to the geometric area of GC.

The specific activity of O_2 reduction at 0.9 V are given in Table 12. The SA value of $Pd_{36}Pt_{64}$ was higher than that of Pd nanocubes, but still lower than that of Pt nanocubes. Hoshi et al. have shown that a Pt monolayer on Pd(100) decreases the activity [290]. On the other hand Pd–Pt nanodendrites with 85% of Pt had higher activity than that of Pt/C [145]. In this work the largest Pt content was 64% and it can be observed that SA starts to increase, but still does not surpass that of Pt nanocubes. It has been suggested that with higher Pt content the O_2 adsorption is more favourable and thus increases the ORR activity [145]. Apparently, the lower activity of PdPt nanocubes is related to a decrease in the number of dual Pt–Pt sites as compared to monometallic Pt particles. Another reason for lower SA value of PdPt nanocubes might be the adsorption of anions on the metal that is competing with O_2 adsorption.

Table 12. Kinetic parameters for oxygen reduction on PdPt nanocubes, cubic Pd and cubic Pt in O_2-saturated 0.5 M H_2SO_4, ω = 1900 rpm.

Electrode	A_r (cm^2)	Tafel slope (mV) I region*	Tafel slope (mV) II region*	$E_{1/2}$ (V)	SA at 0.90 V (mA cm^{-2})
$Pd_{36}Pt_{64}$	0.99	–62	–151	0.83	0.089
$Pd_{54}Pt_{46}$	0.89	–62	–152	0.81	0.072
$Pd_{72}Pt_{28}$	0.45	–66	–136	0.79	0.086
Cubic Pd	0.46	–64	–134	0.73	0.078
Cubic Pt	0.75	–58	–142	0.84	0.113

* Region I corresponds to low current densities and Region II to high current densities.

Typical RDE voltammetry curves for O_2 electroreduction on $Pd_{54}Pt_{46}$ nanocubes in 0.1 M $HClO_4$ are demonstrated in Fig. 48a. The ORR polarisation curves showing a single reduction wave were in evidence for all the electrocatalysts studied in the present work.

From the K-L slopes the value of *n* was calculated, which was close to four over the whole range of potentials for all the electrocatalysts studied (see inset in Fig. 48b). This suggests that the main product of the ORR is water and only little peroxide is formed. On hollow Pd-Pt nanostructures using the rotating ring-disk electrode method the H_2O_2 yield was found to be <0.15% [151]. The $4e^-$ pathway of O_2 electroreduction on Pd and Pt electrocatalysts in acid media has been also confirmed in earlier studies [158, 163, 291, 292].

A comparison of the RDE results in perchloric acid at 1900 rpm is shown in Fig. 48c. $Pd_{36}Pt_{64}$ had the highest half-wave potential from the alloys; its $E_{1/2}$ value was comparable with that of pure Pt nanocubes (Table 13). Similar $E_{1/2}$ values have been also found for PdPt nanodendrites [146, 163]. GC electrodes modified with $Pd_{54}Pt_{46}$ and $Pd_{72}Pt_{28}$ nanocubes had the lowest $E_{1/2}$ (0.83 and 0.84 V, respectively), which were similar to that of cubic Pd nanoparticles ($E_{1/2}$ = 0.84 V). Although Pd(100) is recognised to be the most active single-crystal facet for ORR in 0.1 M $HClO_4$ solution [100], the alloy nanocubes with more than 50% Pd had lower electrocatalytic activity towards O_2 reduction. The reason for this observation might be that there are more Pd(110) or Pd(111) sites, which are less electrocatalytically active for ORR than Pd(100), available on the surfaces of $Pd_{54}Pt_{46}$ and $Pd_{72}Pt_{28}$ nanocubes as Fig. 45 suggests. Similar results were found also by Zhang et al., who demonstrated that Pd-Pt bimetallic nanocrystals had lower O_2 reduction activity than commercial Pt/C catalyst [152].

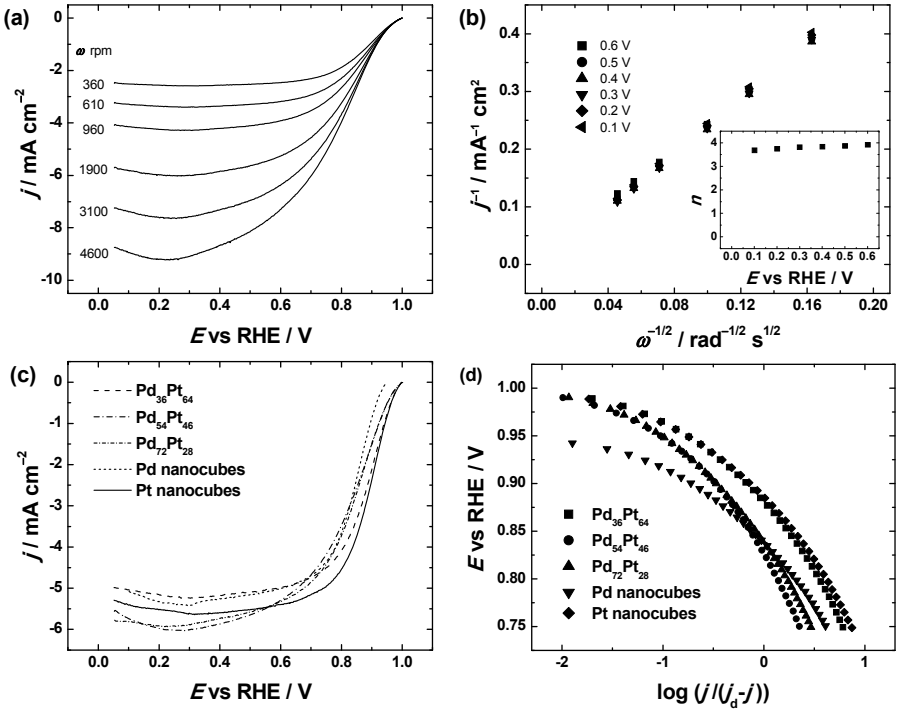

Figure 48. (a) RDE voltammetry curves for oxygen reduction on $Pd_{54}Pt_{46}$ alloy nanocubes in O_2-saturated 0.1 M $HClO_4$ (v = 10 mV s^{-1}), (b) K–L plots for ORR in 0.1 M $HClO_4$ (inset shows the potential dependence of n). (c) Comparison of the RDE results for O_2 reduction on PdPt, Pd and Pt nanocubes in O_2-saturated 0.1 M $HClO_4$ (v = 10 mV s^{-1}, ω = 1900 rpm). (d) Tafel plots for ORR in 0.1 M $HClO_4$ (ω = 1900 rpm). Current densities are normalised to the geometric area of GC.

It has been reported that the addition of defects leads to a remarkable diminution of the electrocatalytic activity for ORR on Pt(111) surfaces [13, 209], but there is still lack of knowledge about the role of defects on Pt(100) facets [14]. Quan et al. have observed that the specific activity towards the O_2 reduction reaction on (720)-bounded Pt concave nanocubes was greater than that of low-indexed Pt nanocubes with similar size [293]. Ma et al. studied the ORR on Pt multicubes and Pt multipods [294]. They found that Pt multicubes are surrounded largely by (100) facets, in contrast to the Pt multipods, which have high-index facets, but still exhibit an increased $E_{1/2}$ value (0.955 and 0.957 V for Pt multicubes and Pt multipods, respectively) and high specific activities (0.729 mA cm^{-2} for multicubes and 0.924 mA cm^{-2} for multipods). In case of Pd concave nanocubes with (730) high-index facets, it has been found that these exhibit enhanced electrocatalytic activity for formic acid oxidation compared to that of conventional Pd nanocubes enclosed by (100) low-index facets [295]. It is still not clear how the high-index facets affect the ORR activity of Pd single crystal basal planes.

Tafel plots were derived from the RDE data of O_2 reduction (shown in Fig. 48c) and two Tafel regions with different slope value were observed (Fig. 48d). In the potential region of low current densities the Tafel slope is close to –60 mV dec^{-1} and in the region of higher current densities the slope values increase over –120 mV dec^{-1}. These Tafel slopes are characteristic to both of the noble metal electrocatalysts studied, Pd and Pt, and the change in the slope is associated with the potential-dependent coverage of oxygen-containing species that inhibit the adsorption of O_2 [96]. For ORR the main barrier for the rate-determining step was identified as the structure-sensitive adsorption of OH species and its inhibiting effect on O_2 adsorption [296]. For pure Pt electrocatalysts Pt–OH is easily formed on the surface of platinum, thus lowering the ORR activity [175]. In comparison with that of pure Pt, the addition of palladium into the Pd-Pt catalysts showed that the degree of Pt–OH appeared on the surface of Pd@Pt is decreased and therefore enhances the activity of O_2 reduction. Similar observation of low OH_{ad} coverage on the surface of Pt-on-Pd has been made by Peng and Yang [297]. The electrocatalytic ORR activity of the hetero-nanostructures increased nearly two times.

The specific activities for O_2 reduction were also calculated in 0.1 M $HClO_4$ solution. The SA values were determined using Eq. (11) and are added to Table 13. In perchloric acid, the specific activities at 0.9 V vs. RHE were lower as compared to those in alkaline solution and the order of the SA values for PdPt alloy nanocubes in 0.1 M $HClO_4$ is adverse to that in 0.1 M KOH. In perchloric acid $Pd_{36}Pt_{64}$ nanocubes demonstrated the highest SA value (0.408 mA cm^{-2}) from the alloyed catalysts and it was comparable to that of pure Pt nanocubes (0.416 mA cm^{-2}). This nanoalloy with highest Pt content exhibited good ORR activity also in sulphuric acid.

Table 13. Kinetic parameters for oxygen reduction on PdPt-nanocubes, cubic Pd and cubic Pt in O_2-saturated 0.1 M $HClO_4$, ω = 1900 rpm.

Electrode	A_r (cm^2)	$E_{1/2}$ (V)	Tafel slope (V) I region*	Tafel slope (V) II region*	SA at 0.9 V (mA cm^{-2})
$Pd_{36}Pt_{64}$	0.61	–0.062	–0.128	0.88	0.408
$Pd_{54}Pt_{46}$	0.59	–0.059	–0.126	0.83	0.241
$Pd_{72}Pt_{28}$	0.65	–0.060	–0.128	0.84	0.216
Cubic Pd	0.41	–0.059	–0.121	0.84	0.249
Cubic Pt	0.73	–0.063	–0.124	0.89	0.416

* Region I corresponds to low current densities and Region II to high current densities.

The O_2 reduction reaction on cubic PdPt nanoalloys was also explored in O_2-saturated 0.1 M KOH solution using the RDE technique. Fig. 49a presents characteristic current density-potential curves for the $Pd_{54}Pt_{46}$-catalyst. Single-wave ORR polarisation curves with well-developed diffusion-limited current plateaus were noticed for all the PdPt electrocatalysts studied.

The Koutecky-Levich analysis results for $Pd_{54}Pt_{46}$ alloy nanocube-modified electrode in alkaline media are presented in Fig. 49b. Linear K-L plots were acquired from the RDE data. The *n* value was found from the slope of the K-L lines and it was close to four for all the electrodes studied (inset to Fig. 49b). The 4-electron O_2 reduction pathway on Pd and Pt catalysts in alkaline media has been also obtained in previous studies [II, V, 47, 117, 162, 172, 207], however, it has been suggested that on Pt-group metals the ORR proceeds partly via 2-electron pathway [106]. Lee et al. suggested that the ORR kinetic properties on Pt-coated Pd nanocubes are better than on Pt nanoparticles and as a result the production of HO_2^- is lower [172].

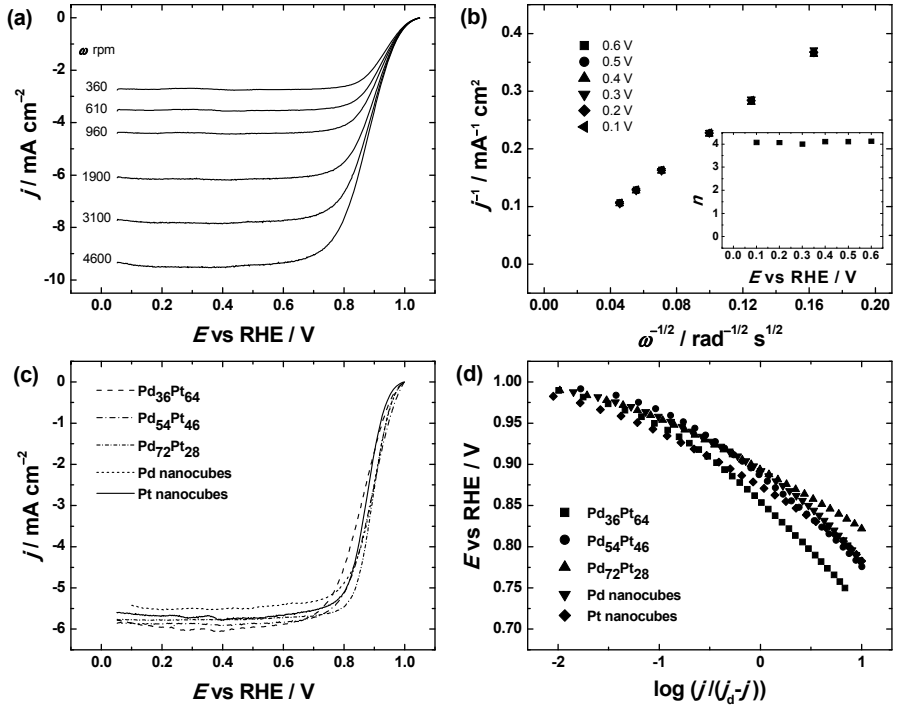

Figure 49. (a) RDE voltammetry curves for oxygen reduction on $Pd_{54}Pt_{46}$ alloy nanocubes in O_2-saturated 0.1 M KOH (v = 10 mV s^{-1}), (b) K–L plots for ORR in 0.1 M KOH (inset shows the potential dependence of *n*). (c) Comparison of the RDE results for O_2 reduction on PdPt, Pd and Pt nanocubes in O_2-saturated 0.1 M KOH (v = 10 mV s^{-1}, ω = 1900 rpm) and (d) Tafel plots for ORR in 0.1 M KOH (ω = 1900 rpm). Current densities are normalised to the geometric area of GC.

A direct comparison of the RDE results of O_2 reduction recorded at 1900 rpm is presented in Fig. 49c. It can be seen that all the cubic-shaped nanocatalysts show similar electrochemical ORR behaviour displaying two distinct regions of mass-transfer (below 0.7 V) and mixed kinetic-diffusion control in the potential range between 0.7 and 1.0 V. The half-wave potential values for all the catalysts are listed in Table 14. $Pd_{36}Pt_{64}$ and pure Pt nanocubes had slightly lower $E_{1/2}$ for O_2 reduction than the other catalysts in this study. Lower electrocatalytic activity could be explained by higher Pt(100) content, which is the least active facet for ORR in alkaline media [8].

Tafel plots (Fig. 49d) were constructed using the RDE data (shown in Fig. 49c) of O_2 reduction at 1900 rpm. Two characteristic regions in Tafel plots with distinct slope values were found. At low current densities the slope value was approximately –60 mV and at higher current densities the slope increased to –120 mV. Similar Tafel behaviour for O_2 reduction has been reported in earlier works [II, 102].

Table 14. Kinetic parameters for oxygen reduction on PdPt nanocubes, cubic Pd and cubic Pt in O_2-saturated 0.1 M KOH, ω = 1900 rpm.

Electrode	A_r (cm^2)	$E_{1/2}$ (V)	Tafel slope (V) I region*	Tafel slope (V) II region*	SA at 0.9 V (mA cm^{-2})
$Pd_{36}Pt_{64}$	0.44	–0.059	–0.119	0.86	0.375
$Pd_{54}Pt_{46}$	0.49	–0.059	–0.114	0.89	0.622
$Pd_{72}Pt_{28}$	0.32	–0.060	–0.126	0.89	1.249
Cubic Pd	0.52	–0.056	–0.122	0.89	0.607
Cubic Pt	0.31	–0.061	–0.121	0.87	0.544

* Region I corresponds to low current densities and Region II to high current densities.

The SA values calculated at 0.9 V are reported in Table 14. Specific activity for PdPt alloy nanocubes increased with increasing Pd content. Interestingly, the SA values for $Pd_{72}Pt_{28}$ and $Pd_{54}Pt_{46}$ alloys are 1.249 and 0.622 mA cm^{-2}, respectively. Thus, the SA for $Pd_{72}Pt_{28}$ is about 2-times higher than that obtained with pure Pd and Pt nanocubes (about 0.55–0.6 mA cm^{-2}) indicating a bimetallic synergetic effect between Pd and Pt at this particular composition. In this regard, it has been found that an insignificant amount of Pt on top of the Pd nanotubes improves the ORR activity in alkaline media [298]. The enhancement of the specific and mass activities for ORR was attributed to electronic effects and higher surface area utilisation.

It has been reported that Pd-Pt concave nanocubes exhibited high electrocatalytic activity for O_2 electroreduction [153]. Enhanced ORR activity was interpreted by higher Pt concentration on the surface of the Pd nanoparticles and

thus being precisely affected in the reaction and also the electronic synergy between Pt and Pd could lead to an increased ORR activity. It has been found for Pd-Pt core-shell systems that the Pd/Pt ratio has a major effect on the activity of O_2 reduction reaction [175]. Compared to pure palladium, Pt is more active. With the increase of the Pt/Pd molar ratio, more Pt nanoclusters were formed on the surface of Pd nanocubes, resulting in the enhanced electrocatalytic activity. Liu et al. studied the ORR electrocatalytic activity of conventional PdPt alloy nanoparticles and compared their specific activity with that of Pd(core)-Pt(shell) and Pt/C catalysts [166]. It was found that in 0.1 M $HClO_4$ solution the SA for PdPt nanoalloys increased with the increased Pt/Pd ratio. The SA values for O_2 reduction of PdPt alloy nanocrystals were even higher with those of Pd-Pt core-shell catalysts. The electrocatalytic trends observed in the present work in $HClO_4$ are in good agreement with those reported for conventional PdPt alloy nanoparticles by Liu et al. [166]. These observations suggest that alloy formation between Pd and Pt may have a large role for the specific activities observed in the present work.

7. SUMMARY

The electroreduction of oxygen on platinum and palladium based nanocomposites was studied in acidic and alkaline media employing the rotating disk electrode technique. For the preparation of nanostructured platinum and palladium catalysts chemical and physical methods were used. For anchoring Pt and Pd nanoparticles to MWCNT surface magnetron sputtering was employed. Metal nanoparticles were supported on nitrogen-doped graphene by chemical reduction of metal salt using either sodium borohydride or ethylene glycol as reducing agents. Shape-controlled Pt nanoparticles were synthesised in the presence of oleylamine/oleic acid and then supported on Vulcan carbon. PdPt nanocubes were prepared in the presence of polyvinylpyrrolidone.

The oxygen reduction studies on magnetron-sputtered PtNP supported on MWCNT with three different Pt layer thicknesses were carried out in 0.5 M H_2SO_4 and 0.1 M KOH solutions [I]. The PtNP/MWCNT electrodes exhibited a higher electrocatalytic activity for the four-electron reduction of oxygen than bulk Pt electrodes. Tafel analysis revealed that the mechanism of the ORR is the same for the prepared nanocomposites and bulk materials.

In the next part, Pt-TiO_2/MWCNT nanocomposites were employed as electrocatalysts for ORR [II]. Incorporating TiO_2 into the structure of fuel cell catalyst supports could improve the electrocatalytic activity of Pt nanoparticles towards the ORR. The specific activity of Pt–TiO_2/MWCNT catalysts for oxygen reduction was slightly higher than that of commercial Pt/C in acid media. The prepared composite materials showed also a substantial electrocatalytic activity for ORR in alkaline solution.

The reduction of oxygen was also studied on Pt/NG nanomaterials and their ORR kinetics were compared to that of commercial Pt/C catalyst [III]. In acidic solution, 20 wt% Pt/NG catalyst prepared by borohydride reduction showed the highest specific activity for O_2 reduction from all the Pt/NG materials studied. Pt/NG nanomaterials exhibited excellent electrocatalytic activity in alkaline media and their half-wave potentials were similar to that of commercial Pt/C catalyst.

Loading effect of carbon-supported Pt nanocubes on oxygen electroreduction was explored in acidic and alkaline media [IV]. Cyclic voltammetry experiments showed characteristic hydrogen adsorption/desorption peaks of Pt(100) facets in all three electrolytes studied. The RDE measurements showed increased overall ORR electrocatalytic activity with increasing Pt content in the catalyst. The specific and mass activities were found to be constant for all the Pt loadings studied, indicating that these are independent of the amount of Pt dispersed on the carbon support.

The electrochemical reduction of oxygen on Pd nanoparticle/multi-walled carbon nanotube composites prepared by magnetron sputtering has been studied in acid and alkaline solution [V]. In 0.5 M H_2SO_4 solution the specific activity of PdNP/MWCNT catalysts was slightly lower than that of bulk Pd, it is due to different surface morphology and size of Pd nanoparticles. In 0.1 M KOH

solution the specific activities were comparable. Magnetron-sputtered catalysts heat-treated at three different temperatures (300–500 °C) [VI] showed similar electrocatalytic behaviour to bulk Pd. The PdNP/MWCNT composite annealed at 500 °C is the most active catalyst for the four-electron reduction of O_2.

The ORR kinetics was evaluated for Pd/NG electrocatalysts [VII]. The TEM images showed the uniform distribution of Pd nanoparticles over the N-doped graphene nanosheets. The RDE results indicated that Pd/NG catalysts possess a high electrocatalytic activity towards the ORR. The prepared materials catalyse a 4-electron reduction of oxygen. The Tafel behaviour of O_2 reduction on Pd/NG catalysts was similar to that of bare Pd. The Pd/NG composite showed excellent ORR performance in alkaline media and is a promising material to be used as a cathode catalyst for alkaline membrane fuel cells.

The electrochemical kinetic behaviour of the ORR on PdPt alloy nanocubes of various compositions was investigated in 0.5 M H_2SO_4, 0.1 M $HClO_4$ and 0.1 M KOH solutions [VIII, IX]. All the alloyed catalysts showed enhanced electrocatalytic activity for ORR as compared to the monometallic cubic Pd nanoparticles. In sulphuric acid, half-wave potential values for PdPt catalysts were comparable with that of Pt nanocubes. In acid media, $Pd_{36}Pt_{64}$ showed the highest specific activity for ORR from the alloyed catalysts studied, but this activity was similar to that found with Pt and Pd nanocubes. However, in alkaline solution, the SA value for $Pd_{72}Pt_{28}$ was about two times higher than that of Pd and Pt nanocubes.

In summary, all the catalyst materials studied exhibited enhanced oxygen reduction activity and good stability. The reduction of oxygen on all the platinum and palladium based nanocomposites proceeds via 4-electron pathway.

8. REFERENCES

[1] K. Kinoshita, Electrochemical Oxygen Technology, Wiley, New York, 1992.

[2] R. Adžic, Recent advances in the kinetics of oxygen reduction, in: J. Lipkowski, P.N. Ross (Eds.), Electrocatalysis, Wiley-VCH, New York, 1998, pp. 197–242.

[3] M.R. Tarasevich, A. Sadkowski, E. Yeager, Oxygen electrochemistry in: B.E. Conway, J.O.M. Bockris, E. Yeager, S.U.M. Khan, R.E. White (Eds.), Comprehensive Treatise of Electrochemistry, Vol. 7, Plenum Press, New York, 1983, pp. 301–398.

[4] E. Yeager, Dioxygen electrocatalysis – Mechanisms in relation to catalyst structure, Journal of Molecular Catalysis 38 (1986) 5–25.

[5] A. Damjanovic, Mechanistic analysis of oxygen electrode reactions, in: J.O.M. Bockris, B.E. Conway (Eds.), Modern Aspects of Electrochemistry, Vol. 5, Plenum Press, New York, 1969, pp. 369–483.

[6] V. Stamenkovic, N. M. Markovic, P.N. Ross Jr, Structure-relationships in electrocatalysis: oxygen reduction and hydrogen oxidation reactions on Pt(111) and Pt(100) in solutions containing chloride ions, Journal of Electroanalytical Chemistry 500 (2001) 44–51.

[7] N.M. Marković, R.R. Adžić, B.D. Cahan, E.B. Yeager, Structural effects in electrocatalysis: oxygen reduction on platinum low index single-crystal surfaces in perchloric acid solutions, Journal of Electroanalytical Chemistry 377 (1994) 249–259.

[8] N. Markovic, H. Gasteiger, P.N. Ross, Kinetics of oxygen reduction on Pt(hkl) electrodes: Implications for the crystallite size effect with supported Pt electrocatalysts, Journal of The Electrochemical Society 144 (1997) 1591–1597.

[9] N.M. Markovic, H.A. Gasteiger, P.N. Ross, Oxygen reduction on platinum low-index single-crystal surfaces in sulfuric acid solution: Rotating ring-Pt(hkl) disk studies, Journal of Physical Chemistry 99 (1995) 3411–3415.

[10] N.M. Marković, H.A. Gasteiger, P.N. Ross, Oxygen reduction on platinum low-index single-crystal surfaces in alkaline solution: Rotating ring disk Pt(hkl) studies, Journal of Physical Chemistry 100 (1996) 6715–6721.

[11] N.M. Marković, T.J. Schmidt, V. Stamenković, P.N. Ross, Oxygen reduction reaction on Pt and Pt bimetallic surfaces: A selective review, Fuel Cells 1 (2001) 105–116.

[12] N.M. Marković, P.N. Ross Jr, Surface science studies of model fuel cell electrocatalysts, Surface Science Reports 45 (2002) 117–229.

[13] A. Kuzume, E. Herrero, J.M. Feliu, Oxygen reduction on stepped platinum surfaces in acidic media, Journal of Electroanalytical Chemistry 599 (2007) 333–343.

[14] M.D. Maciá, J.M. Campiña, E. Herrero, J.M. Feliu, On the kinetics of oxygen reduction on platinum stepped surfaces in acidic media, Journal of Electroanalytical Chemistry 564 (2004) 141–150.

[15] G.A. Attard, A. Brew, Cyclic voltammetry and oxygen reduction activity of the Pt{1 1 0}–(1 × 1) surface, Journal of Electroanalytical Chemistry 747 (2015) 123–129.

[16] K. Kinoshita, Particle size effects for oxygen reduction on highly dispersed platinum in acid electrolytes, Journal of The Electrochemical Society 137 (1990) 845–848.

[17] E. Antolini, Structural parameters of supported fuel cell catalysts: The effect of particle size, inter-particle distance and metal loading on catalytic activity and fuel cell performance, Applied Catalysis B: Environmental 181 (2016) 298–313.
[18] A. Kabbabi, F. Gloaguen, F. Andolfatto, R. Durand, Particle size effect for oxygen reduction and methanol oxidation on Pt/C inside a proton exchange membrane, Journal of Electroanalytical Chemistry 373 (1994) 251–254.
[19] S. Mukerjee, J. McBreen, Effect of particle size on the electrocatalysis by carbon-supported Pt electrocatalysts: An in situ XAS investigation, Journal of Electro-analytical Chemistry 448 (1998) 163–171.
[20] K.J.J. Mayrhofer, B.B. Blizanac, M. Arenz, V.R. Stamenkovic, P.N. Ross, N.M. Markovic, The impact of geometric and surface electronic properties of Pt-catalysts on the particle size effect in electrocatalysis, Journal of Physical Chemistry B 109 (2005) 14433–14440.
[21] K.J.J. Mayrhofer, D. Strmcnik, B.B. Blizanac, V. Stamenkovic, M. Arenz, N.M. Markovic, Measurement of oxygen reduction activities via the rotating disc electrode method: From Pt model surfaces to carbon-supported high surface area catalysts, Electrochimica Acta 53 (2008) 3181–3188.
[22] W. Sheng, S. Chen, E. Vescovo, Y. Shao-Horn, Size influence on the oxygen re-duction reaction activity and instability of supported Pt nanoparticles, Journal of The Electrochemical Society 159 (2011) B96–B103.
[23] M. Shao, A. Peles, K. Shoemaker, Electrocatalysis on platinum nanoparticles: Particle size effect on oxygen reduction reaction activity, Nano Letters 11 (2011) 3714–3719.
[24] K. Yamamoto, T. Imaoka, W.-J. Chun, O. Enoki, H. Katoh, M. Takenaga, A. Sonoi, Size-specific catalytic activity of platinum clusters enhances oxygen reduction reactions, Nature Chemistry 1 (2009) 397–402.
[25] S.J. Ashton, A. Novo, K.J. Mayrhofer, M. Arenz, Influence of the electrolyte on the particle size effect of the oxygen reduction reaction on Pt nanoparticles, ECS Transactions 25 (2009) 455–462.
[26] A. Anastasopoulos, J.C. Davies, L. Hannah, B.E. Hayden, C.E. Lee, C. Milhano, C. Mormiche, L. Offin, The particle size dependence of the oxygen reduction reaction for carbon-supported platinum and palladium, ChemSusChem 6 (2013) 1973–1982.
[27] K. Shinozaki, Y. Morimoto, B.S. Pivovar, S.S. Kocha, Re-examination of the Pt particle size effect on the oxygen reduction reaction for ultrathin uniform Pt/C catalyst layers without influence from Nafion, Electrochimica Acta 213 (2016) 783–790.
[28] D. Li, C. Wang, D.S. Strmcnik, D.V. Tripkovic, X. Sun, Y. Kang, M. Chi, J.D. Snyder, D. van der Vliet, Y. Tsai, V.R. Stamenkovic, S. Sun, N.M. Markovic, Functional links between Pt single crystal morphology and nanoparticles with different size and shape: the oxygen reduction reaction case, Energy and Environmental Science 7 (2014) 4061–4069.
[29] A. Damjanovic, V. Brusic, Electrode kinetics of oxygen reduction on oxide-free platinum electrodes, Electrochimica Acta 12 (1967) 615–628.
[30] N. Punbusayakul, S. Talapatra, L. Ci, W. Surareungchai, P.M. Ajayan, Double-walled carbon nanotube electrodes for electrochemical sensing, Electrochemical and Solid-State Letters 10 (2007) F13–F17.
[31] G. Che, B.B. Lakshmi, E.R. Fisher, C.R. Martin, Carbon nanotubule membranes for electrochemical energy storage and production, Nature 393 (1998) 346–349.

[32] C.-T. Hsieh, J.-Y. Lin, J.-L. Wei, Deposition and electrochemical activity of Pt-based bimetallic nanocatalysts on carbon nanotube electrodes, International Journal of Hydrogen Energy 34 (2009) 685–693.
[33] W. Li, C. Liang, W. Zhou, J. Qiu, Zhou, G. Sun, Q. Xin, preparation and characterization of multiwalled carbon nanotube-supported platinum for cathode catalysts of direct methanol fuel cells, Journal of Physical Chemistry B 107 (2003) 6292–6299.
[34] G. Che, B.B. Lakshmi, C.R. Martin, E.R. Fisher, Metal-nanocluster-filled carbon nanotubes: catalytic properties and possible applications in electrochemical energy storage and production, Langmuir 15 (1999) 750–758.
[35] Y. Shao, G. Yin, Y. Gao, P. Shi, Durability study of Pt/C and Pt/CNTs catalysts under simulated PEM fuel cell conditions, Journal of The Electrochemical Society 153 (2006) A1093–A1097.
[36] X. Wang, W. Li, Z. Chen, M. Waje, Y. Yan, Durability investigation of carbon nanotube as catalyst support for proton exchange membrane fuel cell, Journal of Power Sources 158 (2006) 154–159.
[37] M.S. Ahmed, D. Kim, S. Jeon, Covalently grafted platinum nanoparticles to multi walled carbon nanotubes for enhanced electrocatalytic oxygen reduction, Electrochimica Acta 92 (2013) 168–175.
[38] R.-S. Zhong, Y.-H. Qin, D.-F. Niu, X.-S. Zhang, X.-G. Zhou, S.-G. Sun, W.-K. Yuan, Effect of carbon nanofiber surface groups on oxygen reduction reaction of supported Pt electrocatalyst, Electrochimica Acta 89 (2013) 157–162.
[39] T.K. Lee, J.H. Jung, J.B. Kim, S.H. Hur, Improved durability of Pt/CNT catalysts by the low temperature self-catalyzed reduction for the PEM fuel cells, International Journal of Hydrogen Energy 37 (2012) 17992–18000.
[40] L. Zhang, N. Zheng, A. Gao, C. Zhu, Z. Wang, Y. Wang, Z. Shi, Y. Liu, A robust fuel cell cathode catalyst assembled with nitrogen-doped carbon nanohorn and platinum nanoclusters, Journal of Power Sources 220 (2012) 449–454.
[41] Z. Liu, F. Peng, H. Wang, H. Yu, C. Chen, Q. Shi, Design of Pt catalyst with high electrocatalytic activity and well tolerance to methanol for oxygen reduction in acidic medium, Catalysis Communications 29 (2012) 11–14.
[42] B.P. Vinayan, R.I. Jafri, R. Nagar, N. Rajalakshmi, K. Sethupathi, S. Ramaprabhu, Catalytic activity of platinum–cobalt alloy nanoparticles decorated functionalized multiwalled carbon nanotubes for oxygen reduction reaction in PEMFC, International Journal of Hydrogen Energy 37 (2012) 412–421.
[43] P. Hernández-Fernández, M. Montiel, P. Ocón, J.L.G. de la Fuente, S. García-Rodríguez, S. Rojas, J.L.G. Fierro, Functionalization of multi-walled carbon nanotubes and application as supports for electrocatalysts in proton-exchange membrane fuel cell, Applied Catalysis B: Environmental 99 (2010) 343–352.
[44] J. Kim, S.W. Lee, C. Carlton, Y. Shao-Horn, Pt-covered multiwall carbon nanotubes for oxygen reduction in fuel cell applications, Journal of Physical Chemistry Letters 2 (2011) 1332–1336.
[45] S.N. Stamatin, M. Borghei, R. Dhiman, S.M. Andersen, V. Ruiz, E. Kauppinen, E.M. Skou, Activity and stability studies of platinized multi-walled carbon nanotubes as fuel cell electrocatalysts, Applied Catalysis B: Environmental 162 (2015) 289–299.
[46] W. Huang, J.M. Ahlfield, X. Zhang, P.A. Kohl, Platinum supported on functionalized carbon nanotubes for oxygen reduction reaction in PEM/AEM hybrid fuel cells, Journal of The Electrochemical Society 164 (2017) F217–F223.

[47] N. Alexeyeva, K. Tammeveski, A. Lopez-Cudero, J. Solla-Gullón, J.M. Feliu, Electroreduction of oxygen on Pt nanoparticle/carbon nanotube nanocomposites in acid and alkaline solutions, Electrochimica Acta 55 (2010) 794–803.
[48] J.-S. Zheng, X.-Z. Wang, R. Fu, D.-J. Yang, P. Li, H. Lv, J.-X. Ma, Microstructure effect of carbon nanofibers on Pt/CNFs electrocatalyst for oxygen reduction, International Journal of Hydrogen Energy 37 (2012) 4639–4647.
[49] Y. Chen, J. Xu, X. Liu, Y. Tang, T. Lu, Electrostatic self-assembly of platinum nanochains on carbon nanotubes: A highly active electrocatalyst for the oxygen reduction reaction, Applied Catalysis B: Environmental 140–141 (2013) 552–558.
[50] C. Wang, M. Waje, X. Wang, J.M. Tang, R.C. Haddon, Yan, Proton exchange membrane fuel cells with carbon nanotube based electrodes, Nano Letters 4 (2004) 345–348.
[51] G. Girishkumar, K. Vinodgopal, P.V. Kamat, Carbon nanostructures in portable fuel cells: Single-walled carbon nanotube electrodes for methanol oxidation and oxygen reduction, Journal of Physical Chemistry B 108 (2004) 19960–19966.
[52] H. Tang, J.H. Chen, Z.P. Huang, D.Z. Wang, Z.F. Ren, L.H. Nie, Y.F. Kuang, S.Z. Yao, High dispersion and electrocatalytic properties of platinum on well-aligned carbon nanotube arrays, Carbon 42 (2004) 191–197.
[53] H.-F. Cui, J.-S. Ye, W.-D. Zhang, J. Wang, F.-S. Sheu, Electrocatalytic reduction of oxygen by a platinum nanoparticle/carbon nanotube composite electrode, Journal of Electroanalytical Chemistry 577 (2005) 295–302.
[54] X. Chen, K. Eckhard, M. Zhou, M. Bron, W. Schuhmann, Electrocatalytic activity of spots of electrodeposited noble-metal catalysts on carbon nanotubes modified glassy carbon, Analytical Chemistry 81 (2009) 7597–7603.
[55] P.S. Ruvinskiy, A. Bonnefont, E.R. Savinova, Further insight into the oxygen reduction reaction on Pt nanoparticles supported on spatially structured catalytic layers, Electrocatalysis 2 (2011) 123–133.
[56] R. Sharma, K.K. Kar, Hierarchically structured catalyst layer for the oxygen reduction reaction fabricated by electrodeposition of platinum on carbon nanotube coated carbon fiber, RSC Advances 5 (2015) 66518–66527.
[57] Z. Hamoudi, A. Brahim, M.A. El Khakani, M. Mohamedi, Electroanalytical study of methanol oxidation and oxygen reduction at carbon nanohorns-Pt nano-structured electrodes, Electroanalysis 25 (2013) 538–545.
[58] A.K. Roy, C.-T. Hsieh, Pulse microwave-assisted synthesis of Pt nanoparticles onto carbon nanotubes as electrocatalysts for proton exchange membrane fuel cells, Electrochimica Acta 87 (2013) 63–72.
[59] L.V. Kumar, S. Addo Ntim, O. Sae-Khow, C. Janardhana, V. Lakshminarayanan, S. Mitra, Electro-catalytic activity of multiwall carbon nanotube-metal (Pt or Pd) nanohybrid materials synthesized using microwave-induced reactions and their possible use in fuel cells, Electrochimica Acta 83 (2012) 40–46.
[60] C.-T. Hsieh, W.-Y. Chen, I.L. Chen, A.K. Roy, Deposition and activity stability of Pt–Co catalysts on carbon nanotube-based electrodes prepared by microwave-assisted synthesis, Journal of Power Sources 199 (2012) 94–102.
[61] B. Ha, O.H. Han, Platinum-catalyzed carbon nanotubes for durability enhancement of low-temperature fuel cells, Journal of Power Sources 223 (2013) 246–253.
[62] A.A. Dameron, S. Pylypenko, J.B. Bult, K.C. Neyerlin, C. Engtrakul, C. Bochert, G.J. Leong, S.L. Frisco, L. Simpson, H.N. Dinh, B. Pivovar, Aligned carbon nano-tube array functionalization for enhanced atomic layer deposition of platinum electrocatalysts, Applied Surface Science 258 (2012) 5212–5221.

[63] T. Shu, S.-J. Liao, C.-T. Hsieh, A.K. Roy, Y.-Y. Liu, D.-Y. Tzou, W.-Y. Chen, Fabrication of platinum electrocatalysts on carbon nanotubes using atomic layer deposition for proton exchange membrane fuel cells, Electrochimica Acta 75 (2012) 101–107.
[64] S. Swann, Magnetron sputtering, Physics in Technology 19 (1988) 67.
[65] T.S. Olson, A.A. Dameron, K. Wood, S. Pylpenko, K.E. Hurst, S. Christensen, J.B. Bult, D.S. Ginley, R. O'Hayre, H. Dinh, T. Gennett, Enhanced fuel cell catalyst durability with nitrogen modified carbon supports, Journal of The Electrochemical Society 160 (2013) F389–F394.
[66] K.-C. Pham, D.S. McPhail, C. Mattevi, A.T.S. Wee, D.H.C. Chua, Graphene-carbon nanotube hybrids as robust catalyst supports in proton exchange membrane fuel cells, Journal of The Electrochemical Society 163 (2016) F255–F263.
[67] S. Hussain, H. Erikson, N. Kongi, M. Merisalu, P. Ritslaid, V. Sammelselg, K. Tammeveski, Heat-treatment effects on the ORR activity of Pt nanoparticles deposited on multi-walled carbon nanotubes using magnetron sputtering technique, International Journal of Hydrogen Energy 42 (2017) 5958–5970.
[68] S. Sharma, B.G. Pollet, Support materials for PEMFC and DMFC electrocatalysts – A review, Journal of Power Sources 208 (2012) 96–119.
[69] E. Antolini, Graphene as a new carbon support for low-temperature fuel cell catalysts, Applied Catalysis B: Environmental 123–124 (2012) 52–68.
[70] L.T. Soo, K.S. Loh, A.B. Mohamad, W.R.W. Daud, W.Y. Wong, An overview of the electrochemical performance of modified graphene used as an electrocatalyst and as a catalyst support in fuel cells, Applied Catalysis A: General 497 (2015) 198–210.
[71] M.H. Seo, S.M. Choi, H.J. Kim, W.B. Kim, The graphene-supported Pd and Pt catalysts for highly active oxygen reduction reaction in an alkaline condition, Electrochemistry Communications 13 (2011) 182–185.
[72] D.A.C. Brownson, G.E. Banks, The Handbook of Graphene Electrochemistry, Springer, London, 2014.
[73] G.V. Fortunato, F. de Lima, G. Maia, Oxygen-reduction reaction strongly electrocatalyzed by Pt electrodeposited onto graphene or graphene nanoribbons, Journal of Power Sources 302 (2016) 247–258.
[74] N. Shaari, S.K. Kamarudin, Graphene in electrocatalyst and proton conductiong membrane in fuel cell applications: An overview, Renewable and Sustainable Energy Reviews 69 (2017) 862–870.
[75] A. Ghosh, S. Basu, A. Verma, Graphene and functionalized graphene supported platinum catalyst for PEMFC, Fuel Cells 13 (2013) 355–363.
[76] H.-W. Ha, I.Y. Kim, S.-J. Hwang, R.S. Ruoff, One-pot synthesis of platinum nanoparticles embedded on reduced graphene oxide for oxygen reduction in methanol fuel cells, Electrochemical and Solid-State Letters 14 (2011) B70-B73.
[77] H. Wu, T. Peng, Z. Kou, J. Zhang, K. Cheng, D. He, M. Pan, S. Mu, Core-shell graphene@amorphous carbon composites supported platinum catalysts for oxygen reduction reaction, Chinese Journal of Catalysis 36 (2015) 490–495.
[78] Y. Zhou, K. Neyerlin, T.S. Olson, S. Pylypenko, J. Bult, H.N. Dinh, T. Gennett, Z. Shao, R. O'Hayre, Enhancement of Pt and Pt-alloy fuel cell catalyst activity and durability via nitrogen-modified carbon supports, Energy and Environmental Science 3 (2010) 1437–1446.
[79] M.S. Saha, R. Li, X. Sun, S. Ye, 3-D composite electrodes for high performance PEM fuel cells composed of Pt supported on nitrogen-doped carbon nanotubes grown on carbon paper, Electrochemistry Communications 11 (2009) 438–441.

[80] G. Vijayaraghavan, K.J. Stevenson, Synergistic assembly of dendrimer-templated platinum catalysts on nitrogen-doped carbon nanotube electrodes for oxygen reduction, Langmuir 23 (2007) 5279–5282.
[81] Y. Chen, J. Wang, H. Liu, R. Li, X. Sun, S. Ye, S. Knights, Enhanced stability of Pt electrocatalysts by nitrogen doping in CNTs for PEM fuel cells, Electrochemistry Communications 11 (2009) 2071–2076.
[82] Y. Chen, J. Wang, H. Liu, M.N. Banis, R. Li, X. Sun, T.-K. Sham, S. Ye, S. Knights, Nitrogen doping effects on carbon nanotubes and the origin of the enhanced electrocatalytic activity of supported Pt for proton-exchange membrane fuel cells, Journal of Physical Chemistry C 115 (2011) 3769–3776.
[83] S. Jiang, Y. Ma, G. Jian, H. Tao, X. Wang, Y. Fan, Y. Lu, Z. Hu, Y. Chen, Facile construction of Pt–Co/CN_x nanotube electrocatalysts and their application to the oxygen reduction reaction, Advanced Materials 21 (2009) 4953–4956.
[84] Y. Jiang, J. Zhang, Y.-H. Qin, D.-F. Niu, X.-S. Zhang, L. Niu, X.-G. Zhou, T.-H. Lu, W.-K. Yuan, Ultrasonic synthesis of nitrogen-doped carbon nanofibers as platinum catalyst support for oxygen reduction, Journal of Power Sources 196 (2011) 9356–9360.
[85] T. Palaniselvam, A. Irshad, B. Unni, S. Kurungot, Activity modulated low platium content oxygen reduction electrocatalysts prepared by inducing nano-order dislocations on carbon nanofiber through N_2-doping, Journal of Physical Chemistry C 116 (2012) 14754–14763.
[86] J. Melke, B. Peter, A. Habereder, J. Ziegler, C. Fasel, A. Nefedov, H. Sezen, C. Wöll, H. Ehrenberg, C. Roth, Metal–support interactions of platinum nanoparticles decorated N-doped carbon nanofibers for the oxygen reduction reaction, ACS Applied Materials and Interfaces 8 (2016) 82–90.
[87] Z.-H. Sheng, H.-L. Gao, W.-J. Bao, F.-B. Wang, X.-H. Xia, Synthesis of boron doped graphene for oxygen reduction reaction in fuel cells, Journal of Materials Chemistry 22 (2012) 390–395.
[88] D. Higgins, M.A. Hoque, M.H. Seo, R. Wang, F. Hassan, J.-Y. Choi, M. Pritzker, A. Yu, J. Zhang, Z. Chen, Development and simulation of sulfur-doped graphene supported platinum with exemplary stability and activity towards oxygen reduction, Advanced Functional Materials 24 (2014) 4325–4336.
[89] E. Gracia-Espino, X. Jia, T. Wågberg, Improved oxygen reduction performance of Pt–Ni nanoparticles by adhesion on nitrogen-doped graphene, Journal of Physical Chemistry C 118 (2014) 2804–2811.
[90] P. Hu, K. Liu, C.P. Deming, S. Chen, Multifunctional graphene-based nanostructures for efficient electrocatalytic reduction of oxygen, Journal of Chemical Technology and Biotechnology 90 (2015) 2132–2151.
[91] R. Imran Jafri, N. Rajalakshmi, S. Ramaprabhu, Nitrogen doped graphene nanoplatelets as catalyst support for oxygen reduction reaction in proton exchange membrane fuel cell, Journal of Materials Chemistry 20 (2010) 7114–7117.
[92] D. He, Y. Jiang, H. Lv, M. Pan, S. Mu, Nitrogen-doped reduced graphene oxide supports for noble metal catalysts with greatly enhanced activity and stability, Applied Catalysis B: Environmental 132–133 (2013) 379–388.
[93] C.-S. Liu, X.-C. Liu, G.-C. Wang, R.-P. Liang, J.-D. Qiu, Preparation of nitrogen-doped graphene supporting Pt nanoparticles as a catalyst for oxygen reduction and methanol oxidation, Journal of Electroanalytical Chemistry 728 (2014) 41–50.
[94] Z. Li, Q. Gao, H. Zhang, W. Tian, Y. Tan, W. Qian, Z. Liu, Low content Pt nanoparticles anchored on N-doped reduced graphene oxide with high and stable

electrocatalytic activity for oxygen reduction reaction, Scientific Reports 7 (2017) 43352.
[95] E. Antolini, Palladium in fuel cell catalysis, Energy and Environmental Science 2 (2009) 915–931.
[96] L.M. Vracar, D.B. Sepa, A. Damjanovic, Palladium electrode in oxygen-saturated aqueous solutions: Reduction of oxygen in the activation-controlled region, Journal of The Electrochemical Society 133 (1986) 1835–1839.
[97] L.M. Vracar, D.B. Sepa, A. Damjanovic, Palladium electrode in oxygen-saturated aqueous solutions: Potential dependent adsorption of oxygen containing species and their effect on oxygen reduction, Journal of The Electrochemical Society 136 (1989) 1973–1977.
[98] H. Erikson, A. Kasikov, C. Johans, K. Kontturi, K. Tammeveski, A. Sarapuu, Oxygen reduction on Nafion-coated thin-film palladium electrodes, Journal of Electroanalytical Chemistry 652 (2011) 1–7.
[99] M. Shao, Palladium-based electrocatalysts for hydrogen oxidation and oxygen reduction reactions, Journal of Power Sources 196 (2011) 2433–2444.
[100] S. Kondo, M. Nakamura, N. Maki, N. Hoshi, Active sites for the oxygen reduction reaction on the low and high index planes of palladium, Journal of Physical Chemistry C 113 (2009) 12625–12628.
[101] M. Shao, T. Yu, J.H. Odell, M. Jin, Y. Xia, Structural dependence of oxygen reduction reaction on palladium nanocrystals, Chemical Communications 47 (2011) 6566–6568.
[102] H. Erikson, A. Sarapuu, N. Alexeyeva, K. Tammeveski, J. Solla-Gullón, J.M. Feliu, Electrochemical reduction of oxygen on palladium nanocubes in acid and alkaline solutions, Electrochimica Acta 59 (2012) 329–335.
[103] H. Erikson, A. Sarapuu, K. Tammeveski, J. Solla-Gullón, J.M. Feliu, Enhanced electrocatalytic activity of cubic Pd nanoparticles towards the oxygen reduction reaction in acid media, Electrochemistry Communications 13 (2011) 734–737.
[104] C.-L. Lee, H.-P. Chiou, C.-R. Liu, Palladium nanocubes enclosed by (100) planes as electrocatalyst for alkaline oxygen electroreduction, International Journal of Hydrogen Energy 37 (2012) 3993–3997.
[105] C.-L. Lee, H.-P. Chiou, Methanol-tolerant Pd nanocubes for catalyzing oxygen reduction reaction in H_2SO_4 electrolyte, Applied Catalysis B: Environmental 117–118 (2012) 204–211.
[106] J.S. Spendelow, A. Wieckowski, Electrocatalysis of oxygen reduction and small alcohol oxidation in alkaline media, Physical Chemistry Chemical Physics 9 (2007) 2654–2675.
[107] T.G. Nikiforova, Y.V. Kabeneva, O.A. Runova, Carbon-supported palladium catalysts for fuel cells, Russian Journal of Applied Chemistry 83 (2010) 1001–1009.
[108] J.J. Salvador-Pascual, S. Citalán-Cigarroa, O. Solorza-Feria, Kinetics of oxygen reduction reaction on nanosized Pd electrocatalyst in acid media, Journal of Power Sources 172 (2007) 229–234.
[109] S.M. Senthil Kumar, J. Soler Herrero, S. Irusta, K. Scott, The effect of pretreatment of Vulcan XC-72R carbon on morphology and electrochemical oxygen reduction kinetics of supported Pd nano-particle in acidic electrolyte, Journal of Electroanalytical Chemistry 647 (2010) 211–221.
[110] G.F. Alvarez, M. Mamlouk, S.M. Senthil Kumar, K. Scott, Preparation and characterisation of carbon-supported palladium nanoparticles for oxygen reduction in low

temperature PEM fuel cells, Journal of Applied Electrochemistry 41 (2011) 925–937.
[111] H. Li, G. Sun, N. Li, S. Sun, D. Su, Q. Xin, Design and preparation of highly active Pt−Pd/C catalyst for the oxygen reduction reaction, Journal of Physical Chemistry C 111 (2007) 5605–5617.
[112] H. Li, Q. Xin, W. Li, Z. Zhou, L. Jiang, S. Yang, G. Sun, An improved palladium-based DMFCs cathode catalyst, Chemical Communications (2004) 2776–2777.
[113] A.C. Garcia, V.A. Paganin, E.A. Ticianelli, CO tolerance of PdPt/C and PdPtRu/C anodes for PEMFC, Electrochimica Acta 53(12) (2008) 4309–4315.
[114] Z. Liu, L. Hong, M.P. Tham, T.H. Lim, H. Jiang, Nanostructured Pt/C and Pd/C catalysts for direct formic acid fuel cells, Journal of Power Sources 161(2) (2006) 831–835.
[115] L. Jiang, A. Hsu, D. Chu, R. Chen, Size-dependent activity of palladium nanoparticles for oxygen electroreduction in alkaline solutions, Journal of The Electrochemical Society 156 (2009) B643–B649.
[116] N. Alexeyeva, A. Sarapuu, K. Tammeveski, F.J. Vidal-Iglesias, J. Solla-Gullón, J.M. Feliu, Electroreduction of oxygen on Vulcan carbon supported Pd nanoparticles and Pd–M nanoalloys in acid and alkaline solutions, Electrochimica Acta 56 (2011) 6702–6708.
[117] K. Jukk, N. Alexeyeva, C. Johans, K. Kontturi, K. Tammeveski, Oxygen reduction on Pd nanoparticle/multi-walled carbon nanotube composites, Journal of Electroanalytical Chemistry 666 (2012) 67–75.
[118] C.-L. Lee, Y.-C. Huang, L.-C. Kuo, Y.-W. Lin, Preparation of carbon nanotube-supported palladium nanoparticles by self-regulated reduction of surfactant, Carbon 45 (2007) 203–206.
[119] C.-L. Lee, Synthesis and electroactivity of carbon-nanomaterials-supported Pd nanoparticles from self-regulated reduction of sodium n-dodecyl sulfate, Journal of Solid State Electrochemistry 11 (2007) 1313–1317.
[120] S. Chakraborty, C. Retna Raj, Electrocatalytic performance of carbon nanotube-supported palladium particles in the oxidation of formic acid and the reduction of oxygen, Carbon 48 (2010) 3242–3249.
[121] B.P. Vinayan, K. Sethupathi, S. Ramaprabhu, Facile synthesis of triangular shaped palladium nanoparticles decorated nitrogen doped graphene and their catalytic study for renewable energy applications, International Journal of Hydrogen Energy 38 (2013) 2240–2250.
[122] A.D. Franklin, J.T. Smith, T. Sands, T.S. Fisher, K.-S. Choi, D.B. Janes, Controlled decoration of single-walled carbon nanotubes with Pd nanocubes, Journal of Physical Chemistry C 111 (2007) 13756–13762.
[123] C.-T. Hsieh, Y.-Y. Liu, A.K. Roy, Pulse electrodeposited Pd nanoclusters on graphene-based electrodes for proton exchange membrane fuel cells, Electrochimica Acta 64 (2012) 205–210.
[124] H. Erikson, M. Liik, A. Sarapuu, J. Kozlova, V. Sammelselg, K. Tammeveski, Oxygen reduction on electrodeposited Pd coatings on glassy carbon, Electrochimica Acta 88 (2013) 513–518.
[125] C. Liang, W. Xia, H. Soltani-Ahmadi, O. Schluter, R.A. Fischer, M. Muhler, The two-step chemical vapor deposition of Pd(allyl)Cp as an atom-efficient route to synthesize highly dispersed palladium nanoparticles on carbon nanofibers, Chemical Communications (2005) 282–284.

[126] J. Wang, C. Liu, A. Lushington, N. Cheng, M.N. Banis, A. Riese, X. Sun, Pd on carbon nanotubes-supported Ag for formate oxidation: The effect of Ag on anti-poisoning performance, Electrochimica Acta 210 (2016) 285–292.
[127] Y. Jiang, J. Chen, J. Zhang, A. Li, Y. Zeng, F. Zhou, G. Wang, R. Wang, Ultralow loading palladium nanocatalysts prepared by atomic layer deposition on three-dimensional graphite-coated nickel foam to enhance the ethanol electro-oxidation reaction, RSC Advances 6 (2016) 13207–13216.
[128] J.-S. Ye, Y.-C. Bai, W.-D. Zhang, Modification of vertically aligned carbon nanotube arrays with palladium nanoparticles for electrocatalytic reduction of oxygen, Microchimica Acta 165 (2009) 361–366.
[129] Y.S. Li, T.S. Zhao, Ultra-low catalyst loading cathode electrode for anion-exchange membrane fuel cells, International Journal of Hydrogen Energy 37 (2012) 15334–15338.
[130] M. Cano, A. Benito, W.K. Maser, E.P. Urriolabeitia, One-step microwave synthesis of palladium–carbon nanotube hybrids with improved catalytic performance, Carbon 49 (2011) 652–658.
[131] J.-S. Zheng, X.-S. Zhang, P. Li, J. Zhu, X.-G. Zhou, W.-K. Yuan, Effect of carbon nanofiber microstructure on oxygen reduction activity of supported palladium electrocatalyst, Electrochemistry Communications 9 (2007) 895–900.
[132] Y.-X. Huang, J.-F. Xie, X. Zhang, L. Xiong, H.-Q. Yu, Reduced graphene oxide supported palladium nanoparticles via photoassisted citrate reduction for enhanced electrocatalytic activities, ACS Applied Materials and Interfaces 6 (2014) 15795–15801.
[133] K. Kakaei, H. Gharibi, Palladium nanoparticle catalysts synthesis on graphene in sodium dodecyl sulfate for oxygen reduction reaction, Energy 65 (2014) 166–171.
[134] Z.-T. Liu, K.-L. Huang, Y.-S. Wu, Y.-P. Lyu, C.-L. Lee, A comparison of physically and chemically defective graphene nanosheets as catalyst supports for cubic Pd nanoparticles in an alkaline oxygen reduction reaction, Electrochimica Acta 186 (2015) 552–561.
[135] C.P. Deming, R. Mercado, V. Gadiraju, S.W. Sweeney, M. Khan, S. Chen, Graphene quantum dots-supported palladium nanoparticles for efficient electrocatalytic reduction of oxygen in alkaline media, ACS Sustainable Chemistry and Engineering 3 (2015) 3315–3323.
[136] S. Kabir, A. Serov, P. Atanassov, Palladium nanoparticles supported on 3D-graphene nanosheets for oxygen reduction reactions in alkaline media, ECS Transactions 72 (2016) 39–47.
[137] S. Kabir, A. Serov, A. Zadick, K. Artyushkova, P. Atanassov, Palladium nanoparticles supported on three-dimensional graphene nanosheets: Superior cathode electrocatalysts, ChemElectroChem 3 (2016) 1655–1666.
[138] C.P. Deming, R. Mercado, J.E. Lu, V. Gadiraju, M. Khan, S. Chen, Oxygen electroreduction catalyzed by palladium nanoparticles supported on nitrogen-doped graphene quantum dots: Impacts of nitrogen dopants, ACS Sustainable Chemistry and Engineering 4 (2016) 6580–6589.
[139] H. Kim, K. Lee, S.I. Woo, Y. Jung, On the mechanism of enhanced oxygen reduction reaction in nitrogen-doped graphene nanoribbons, Physical Chemistry Chemical Physics 13 (2011) 17505–17510.
[140] K.D. Beard, J.W. Van Zee, J.R. Monnier, Preparation of carbon-supported Pt–Pd electrocatalysts with improved physical properties using electroless deposition methods, Applied Catalysis B: Environmental 88 (2009) 185–193.

[141] S. Ghosh, R.K. Sahu, C.R. Raj, Pt–Pd alloy nanoparticle-decorated carbon nanotubes: A durable and methanol tolerant oxygen reduction electrocatalyst, Nanotechnology 23 (2012) 385602.
[142] F.J. Vidal-Iglesias, A. López-Cudero, J. Solla-Gullón, A. Aldaz, J.M. Feliu, Pd-modified shape-controlled Pt nanoparticles towards formic acid electrooxidation, Electrocatalysis 3 (2012) 313–323.
[143] C. Kim, J. Kim, S. Yang, H. Lee, One-pot synthesis of Pd@PdPt core-shell nanocubes on carbon supports, RSC Advances 4 (2014) 63677–63680.
[144] Z.-C. Zhang, J.-F. Hui, Z.-G. Guo, Q.-Y. Yu, B. Xu, X. Zhang, Z.-C. Liu, C.-M. Xu, J.-S. Gao, X. Wang, Solvothermal synthesis of Pt-Pd alloys with selective shapes and their enhanced electrocatalytic activities, Nanoscale 4 (2012) 2633–2639.
[145] B. Lim, M. Jiang, P.H.C. Camargo, E.C. Cho, J. Tao, X. Lu, Y. Zhu, Y. Xia, Pd-Pt bimetallic nanodendrites with high activity for oxygen reduction, Science 324 (2009) 1302.
[146] L. Sun, H. Wang, K. Eid, S.M. Alshehri, V. Malgras, Y. Yamauchi, L. Wang, One-Step synthesis of dendritic bimetallic PtPd nanoparticles on reduced graphene oxide and its electrocatalytic properties, Electrochimica Acta 188 (2016) 845–851.
[147] J.-J. Lv, J.-N. Zheng, H.-B. Zhang, M. Lin, A.-J. Wang, J.-R. Chen, J.-J. Feng, Simple synthesis of platinum–palladium nanoflowers on reduced graphene oxide and their enhanced catalytic activity for oxygen reduction reaction, Journal of Power Sources 269 (2014) 136–143.
[148] J.-N. Zheng, L.-L. He, F.-Y. Chen, A.-J. Wang, M.-W. Xue, J.-J. Feng, Simple one-pot synthesis of platinum-palladium nanoflowers with enhanced catalytic activity and methanol-tolerance for oxygen reduction in acid media, Electrochimica Acta 137 (2014) 431–438.
[149] J.-J. Lv, N. Wisitruangsakul, J.-J. Feng, J. Luo, K.-M. Fang, A.-J. Wang, Biomolecule-assisted synthesis of porous PtPd alloyed nanoflowers supported on reduced graphene oxide with highly electrocatalytic performance for ethanol oxidation and oxygen reduction, Electrochimica Acta 160 (2015) 100–107.
[150] G. Fu, K. Wu, J. Lin, Y. Tang, Y. Chen, Y. Zhou, T. Lu, One-pot water-based synthesis of Pt–Pd alloy nanoflowers and their superior electrocatalytic activity for theoxygen reduction reaction and remarkable methanol-tolerant ability in acid media, Journal of Physical Chemistry C 117 (2013) 9826–9834.
[151] J.W. Hong, S.W. Kang, B.-S. Choi, D. Kim, S.B. Lee, S.W. Han, Controlled synthesis of Pd–Pt alloy hollow nanostructures with enhanced catalytic activities for oxygen reduction, ACS Nano 6 (2012) 2410–2419.
[152] H. Zhang, M. Jin, J. Wang, W. Li, P.H.C. Camargo, M.J. Kim, D. Yang, Z. Xie, Y. Xia, Synthesis of Pd−Pt bimetallic nanocrystals with a concave structure through a bromide-induced galvanic replacement reaction, Journal of the American Chemical Society 133 (2011) 6078–6089.
[153] H. Zhang, M. Jin, Y. Xia, Enhancing the catalytic and electrocatalytic properties of Pt-based catalysts by forming bimetallic nanocrystals with Pd, Chemical Society Reviews 41 (2012) 8035–8049.
[154] Z.-T. Liu, H.-R. Chen, C.-L. Lee, Promising activity of concave Pd@Pd-Pt nanocubes for the oxygen reduction reaction, Electrochimica Acta 226 (2017) 1–9.
[155] C. Koenigsmann, E. Sutter, T.A. Chiesa, R.R. Adzic, S.S. Wong, Highly enhanced electrocatalytic oxygen reduction performance observed in bimetallic palladium-based nanowires prepared under ambient, surfactantless conditions, Nano Letters 12 (2012) 2013–2020.

[156] Z. Zhu, Y. Zhai, C. Zhu, Z. Wang, S. Dong, Bimetallic alloy nanowires and nanosponges: A comparative study of peroxidase mimetics and as enhanced catalysts for oxygen reduction reaction, Electrochemistry Communications 36 (2013) 22–25.
[157] T.-H. Yeh, C.-W. Liu, H.-S. Chen, K.-W. Wang, Preparation of carbon-supported PtM (M = Au, Pd, or Cu) nanorods and their application in oxygen reduction reaction, Electrochemistry Communications 31 (2013) 125–128.
[158] Y. Lu, Y. Jiang, W. Chen, PtPd porous nanorods with enhanced electrocatalytic activity and durability for oxygen reduction reaction, Nano Energy 2 (2013) 836–844.
[159] L. Wu, Z. Liu, M. Xu, J. Zhang, X. Yang, Y. Huang, J. Lin, D. Sun, L. Xu, Y. Tang, Facile synthesis of ultrathin Pd–Pt alloy nanowires as highly active and durable catalysts for oxygen reduction reaction, International Journal of Hydrogen Energy 41 (2016) 6805–6813.
[160] Y.-W. Lee, S.-E. Oh, K.-W. Park, Highly active Pt–Pd alloy catalyst for oxygen reduction reaction in buffer solution, Electrochemistry Communications 13 (2011) 1300–1303.
[161] Y. Tang, F. Gao, S. Yu, Z. Li, Y. Zhao, Surfactant-free synthesis of highly methanol-tolerant, polyhedral Pd–Pt nanocrystallines for oxygen reduction reaction, Journal of Power Sources 239 (2013) 374–381.
[162] J.-J. Lv, J.-N. Zheng, L.-L. Chen, M. Lin, A.-J. Wang, J.-R. Chen, J.-J. Feng, Facile synthesis of bimetallic alloyed Pt-Pd nanocubes on reduced graphene oxide with enhanced eletrocatalytic properties, Electrochimica Acta 143 (2014) 36–43.
[163] Y. Ye, J. Joo, S. Lee, J. Lee, A direct one-step synthetic route to Pd-Pt nanostructures with controllable shape, size, and composition for electrocatalytic applications, Journal of Materials Chemistry A 2 (2014) 19239–19246.
[164] J. Yang, J.Y. Lee, Q. Zhang, W. Zhou, Z. Liu, Carbon-supported pseudo-core–shell Pd–Pt nanoparticles for ORR with and without methanol, Journal of The Electrochemical Society 155 (2008) B776–B781.
[165] K. Sasaki, H. Naohara, Y. Cai, Y.M. Choi, P. Liu, M.B. Vukmirovic, J.X. Wang, R.R. Adzic, Core-protected platinum monolayer shell high-stability electrocatalysts for fuel-cell cathodes, Angewandte Chemie International Edition 49 (2010) 8602–8607.
[166] L. Liu, G. Samjeske, S.-i. Nagamatsu, O. Sekizawa, K. Nagasawa, S. Takao, Y. Imaizumi, T. Yamamoto, T. Uruga, Y. Iwasawa, Enhanced oxygen reduction reaction activity and characterization of Pt–Pd/C bimetallic fuel cell catalysts with Pt-enriched surfaces in acid media, Journal of Physical Chemistry C 116 (2012) 23453–23464.
[167] K. Gong, M.B. Vukmirovic, C. Ma, Y. Zhu, R.R. Adzic, Synthesis and catalytic activity of Pt monolayer on Pd tetrahedral nanocrystals with CO-adsorption-induced removal of surfactants, Journal of Electroanalytical Chemistry 662 (2011) 213–218.
[168] G. Zhang, Z.-G. Shao, W. Lu, H. Xiao, F. Xie, X. Qin, J. Li, F. Liu, B. Yi, Aqueous-phase synthesis of sub 10 nm Pdcore@Ptshell nanocatalysts for oxygen reduction reaction using amphiphilic triblock copolymers as the reductant and capping agent, Journal of Physical Chemistry C 117 (2013) 13413–13423.
[169] R. Choi, S.-I. Choi, C.H. Choi, K.M. Nam, S.I. Woo, J.T. Park, S.W. Han, Designed synthesis of well-defined Pd@Pt core–shell nanoparticles with controlled shell thickness as efficient oxygen reduction electrocatalysts, Chemistry – A European Journal 19 (2013) 8190–8198.

[170] M. Shao, G. He, A. Peles, J.H. Odell, J. Zeng, D. Su, J. Tao, T. Yu, Y. Zhu, Y. Xia, Manipulating the oxygen reduction activity of platinum shells with shape-controlled palladium nanocrystal cores, Chemical Communications 49 (2013) 9030–9032.
[171] M. Shao, A. Peles, J. Odell, Enhanced oxygen reduction activity of platinum monolayer with a gold interlayer on palladium, Journal of Physical Chemistry C 118 (2014) 18505–18509.
[172] C.-L. Lee, C.-C. Yang, C.-R. Liu, Z.-T. Liu, J.-S. Ye, Pt-coated Pd nanocubes as catalysts for alkaline oxygen reduction activity, Journal of Power Sources 268 (2014) 712–717.
[173] C.-C. Yang, H.-R. Chen, C.-L. Lee, Sub 10-nm Pd nanocubes and their coating with multi-armed Pt shells: Facile synthesis and catalysis of alkaline oxygen reduction, Journal of The Electrochemical Society 162 (2015) H512–H517.
[174] S.M. Alia, K.O. Jensen, B.S. Pivovar, Y. Yan, Platinum-coated palladium nanotubes as oxygen reduction reaction electrocatalysts, ACS Catalysis 2 (2012) 858–863.
[175] H. Zhang, Y. Yin, Y. Hu, C. Li, P. Wu, S. Wei, C. Cai, Pd@Pt core−shell nanostructures with controllable composition synthesized by a microwave method and their enhanced electrocatalytic activity toward oxygen reduction and methanol oxidation, Journal of Physical Chemistry C 114 (2010) 11861–11867.
[176] W. Wang, Z.Y. Wang, J.J. Wang, C.J. Zhong, C.J. Liu, Highly active and stable Pt–Pd alloy catalysts synthesized by room-temperature electron reduction for oxygen reduction reaction, Advanced Science 4 (2017) 1600486.
[177] N. Alexeyeva, K. Tammeveski, Electrochemical reduction of oxygen on multi-walled carbon nanotube modified glassy carbon electrodes in acid media, Electrochemical and Solid-State Letters 10 (2007) F18–F21.
[178] M. Vikkisk, I. Kruusenberg, U. Joost, E. Shulga, I. Kink, K. Tammeveski, Electrocatalytic oxygen reduction on nitrogen-doped graphene in alkaline media, Applied Catalysis B: Environmental 147 (2014) 369–376.
[179] A.J. Hart, L. van Laake, A.H. Slocum, Desktop growth of carbon-nanotube monoliths with in situ optical imaging, Small 3 (2007) 772–777.
[180] K. Tiido, N. Alexeyeva, M. Couillard, C. Bock, B.R. MacDougall, K. Tammeveski, Graphene–TiO_2 composite supported Pt electrocatalyst for oxygen reduction reaction, Electrochimica Acta 107 (2013) 509–517.
[181] J. Zhang, J. Fang, A general strategy for preparation of Pt 3d-transition metal (Co, Fe, Ni) nanocubes, Journal of the American Chemical Society 131 (2009) 18543–18547.
[182] R.M. Arán-Ais, F.J. Vidal-Iglesias, J. Solla-Gullón, E. Herrero, J.M. Feliu, Electrochemical characterization of clean shape-controlled Pt nanoparticles prepared in presence of oleylamine/oleic acid, Electroanalysis 27 (2015) 945–956.
[183] X. Huang, Y. Li, Y. Li, H. Zhou, X. Duan, Y. Huang, Synthesis of PtPd bimetal nanocrystals with controllable shape, composition, and their tunable catalytic properties, Nano Letters 12 (2012) 4265–4270.
[184] J. Solla-Gullón, F.J. Vidal-Iglesias, E. Herrero, J.M. Feliu, A. Aldaz, CO monolayer oxidation on semi-spherical and preferentially oriented (1 0 0) and (1 1 1) platinum nanoparticles, Electrochemistry Communications 8 (2006) 189–194.
[185] O.V. Cherstiouk, P.A. Simonov, V.I. Zaikovskii, E.R. Savinova, CO monolayer oxidation at Pt nanoparticles supported on glassy carbon electrodes, Journal of Electroanalytical Chemistry 554–555 (2003) 241–251.

[186] F. Maillard, E.R. Savinova, P.A. Simonov, V.I. Zaikovskii, U. Stimming, Infrared spectroscopic study of CO adsorption and electro-oxidation on carbon-supported Pt nanoparticles: Interparticle versus intraparticle heterogeneity, Journal of Physical Chemistry B 108 (2004) 17893–17904.
[187] S. Guerin, B.E. Hayden, C.E. Lee, C. Mormiche, J.R. Owen, A.E. Russell, B. Theobald, D. Thompsett, Combinatorial electrochemical screening of fuel cell electrocatalysts, Journal of Combinatorial Chemistry 6 (2004) 149–158.
[188] A. López-Cudero, J. Solla-Gullón, E. Herrero, A. Aldaz, J.M. Feliu, CO electro-oxidation on carbon supported platinum nanoparticles: Effect of aggregation, Journal of Electroanalytical Chemistry 644 (2010) 117–126.
[189] F. Maillard, E.R. Savinova, U. Stimming, CO monolayer oxidation on Pt nanoparticles: Further insights into the particle size effects, Journal of Electroanalytical Chemistry 599 (2007) 221–232.
[190] K.J.J. Mayrhofer, M. Arenz, B.B. Blizanac, V. Stamenkovic, P.N. Ross, N.M. Markovic, CO surface electrochemistry on Pt-nanoparticles: A selective review, Electrochimica Acta 50 (2005) 5144–5154.
[191] J. Solla-Gullón, A. Rodes, V. Montiel, A. Aldaz, J. Clavilier, Electrochemical characterisation of platinum–palladium nanoparticles prepared in a water-in-oil microemulsion, Journal of Electroanalytical Chemistry 554–555 (2003) 273–284.
[192] R. Chetty, S. Kundu, W. Xia, M. Bron, W. Schuhmann, V. Chirila, W. Brandl, T. Reinecke, M. Muhler, PtRu nanoparticles supported on nitrogen-doped multi-walled carbon nanotubes as catalyst for methanol electrooxidation, Electrochimica Acta 54 (2009) 4208–4215.
[193] D.C. Higgins, D. Meza, Z. Chen, Nitrogen-doped carbon nanotubes as platinum catalyst supports for oxygen reduction reaction in proton exchange membrane fuel cells, Journal of Physical Chemistry C 114 (2010) 21982–21988.
[194] D.Z. Mezalira, M. Bron, High stability of low Pt loading high surface area electrocatalysts supported on functionalized carbon nanotubes, Journal of Power Sources 231 (2013) 113–121.
[195] O.A. Baturina, B.D. Gould, Y. Garsany, K.E. Swider-Lyons, Insights on the SO_2 poisoning of Pt_3Co/VC and Pt/VC fuel cell catalysts, Electrochimica Acta 55 (2010) 6676–6686.
[196] A.J. Bard, L.R. Faulkner, Electrochemical Methods: Fundamentals and Applications, 2nd ed., Wiley, New York, 2001.
[197] S. Gottesfeld, I.D. Raistrick, S. Srinivasan, Oxygen reduction kinetics on a platinum RDE coated with a recast Nafion film, Journal of The Electrochemical Society 134 (1987) 1455–1462.
[198] D.R. Lide, CRC Handbook of Chemistry and Physics, 82nd ed., CRC Press, Boca Raton, 2001.
[199] A. Sarapuu, A. Kasikov, T. Laaksonen, K. Kontturi, K. Tammeveski, Electrochemical reduction of oxygen on thin-film Pt electrodes in acid solutions, Electrochimica Acta 53 (2008) 5873–5880.
[200] W. Sheng, S. Woo Lee, E.J. Crumlin, S. Chen, Y. Shao-Horn, Synthesis, activity and durability of Pt nanoparticles supported on multi-walled carbon nanotubes for oxygen reduction, Journal of The Electrochemical Society 158 (2011) B1398–B1404.
[201] M. Fowler, R.F. Mann, J.C. Amphlett, B.A. Peppley, P.R. Roberge, Reliability issues and voltage degradation, in: W. Vielstich, H.A. Gasteiger, A. Lamm (Eds.), Handbook of Fuel Cells: Fundamentals, Technology and Applications, Wiley, New York, 2003, p. 663.

[202] H.A. Gasteiger, S.S. Kocha, B. Sompalli, F.T. Wagner, Activity benchmarks and requirements for Pt, Pt-alloy, and non-Pt oxygen reduction catalysts for PEMFCs, Applied Catalysis B: Environmental 56 (2005) 9–35.
[203] D. Thompsett, Pt alloys as oxygen reduction catalysts, in: W. Vielstich, H.A. Gasteiger, A. Lamm (Eds.), Handbook of Fuel Cells: Fundamentals, Technology and Applications, Wiley, Chichester, 2003, p. 467.
[204] H. Yang, W. Vogel, C. Lamy, N. Alonso-Vante, Structure and electrocatalytic activity of carbon-supported Pt−Ni alloy nanoparticles toward the oxygen reduction reaction, Journal of Physical Chemistry B 108 (2004) 11024–11034.
[205] R.E. Davis, G.L. Horvath, C.W. Tobias, The solubility and diffusion coefficient of oxygen in potassium hydroxide solutions, Electrochimica Acta 12 (1967) 287–297.
[206] K. Tammeveski, M. Arulepp, T. Tenno, C. Ferrater, J. Claret, Oxygen electroreduction on titanium-supported thin Pt films in alkaline solution, Electrochimica Acta 42 (1997) 2961–2967.
[207] K. Tammeveski, T. Tenno, J. Claret, C. Ferrater, Electrochemical reduction of oxygen on thin-film Pt electrodes in 0.1 M KOH, Electrochimica Acta 42 (1997) 893–897.
[208] K. Liu, X. Kang, Z.-Y. Zhou, Y. Song, L.J. Lee, D. Tian, S. Chen, Platinum nanoparticles functionalized with acetylene derivatives: Electronic conductivity and electrocatalytic activity in oxygen reduction, Journal of Electroanalytical Chemistry 688 (2013) 143–150.
[209] R. Rizo, E. Herrero, J.M. Feliu, Oxygen reduction reaction on stepped platinum surfaces in alkaline media, Physical Chemistry Chemical Physics 15 (2013) 15416–15425.
[210] K.L. Hsueh, E.R. Gonzalez, S. Srinivasan, Electrolyte effects on oxygen reduction kinetics at platinum: A rotating ring-disc electrode analysis, Electrochimica Acta 28 (1983) 691–697.
[211] S.-Y. Lu, C.-W. Tang, Y.-H. Lin, H.-F. Kuo, Y.-C. Lai, M.-Y. Tsai, H. Ouyang, W.-K. Hsu, TiO_2-coated carbon nanotubes: A redshift enhanced photocatalysis at visible light, Applied Physics Letters 96 (2010) 231915.
[212] P.S. Ruvinskiy, A. Bonnefont, M. Houllé, C. Pham-Huu, E.R. Savinova, Preparation, testing and modeling of three-dimensionally ordered catalytic layers for electrocatalysis of fuel cell reactions, Electrochimica Acta 55 (2010) 3245–3256.
[213] N. Alexeyeva, E. Shulga, V. Kisand, I. Kink, K. Tammeveski, Electroreduction of oxygen on nitrogen-doped carbon nanotube modified glassy carbon electrodes in acid and alkaline solutions, Journal of Electroanalytical Chemistry 648 (2010) 169–175.
[214] K. Tammeveski, T. Tenno, A. Rosental, P. Talonen, L.S. Johansson, L. Niinistö, The reduction of oxygen on Pt-TiO_2 coated Ti electrodes in alkaline solution, Journal of The Electrochemical Society 146 (1999) 669–676.
[215] T. Ioroi, Z. Siroma, N. Fujiwara, S.-i. Yamazaki, K. Yasuda, Sub-stoichiometric titanium oxide-supported platinum electrocatalyst for polymer electrolyte fuel cells, Electrochemistry Communications 7 (2005) 183–188.
[216] T. Binninger, E. Fabbri, R. Kötz, T.J. Schmidt, Determination of the electrochemically active surface area of metal-oxide supported platinum catalyst, Journal of The Electrochemical Society 161 (2014) H121–H128.
[217] I. Kruusenberg, N. Alexeyeva, K. Tammeveski, J. Kozlova, L. Matisen, V. Sammelselg, J. Solla-Gullón, J.M. Feliu, Effect of purification of carbon nanotubes on their electrocatalytic properties for oxygen reduction in acid solution, Carbon 49 (2011) 4031–4039.

[218] B.E. Hayden, D. Pletcher, J.-P. Suchsland, L.J. Williams, The influence of support and particle size on the platinum catalysed oxygen reduction reaction, Physical Chemistry Chemical Physics 11 (2009) 9141–9148.
[219] O.A. Baturina, Y. Garsany, T.J. Zega, R.M. Stroud, T. Schull, K.E. Swider-Lyons, Oxygen reduction reaction on platinum/tantalum oxide electrocatalysts for PEM fuel cells, Journal of The Electrochemical Society 155 (2008) B1314–B1321.
[220] N.R. Elezović, B.M. Babić, L. Gajić-Krstajić, V. Radmilović, N.V. Krstajić, L.J. Vračar, Synthesis, characterization and electrocatalytical behavior of Nb–TiO_2/Pt nanocatalyst for oxygen reduction reaction, Journal of Power Sources 195 (2010) 3961–3968.
[221] B. Ruiz-Camacho, M.A. Valenzuela, R.G. González-Huerta, K. Suarez-Alcantara, S.E. Canton, F. Pola-Albores, Electrochemical and XAS investigation of oxygen reduction reaction on Pt-TiO_2-C catalysts, International Journal of Hydrogen Energy 38 (2013) 12648–12656.
[222] G. Jürmann, K. Tammeveski, Electroreduction of oxygen on multi-walled carbon nanotubes modified highly oriented pyrolytic graphite electrodes in alkaline solution, Journal of Electroanalytical Chemistry 597 (2006) 119–126.
[223] I. Kruusenberg, M. Marandi, V. Sammelselg, K. Tammeveski, Hydrodynamic deposition of carbon nanotubes onto HOPG: The reduction of oxygen on CNT/HOPG electrodes in alkaline solution, Electrochemical and Solid-State Letters 12 (2009) F31–F34.
[224] K. Tammeveski, T. Tenno, Oxygen reduction on thin-layer platinum-electrode in alkaline-solution, Russian Journal of Electrochemistry 31 (1995) 603–606.
[225] N.R. Elezovic, B.M. Babic, V.R. Radmilovic, L.M. Vracar, N.V. Krstajic, Nb–TiO_2 supported platinum nanocatalyst for oxygen reduction reaction in alkaline solutions, Electrochimica Acta 56 (2011) 9020–9026.
[226] M. Gustavsson, H. Ekström, P. Hanarp, L. Eurenius, G. Lindbergh, E. Olsson, B. Kasemo, Thin film Pt/TiO_2 catalysts for the polymer electrolyte fuel cell, Journal of Power Sources 163 (2007) 671–678.
[227] J. Ma, A. Habrioux, N. Alonso-Vante, The effect of substrates at cathodes in low-temperature fuel cells, ChemElectroChem 1 (2014) 37–46.
[228] L. Timperman, A. Lewera, W. Vogel, N. Alonso-Vante, Nanostructured platinum becomes alloyed at oxide-composite substrate, Electrochemistry Communications 12 (2010) 1772–1775.
[229] G. Sakai, T. Arai, T. Matsumoto, T. Ogawa, M. Yamada, K. Sekizawa, T. Taniguchi, Electrochemical and ESR study on Pt-TiO_x/C electrocatalysts with enhanced activity for ORR, ChemElectroChem 1 (2014) 366–370.
[230] A. Bauer, R. Hui, A. Ignaszak, J. Zhang, D.J. Jones, Application of a composite structure of carbon nanoparticles and Nb–TiO_2 nanofibers as electrocatalyst support for PEM fuel cells, Journal of Power Sources 210 (2012) 15–20.
[231] I. Savych, J. Bernard d'Arbigny, S. Subianto, S. Cavaliere, D.J. Jones, J. Rozière, On the effect of non-carbon nanostructured supports on the stability of Pt nanoparticles during voltage cycling: A study of TiO_2 nanofibres, Journal of Power Sources 257 (2014) 147–155.
[232] D. Huang, B. Zhang, J. Bai, Y. Zhang, G. Wittstock, M. Wang, Y. Shen, Pt catalyst supported within TiO_2 mesoporous films for oxygen reduction reaction, Electrochimica Acta 130 (2014) 97–103.
[233] S.-Y. Huang, P. Ganesan, S. Park, B.N. Popov, Development of a titanium dioxide-supported platinum catalyst with ultrahigh stability for polymer electrolyte

membrane fuel cell applications, Journal of the American Chemical Society 131 (2009) 13898–13899.
[234] W.-J. Lee, D.-H. Lim, W.H. Smyrl, Miniature H_2/O_2 fuel cells using TiO_2 nanotube substrates and sputtered Pt catalyst, Journal of Power Sources 240 (2013) 612–617.
[235] B.P. Vinayan, S. Ramaprabhu, Platinum-TM (TM = Fe, Co) alloy nanoparticles dispersed nitrogen doped (reduced graphene oxide-multiwalled carbon nanotube) hybrid structure cathode electrocatalysts for high performance PEMFC applications, Nanoscale 5 (2013) 5109–5118.
[236] D. Wei, Y. Liu, Y. Wang, H. Zhang, L. Huang, G. Yu, Synthesis of N-doped graphene by chemical vapor deposition and its electrical properties, Nano Letters 9 (2009) 1752–1758.
[237] N.P. Subramanian, X. Li, V. Nallathambi, S.P. Kumaraguru, H. Colon-Mercado, G. Wu, J.-W. Lee, B.N. Popov, Nitrogen-modified carbon-based catalysts for oxygen reduction reaction in polymer electrolyte membrane fuel cells, Journal of Power Sources 188 (2009) 38–44.
[238] H. Niwa, K. Horiba, Y. Harada, M. Oshima, T. Ikeda, K. Terakura, J.-i. Ozaki, S. Miyata, X-ray absorption analysis of nitrogen contribution to oxygen reduction reaction in carbon alloy cathode catalysts for polymer electrolyte fuel cells, Journal of Power Sources 187 (2009) 93–97.
[239] B.P. Vinayan, R. Nagar, N. Rajalakshmi, S. Ramaprabhu, Novel platinum–cobalt alloy nanoparticles dispersed on nitrogen-doped graphene as a cathode electrocatalyst for PEMFC applications, Advanced Functional Materials 22 (2012) 3519–3526.
[240] J. Solla-Gullón, V. Montiel, A. Aldaz, J. Clavilier, Electrochemical characterisation of platinum nanoparticles prepared by microemulsion: how to clean them without loss of crystalline surface structure, Journal of Electroanalytical Chemistry 491 (2000) 69–77.
[241] P. Urchaga, S. Baranton, C. Coutanceau, G. Jerkiewicz, Electro-oxidation of CO_{chem} on Pt nanosurfaces: Solution of the peak multiplicity puzzle, Langmuir 28 (2012) 3658–3663.
[242] P. Urchaga, S. Baranton, C. Coutanceau, G. Jerkiewicz, Evidence of an Eley–Rideal mechanism in the stripping of a saturation layer of chemisorbed CO on platinum nanoparticles, Langmuir 28 (2012) 13094–13104.
[243] J. Solla-Gullon, F.J. Vidal-Iglesias, A. Lopez-Cudero, E. Garnier, J.M. Feliu, A. Aldaz, Shape-dependent electrocatalysis: Methanol and formic acid electrooxidation on preferentially oriented Pt nanoparticles, Physical Chemistry Chemical Physics 10 (2008) 3689–3698.
[244] L. Guo, W.-J. Jiang, Y. Zhang, J.-S. Hu, Z.-D. Wei, L.-J. Wan, Embedding Pt nanocrystals in N-doped porous carbon/carbon nanotubes toward highly stable electrocatalysts for the oxygen reduction reaction, ACS Catalysis 5 (2015) 2903–2909.
[245] M. Nesselberger, S. Ashton, J.C. Meier, I. Katsounaros, K.J.J. Mayrhofer, M. Arenz, The particle size effect on the oxygen reduction reaction activity of Pt catalysts: Influence of electrolyte and relation to single crystal models, Journal of the American Chemical Society 133 (2011) 17428–17433.
[246] R.I. Jafri, N. Rajalakshmi, S. Ramaprabhu, Nitrogen-doped multi-walled carbon nanocoils as catalyst support for oxygen reduction reaction in proton exchange membrane fuel cell, Journal of Power Sources 195 (2010) 8080–8083.
[247] J. Ma, A. Habrioux, Y. Luo, G. Ramos-Sanchez, L. Calvillo, G. Granozzi, P.B. Balbuena, N. Alonso-Vante, Electronic interaction between platinum nanoparticles

and nitrogen-doped reduced graphene oxide: Effect on the oxygen reduction reaction, Journal of Materials Chemistry A 3 (2015) 11891–11904.
[248] F. Su, Z. Tian, C.K. Poh, Z. Wang, S.H. Lim, Z. Liu, J. Lin, Pt nanoparticles supported on nitrogen-doped porous carbon nanospheres as an electrocatalyst for fuel cells, Chemistry of Materials 22 (2010) 832–839.
[249] J. Solla-Gullon, P. Rodriguez, E. Herrero, A. Aldaz, J.M. Feliu, Surface characterization of platinum electrodes, Physical Chemistry Chemical Physics 10 (2008) 1359–1373.
[250] F.J. Vidal-Iglesias, V. Montiel, J. Solla-Gullón, Influence of the metal loading on the electrocatalytic activity of carbon-supported (100) Pt nanoparticles, Journal of Solid State Electrochemistry 20 (2016) 1107–1118.
[251] M.S. McGovern, E.C. Garnett, C. Rice, R.I. Masel, A. Wieckowski, Effects of Nafion as a binding agent for unsupported nanoparticle catalysts, Journal of Power Sources 115 (2003) 35–39.
[252] F.J. Vidal-Iglesias, R.M. Arán-Ais, J. Solla-Gullón, E. Herrero, J.M. Feliu, Electrochemical characterization of shape-controlled Pt nanoparticles in different supporting electrolytes, ACS Catalysis 2 (2012) 901–910.
[253] R.R. Adžić, J. Wang, B.M. Ocko, Structure of metal adlayers during the course of electrocatalytic reactions: O_2 reduction on Au(111) with Tl adlayers in acid solutions, Electrochimica Acta 40 (1995) 83–89.
[254] T.J. Schmidt, U.A. Paulus, H.A. Gasteiger, R.J. Behm, The oxygen reduction reaction on a Pt/carbon fuel cell catalyst in the presence of chloride anions, Journal of Electroanalytical Chemistry 508 (2001) 41–47.
[255] A. Sarapuu, S. Kallip, A. Kasikov, L. Matisen, K. Tammeveski, Electroreduction of oxygen on gold-supported thin Pt films in acid solutions, Journal of Electroanalytical Chemistry 624 (2008) 144–150.
[256] L. Borchardt, F. Hasché, M.R. Lohe, M. Oschatz, F. Schmidt, E. Kockrick, C. Ziegler, T. Lescouet, A. Bachmatiuk, B. Büchner, D. Farrusseng, P. Strasser, S. Kaskel, Transition metal loaded silicon carbide-derived carbons with enhanced catalytic properties, Carbon 50 (2012) 1861–1870.
[257] N. Gavrilov, M. Dašić-Tomić, I. Pašti, G. Ćirić-Marjanović, S. Mentus, Carbonized polyaniline nanotubes/nanosheets-supported Pt nanoparticles: Synthesis, characterization and electrocatalysis, Materials Letters 65 (2011) 962–965.
[258] C. Koenigsmann, W.-p. Zhou, R.R. Adzic, E. Sutter, S.S. Wong, Size-dependent enhancement of electrocatalytic performance in relatively defect-free, processed ultrathin platinum nanowires, Nano Letters 10 (2010) 2806–2811.
[259] E. Fabbri, S. Taylor, A. Rabis, P. Levecque, O. Conrad, R. Kötz, T.J. Schmidt, The effect of platinum nanoparticle distribution on oxygen electroreduction activity and selectivity, ChemCatChem 6 (2014) 1410–1418.
[260] S. Taylor, E. Fabbri, P. Levecque, T.J. Schmidt, O. Conrad, The effect of platinum loading and surface morphology on oxygen reduction activity, Electrocatalysis 7 (2016) 287–296.
[261] N.-I. Kim, J.Y. Cheon, J.H. Kim, J. Seong, J.-Y. Park, S.H. Joo, K. Kwon, Impact of framework structure of ordered mesoporous carbons on the performance of supported Pt catalysts for oxygen reduction reaction, Carbon 72 (2014) 354–364.
[262] G. Fu, K. Wu, X. Jiang, L. Tao, Y. Chen, J. Lin, Y. Zhou, S. Wei, Y. Tang, T. Lu, X. Xia, Polyallylamine-directed green synthesis of platinum nanocubes. Shape and electronic effect codependent enhanced electrocatalytic activity, Physical Chemistry Chemical Physics 15 (2013) 3793–3802.

[263] S.H. Joo, K. Kwon, D.J. You, C. Pak, H. Chang, J.M. Kim, Preparation of high loading Pt nanoparticles on ordered mesoporous carbon with a controlled Pt size and its effects on oxygen reduction and methanol oxidation reactions, Electrochimica Acta 54 (2009) 5746–5753.
[264] F.J. Perez-Alonso, D.N. McCarthy, A. Nierhoff, P. Hernandez-Fernandez, C. Strebel, I.E.L. Stephens, J.H. Nielsen, I. Chorkendorff, The effect of size on the oxygen electroreduction activity of mass-selected platinum nanoparticles, Angewandte Chemie International Edition 51 (2012) 4641–4643.
[265] M.L. Sattler, P.N. Ross, The surface structure of Pt crystallites supported on carbon black, Ultramicroscopy 20 (1986) 21–28.
[266] F. Maillard, S. Pronkin, E.R. Savinova, Influence of size on the electrocatalytic activities of supported metal nanoparticles in fuel cells related reactions, Handbook of Fuel Cells, Wiley, 2010.
[267] S. St. John, I. Dutta, A. P. Angelopoulos, Synthesis and characterization of electrocatalytically active platinum atom clusters and monodisperse single crystals, Journal of Physical Chemistry C 114 (2010) 13515–13525.
[268] F.J. Vidal-Iglesias, Estudio de la electrooxidación de amoniaco en medio básico sobre platino: Superficies bien definidas y nanopartículas, Universidad de Alicante, Alicante, 2005.
[269] N.R. Elezović, B.M. Babić, L. Gajić-Krstajić, P. Ercius, V.R. Radmilović, N.V. Krstajić, L.M. Vračar, Pt supported on nano-tungsten carbide as a beneficial catalyst for the oxygen reduction reaction in alkaline solution, Electrochimica Acta 69 (2012) 239–246.
[270] I. Katsounaros, S. Cherevko, A.R. Zeradjanin, K.J.J. Mayrhofer, Oxygen Electrochemistry as a Cornerstone for Sustainable Energy Conversion, Angewandte Chemie International Edition 53 (2014) 102–121.
[271] M. Grdeń, M. Łukaszewski, G. Jerkiewicz, A. Czerwiński, Electrochemical behaviour of palladium electrode: Oxidation, electrodissolution and ionic adsorption, Electrochimica Acta 53 (2008) 7583–7598.
[272] I. Kruusenberg, N. Alexeyeva, K. Tammeveski, The pH-dependence of oxygen reduction on multi-walled carbon nanotube modified glassy carbon electrodes, Carbon 47 (2009) 651–658.
[273] I. Kruusenberg, L. Matisen, Q. Shah, A.M. Kannan, K. Tammeveski, Non-platinum cathode catalysts for alkaline membrane fuel cells, International Journal of Hydrogen Energy 37 (2012) 4406–4412.
[274] L. Jiang, A. Hsu, D. Chu, R. Chen, Oxygen reduction reaction on carbon supported Pt and Pd in alkaline solutions, Journal of The Electrochemical Society 156 (2009) B370–B376.
[275] S. Ratso, I. Kruusenberg, M. Vikkisk, U. Joost, E. Shulga, I. Kink, T. Kallio, K. Tammeveski, Highly active nitrogen-doped few-layer graphene/carbon nanotube composite electrocatalyst for oxygen reduction reaction in alkaline media, Carbon 73 (2014) 361–370.
[276] P.B. Vinayan, R. Nagar, K. Sethupathi, S. Ramaprabhu, Investigation of spillover mechanism in palladium decorated hydrogen exfoliated functionalized graphene, Journal of Physical Chemistry C 115 (2011) 15679–15685.
[277] L. Qu, Y. Liu, J.-B. Baek, L. Dai, Nitrogen-doped graphene as efficient metal-free electrocatalyst for oxygen reduction in fuel cells, ACS Nano 4 (2010) 1321–1326.
[278] L. Zhang, Z. Xia, Mechanisms of oxygen reduction reaction on nitrogen-doped graphene for fuel cells, Journal of Physical Chemistry C 115 (2011) 11170–11176.

[279] J. Bai, Q. Zhu, Z. Lv, H. Dong, J. Yu, L. Dong, Nitrogen-doped graphene as catalysts and catalyst supports for oxygen reduction in both acidic and alkaline solutions, International Journal of Hydrogen Energy 38 (2013) 1413–1418.
[280] T. Huang, S. Mao, H. Pu, Z. Wen, X. Huang, S. Ci, J. Chen, Nitrogen-doped graphene-vanadium carbide hybrids as a high-performance oxygen reduction reaction electrocatalyst support in alkaline media, Journal of Materials Chemistry A 1 (2013) 13404–13410.
[281] R. Wang, X. Li, H. Li, Q. Wang, H. Wang, W. Wang, J. Kang, Y. Chang, Z. Lei, Highly stable and effective Pt/carbon nitride (CN_x) modified SiO_2 electrocatalyst for oxygen reduction reaction, International Journal of Hydrogen Energy 36 (2011) 5775–5781.
[282] X. Tuaev, J.P. Paraknowitsch, R. Illgen, A. Thomas, P. Strasser, Nitrogen-doped coatings on carbon nanotubes and their stabilizing effect on Pt nanoparticles, Physical Chemistry Chemical Physics 14 (2012) 6444–6447.
[283] P.L. Kuo, C.H. Hsu, H.M. Wu, W.S. Hsu, D. Kuo, Controllable-nitrogen doped carbon layer surrounding carbon nanotubes as novel carbon support for oxygen reduction reaction, Fuel Cells 12 (2012) 649–655.
[284] B.P. Vinayan, R. Nagar, S. Ramaprabhu, Synthesis and investigation of mechanism of platinum-graphene electrocatalysts by novel co-reduction techniques for proton exchange membrane fuel cell applications, Journal of Materials Chemistry 22 (2012) 25325–25334.
[285] C. He, P.K. Shen, Synthesis of the nitrogen-doped carbon nanotube (NCNT) bouquets and their electrochemical properties, Electrochemistry Communications 35 (2013) 80–83.
[286] S. Zhang, S. Chen, Enhanced-electrocatalytic activity of Pt nanoparticles supported on nitrogen-doped carbon for the oxygen reduction reaction, Journal of Power Sources 240 (2013) 60–65.
[287] R. Balgis, G.M. Anilkumar, S. Sago, T. Ogi, K. Okuyama, Ultrahigh oxygen reduction activity of Pt/nitrogen-doped porous carbon microspheres prepared via spray-drying, Journal of Power Sources 229 (2013) 58–64.
[288] S. Shrestha, S. Asheghi, J. Timbro, W.E. Mustain, Effects of pore structure in nitrogen functionalized mesoporous carbon on oxygen reduction reaction activity of platinum nanoparticles, Carbon 60 (2013) 28–40.
[289] G. Wu, C. Dai, D. Wang, D. Li, N. Li, Nitrogen-doped magnetic onion-like carbon as support for Pt particles in a hybrid cathode catalyst for fuel cells, Journal of Materials Chemistry 20 (2010) 3059–3068.
[290] N. Hoshi, M. Nakamura, S. Kondo, Oxygen reduction reaction on the low index planes of palladium electrodes modified with a monolayer of platinum film, Electrochemistry Communications 11 (2009) 2282–2284.
[291] C.-L. Lee, H.-P. Chiou, S.-C. Wu, C.-C. Wu, Alloy ratio effect of Pd/Pt nanoparticles on carbon nanotubes for catalysing methanol-tolerant oxygen reduction, Electrochimica Acta 56 (2010) 687–692.
[292] A. Sarapuu, A. Kasikov, N. Wong, C.A. Lucas, G. Sedghi, R.J. Nichols, K. Tammeveski, Electroreduction of oxygen on gold-supported nanostructured palladium films in acid solutions, Electrochimica Acta 55 (2010) 6768–6774.
[293] Z. Quan, Y. Wang, J. Fang, High-index faceted noble metal nanocrystals, Accounts of Chemical Research 46 (2013) 191–202.
[294] L. Ma, C. Wang, B.Y. Xia, K. Mao, J. He, X. Wu, Y. Xiong, X.W. Lou, Platinum multicubes prepared by Ni^{2+}-mediated shape evolution exhibit high electrocatalytic activity for oxygen reduction, Angewandte Chemie 127 (2015) 5758–5763.

[295] M. Jin, H. Zhang, Z. Xie, Y. Xia, Palladium concave nanocubes with high-index facets and their enhanced catalytic properties, Angewandte Chemie International Edition 50 (2011) 7850–7854.
[296] J. Gu, Y.W. Zhang, F. Tao, Shape control of bimetallic nanocatalysts through well-designed colloidal chemistry approaches, Chemical Society Reviews 41 (2012) 8050–8065.
[297] Z.M. Peng, H. Yang, Synthesis and oxygen reduction electrocatalytic property of Pt-on-Pd bimetallic heteronanostructures, Journal of the American Chemical Society 131 (2009) 7542–7543.
[298] S. St. John, R.W. Atkinson, O. Dyck, C.-J. Sun, T.A. Zawodzinski, A.B. Papandrew, Segregated Pt on Pd nanotubes for enhanced oxygen reduction activity in alkaline electrolyte, Chemical Communications 51 (2015) 16633–16636.

9. SUMMARY IN ESTONIAN

Hapniku elektrokeemiline redutseerumine plaatina- ja pallaadiumipõhistel katalüsaatoritel

Doktoritöö eesmärk oli uurida hapniku elektrokeemilist redutseerumist plaatina- ja pallaadiumipõhistel komposiitmaterjalidel nii happelises kui ka leeliselises keskkonnas, kasutades pöörleva ketaselektroodi meetodit.

Nanostruktuursete plaatina- ja pallaadiumkatalüsaatorite valmistamiseks kasutati nii keemilisi kui ka füüsikalisi meetodeid. Pt ja Pd nanoosakeste mitmeseinalistele süsiniknanotorudele kandmiseks kasutati magnetrontolmustamise meetodit. Metalli nanoosakesed seoti lämmastikuga dopeeritud grafeeni nanoliistakutele metallisoola keemilisel redutseerimisel, kasutades redutseerijatena kas naatrium tetrahüdridoboraati või etüleenglükooli. Etteantud kujuga Pt nanoosakesed sünteesiti oleüülamiini/oleiinhappe ning PdPt sulami nanokuubid polüvinüülpürrolidooni juuresolekul.

Hapniku redutseerumisreaktsiooni uuriti magnetrontolmustamisel valmistatud erinevate nominaalse Pt-kihi paksustega PtNP/MWCNT katalüsaatormaterjalidel 0,5 M H_2SO_4 ja 0,1 M KOH-i lahustes [I]. PtNP/MWCNT elektroodid näitasid kõrgemat elektrokatalüütilist aktiivsust 4-elektroniliseks hapniku redutseerumiseks kui kompaktne Pt-elektrood. Tafeli analüüs näitas, et hapniku redutseerumise mehhanism nii PtNP/MWCNT komposiitidel kui ka kompaktsel Pt-elektroodil oli sama.

Järgnevalt testiti Pt-TiO_2/MWCNT nanomaterjale kui O_2 redutseerumise elektrokatalüsaatoreid [II]. Pt-TiO_2/MWCNT materjalide eriaktiivsus oli happelises keskkonnas veidi kõrgem kui kommertsiaalsel Pt/C materjalil. Ka leeliselises lahuses näitasid valmistatud nanokomposiidid oluliselt kõrgemat aktiivsust O_2 redutseerumisel.

Hapniku elektrokeemilist redutseerumist uuriti ka plaatina nanoosakestest ja lämmastikuga-dopeeritud grafeeni nanoliistakutest koosnevatel komposiitidel ning nende kineetilisi parameetreid võrreldi kommertsiaalse Pt/C katalüsaatoriga [III]. 0,5 M H_2SO_4 lahuses näitas kõige kõrgemat hapniku redutseerumise eriaktiivsust 20% Pt/NG materjal, mis oli valmistatud $NaBH_4$-ga redutseerumisel. Pt/NG nanokomposiitidel oli suurepärane elektrokatalüütiline aktiivsus ka leeliselises lahuses ning nende poollainepotentsiaalid olid sarnased Pt/C katalüsaatoriga.

Plaatina sisalduse mõju hapniku redutseerumisele analüüsiti suurepinnalisele süsinikkandjale seondatud plaatina nanokuupidel [IV]. Tsüklilise voltamperomeetria eksperimendid kinnitasid Pt(100) tahkude olemasolu ning kõigis kolmes uuritud lahuses olid nähtavad Pt(100) iseloomulikud vesiniku adsorptsiooni/desorptsiooni piigid. Pöörleva ketaselektroodi mõõtmistest selgus, et Pt-sisalduse kasvuga kasvab ka üleüldine hapniku redutseerumise aktiivsus. Eriaktiivsused ning massaktiivsused olid konstantsed kõigi Pt-sisalduste korral, seega ei ole eriaktiivsus ega massaktiivsus sõltuvad Pt kogusest Pt/C katalüsaatoris.

Hapniku redutseerumisest uuriti magnetrontolmustamisel valmistatud pallaadiumi nanoosakestest ning mitmeseinalistest süsiniknanotorudest koosnevatel nanomaterjalidel 0,5 M H_2SO_4 ja 0,1 M KOH-i lahustes [V]. Happelises keskkonnas jäi PdNP/MWCNT elektroodide eriaktiivsus madalamaks kui kompaktsel Pd-elektroodil, mis võib olla põhjustatud erinevast Pd osakeste pinna morfoloogiast ning suurusest. 0,1 M KOH-i lahuses oli uuritud komposiitmaterjalide aktiivsus võrreldav kompaktse Pd omaga. PdNP/MWCNT materjalide kuumtöötlemisel kasutati kolme eri temperatuuri (300–500 °C) [VI]. Need elektroodid käitusid sarnaselt kompaktse Pd-elektroodiga. Kõrgeimat elektrokatalüütilist aktiivsust näitas 500 °C juures töödeldud PdNP/MWCNT materjal.

O_2 redutseerumise kineetilised parameetrid määrati ka Pd nanoosakestest ning N-dopeeritud grafeenist koosnevatele katalüsaatoritele [VII]. Läbistuselektronmikroskoobiga saadud kujutistelt oli näha Pt nanoosakeste ühtlane jaotumine süsinikmaterjalile. Pöörleva ketaselektroodi tulemused näitasid, et Pd/NG katalüsaatoritel on kõrge elektrokatalüütiline aktiivsus ning hapniku redutseerumine toimub nelja-elektronilise protsessina. Tafeli analüüsist selgus, et O_2 redutseerumisreaktsiooni mehhanism Pd/NG katalüsaatoritel ja kompaktsel Pd-elektroodil on sama. Pd/NG materjal näitas kõrget elektrokatalüütilist aktiivsust leeliselises lahuses ning võib olla potentsiaalne katoodimaterjal anioonvahetusmembraaniga kütuseelemendis.

Töö viimases osas uuriti erineva koostisega PdPt sulami nanokuupide O_2 elektroredutseerumise kineetilisi omadusi 0,5 M H_2SO_4, 0,1 M $HClO_4$ ja 0,1 M KOH-i lahustes [VIII, IX]. Valmistatud sulamite elektrokatalüütiline aktiivsus oli kõrgem kui monometallilistel Pd nanokuupidel. Väävelhappe lahuses olid PdPt nanokuupide poollainepotentsiaalid võrreldavad kuubikujuliste Pt nanoosakeste omaga. Happelises keskkonnas oli sulamil $Pd_{36}Pt_{64}$ kõrgeim eriaktiivsus, mis oli sarnane Pd ja Pt nanokuupidel saadud hapniku redutseerumise eriaktiivsusega. Kuid leeliselises keskkonnas oli $Pd_{72}Pt_{28}$ eriaktiivsus kaks korda suurem kui monometallilistel Pd ja Pt nanokuupidel.

Kokkuvõtteks näitasid kõik uuritud materjalid O_2 redutseerumisel kõrget elektrokatalüütilist aktiivsust ning stabiilsust. Hapniku redutseerumine toimus kõigil elektroodidel neljaelektronilise protsessina.

10. ACKNOWLEDGEMENTS

First of all, I would like to thank my supervisors, Assoc. Prof. Kaido Tammeveski and Dr. Nadežda Kongi, without whom this challenge would have been almost impossible. They have encouraged to ask more, do more and to be proud of what has been accomplished. I thank them for their patience, support, time and shared knowledge.

I would also like to thank the co-authors from the Institute of Physics of University of Tartu, Prof. Väino Sammelselg and Mrs. Jekaterina Kozlova for SEM measurements, Mr. Peeter Ritslaid for magnetron sputtering experiments, Dr. Leonard Matisen for XPS measurements, Mr. Aivar Tarre for CVD and ALD experiments, Dr. Arnold Rosental, Dr. Aleksei B. Treštšalov, Dr. Aarne Kasikov and Mr. Sergei Tsarenko for technical assistance. I would like to thank Dr. Protima Rauwel for TEM and EDX measurements. I am also grateful to the co-authors from School of Chemical Technology, Aalto University, Dr. Tanja Kallio and Prof. Kyösti Kontturi for TEM measurements. I am also thankful to Dr. Jaan Aruväli (Department of Geology, University of Tartu) for performing the XRD measurements.

I am very grateful to Dr. Jose Solla-Gullón and Prof. Juan M. Feliu from the University of Alicante for giving me chance to stay in their laboratory and make collaboration with them for the preparation of PdPt alloy nanocubes and Pt nanocubes decorated Vulcan XC-72R carbon catalysts. I am really thankful for their support, time and advices. I would also like to thank the co-workers form their laboratory, who supported me on that journey.

I would like to thank my co-workers and former colleagues from our work-group. My special gratitude goes to Dr. Ave Sarapuu, Dr. Heiki Erikson, Dr. Elo Kibena-Põldsepp and Dr. Ivar Kruusenberg.

My special gratitude goes to my family and especially to my mother Ülle and to Meelis for their continuous support. I am also thankful to my friends in Estonia and Spain for their encouragement.

This work has been financially supported by the Estonian Research Council (Grant nos. 8666 and 9323), institutional research funding of the Estonian Ministry of Education and Research (IUT20-16 and IUT2-24), Archimedes Foundation (Project No. 3.2.0501.10-0011) and scholarships, CRDF-ETF grant (Project No. ESC2-2975-TR-09), the project TK117 and Graduate School of Functional materials and technologies receiving funding from the European Reginal Development Fund under project 2014–2020.4.01.16-0027 in University of Tartu, Estonia. This work was also supported by the EU through the European Regional Development Fund (TK141 “Advanced materials and high-technology devices for energy recuperation systems”).

11. PUBLICATIONS

CURRICULUM VITAE

Name: Kristel Jukk
Born: December 12, 1989
Citizenship: Estonian
Address: Ravila 14a, 50411 Tartu, Estonia
E-mail: kristel.jukk@gmail.com

Education:

2013–...	University of Tartu, Faculty of Science and Technology, PhD student
2011–2013	University of Tartu, Faculty of Science and Technology, MSc (chemistry) 2013
2008–2011	University of Tartu, Faculty of Science and Technology, BSc (chemistry) 2011

Professional employment:

2017–…	Mayeri Industries AS, Product Development Manager
2011–2017	University of Tartu, Institute of Chemistry, chemist (0.5)

Major scientific publications:

1. K. Jukk, N. Alexeyeva, C. Johans, K. Kontturi, K. Tammeveski, Oxygen reduction on Pd nanoparticle/multi-walled carbon nanotube composites, Journal of Electroanalytical Chemistry 666 (2012) 67-75.
2. K. Jukk, N. Alexeyeva, A. Sarapuu, P. Ritslaid, J. Kozlova, V. Sammelselg, K. Tammeveski, Electroreduction of oxygen on sputter-deposited Pd nanolayers on multi-walled carbon nanotubes, International Journal of Hydrogen Energy 38 (2013) 3614–3620.
3. K. Jukk, N. Alexeyeva, P. Ritslaid, J. Kozlova, V. Sammelselg, K. Tammeveski, Electrochemical reduction of oxygen on heat-treated Pd nanoparticle/multi-walled carbon nanotube composites in alkaline solution, Electrocatalysis 4 (2013) 42–48.
4. K. Jukk, J. Kozlova, P. Ritslaid, V. Sammelselg, N. Alexeyeva, K. Tammeveski, Sputter-deposited Pt nanoparticle/multi-walled carbon nanotube composite catalyst for oxygen reduction reaction, Journal of Electroanalytical Chemistry 708 (2013) 31–38.
5. K. Jukk, N. Kongi, A. Tarre, A. Rosental, A.B. Treshchalov, J. Kozlova, P. Ritslaid, L. Matisen, V. Sammelselg, K. Tammeveski, Electrochemical oxygen reduction behaviour of platinum nanoparticles supported on multi-walled carbon nanotube/titanium dioxide composites, Journal of Electroanalytical Chemistry 735 (2014) 68–76.
6. K. Jukk, N. Kongi, L. Matisen, T. Kallio, K. Kontturi, K. Tammeveski, Electroreduction of oxygen on palladium nanoparticles supported on nitrogen-doped graphene nanosheets, Electrochimica Acta 137 (2014) 206–212.

7. K. Jukk, N. Kongi, K. Tammeveski, J. Solla-Gullón, J.M. Feliu, PdPt alloy nanocubes as electrocatalysts for oxygen reduction reaction in acid media, Electrochemistry Communications 56 (2015) 11–15.
8. K. Jukk, N. Kongi, P. Rauwel, L. Matisen, K. Tammeveski, Platinum nanoparticles supported on nitrogen-doped graphene nanosheets as electrocatalysts for oxygen reduction reaction, Electrocatalysis 7 (2016) 428–440.
9. K. Jukk, N. Kongi, K. Tammeveski, J. Solla-Gullón, J.M. Feliu, Electroreduction of oxygen on PdPt alloy nanocubes in alkaline and acid media, ChemElectroChem (2017, accepted for publication).
10. K. Jukk, N. Kongi, K. Tammeveski, R.M. Arán-Ais, J. Solla-Gullón, J.M. Feliu, Loading effect of carbon-supported platinum nanocubes on oxygen electroreduction, (manuscript in preparation).

ELULOOKIRJELDUS

Nimi: Kristel Jukk
Sünniaeg: 12. detsember 1989
Kodakondsus: Eesti
Aadress: Ravila 14a, 50411 Tartu, Eesti
E-mail: kristel.jukk@gmail.com

Haridus:

2013–...	Tartu Ülikool, Loodus- ja täppisteaduste valdkond, doktoriõppe üliõpilane
2011–2013	Tartu Ülikool, Loodus- ja tehnoloogiateaduskond, MSc (keemia) 2013
2008–2011	Tartu Ülikool, Loodus- ja tehnoloogiateaduskond, BSc (keemia) 2011

Teenistuskäik:

2017–…	Mayeri Industries AS, Tootearenduse juht
2011–2017	Tartu Ülikool, Keemia Instituut, 0,5 keemik

Olulisemad publikatsioonid:

1. K. Jukk, N. Alexeyeva, C. Johans, K. Kontturi, K. Tammeveski, Oxygen reduction on Pd nanoparticle/multi-walled carbon nanotube composites, Journal of Electroanalytical Chemistry 666 (2012) 67-75.
2. K. Jukk, N. Alexeyeva, A. Sarapuu, P. Ritslaid, J. Kozlova, V. Sammelselg, K. Tammeveski, Electroreduction of oxygen on sputter-deposited Pd nanolayers on multi-walled carbon nanotubes, International Journal of Hydrogen Energy 38 (2013) 3614–3620.
3. K. Jukk, N. Alexeyeva, P. Ritslaid, J. Kozlova, V. Sammelselg, K. Tammeveski, Electrochemical reduction of oxygen on heat-treated Pd nanoparticle/ multi-walled carbon nanotube composites in alkaline solution, Electrocatalysis 4 (2013) 42–48.
4. K. Jukk, J. Kozlova, P. Ritslaid, V. Sammelselg, N. Alexeyeva, K. Tammeveski, Sputter-deposited Pt nanoparticle/multi-walled carbon nanotube composite catalyst for oxygen reduction reaction, Journal of Electroanalytical Chemistry 708 (2013) 31–38.
5. K. Jukk, N. Kongi, A. Tarre, A. Rosental, A.B. Treshchalov, J. Kozlova, P. Ritslaid, L. Matisen, V. Sammelselg, K. Tammeveski, Electrochemical oxygen reduction behaviour of platinum nanoparticles supported on multi-walled carbon nanotube/titanium dioxide composites, Journal of Electroanalytical Chemistry 735 (2014) 68–76.
6. K. Jukk, N. Kongi, L. Matisen, T. Kallio, K. Kontturi, K. Tammeveski, Electroreduction of oxygen on palladium nanoparticles supported on nitrogen-doped graphene nanosheets, Electrochimica Acta 137 (2014) 206–212.

7. K. Jukk, N. Kongi, K. Tammeveski, J. Solla-Gullón, J.M. Feliu, PdPt alloy nanocubes as electrocatalysts for oxygen reduction reaction in acid media, Electrochemistry Communications 56 (2015) 11–15.
8. K. Jukk, N. Kongi, P. Rauwel, L. Matisen, K. Tammeveski, Platinum nanoparticles supported on nitrogen-doped graphene nanosheets as electrocatalysts for oxygen reduction reaction, Electrocatalysis 7 (2016) 428–440.
9. K. Jukk, N. Kongi, K. Tammeveski, J. Solla-Gullón, J.M. Feliu, Electroreduction of oxygen on PdPt alloy nanocubes in alkaline and acid media, ChemElectroChem (2017, accepted for publication).
10. K. Jukk, N. Kongi, K. Tammeveski, R.M. Arán-Ais, J. Solla-Gullón, J.M. Feliu, Loading effect of carbon-supported platinum nanocubes on oxygen electroreduction, (manuscript in preparation).

DISSERTATIONES CHIMICAE UNIVERSITATIS TARTUENSIS

1. **Toomas Tamm.** Quantum-chemical simulation of solvent effects. Tartu, 1993, 110 p.
2. **Peeter Burk.** Theoretical study of gas-phase acid-base equilibria. Tartu, 1994, 96 p.
3. **Victor Lobanov.** Quantitative structure-property relationships in large descriptor spaces. Tartu, 1995, 135 p.
4. **Vahur Mäemets.** The ^{17}O and ^{1}H nuclear magnetic resonance study of H_2O in individual solvents and its charged clusters in aqueous solutions of electrolytes. Tartu, 1997, 140 p.
5. **Andrus Metsala.** Microcanonical rate constant in nonequilibrium distribution of vibrational energy and in restricted intramolecular vibrational energy redistribution on the basis of slater's theory of unimolecular reactions. Tartu, 1997, 150 p.
6. **Uko Maran.** Quantum-mechanical study of potential energy surfaces in different environments. Tartu, 1997, 137 p.
7. **Alar Jänes.** Adsorption of organic compounds on antimony, bismuth and cadmium electrodes. Tartu, 1998, 219 p.
8. **Kaido Tammeveski.** Oxygen electroreduction on thin platinum films and the electrochemical detection of superoxide anion. Tartu, 1998, 139 p.
9. **Ivo Leito.** Studies of Brønsted acid-base equilibria in water and non-aqueous media. Tartu, 1998, 101 p.
10. **Jaan Leis.** Conformational dynamics and equilibria in amides. Tartu, 1998, 131 p.
11. **Toonika Rinken.** The modelling of amperometric biosensors based on oxidoreductases. Tartu, 2000, 108 p.
12. **Dmitri Panov.** Partially solvated Grignard reagents. Tartu, 2000, 64 p.
13. **Kaja Orupõld.** Treatment and analysis of phenolic wastewater with microorganisms. Tartu, 2000, 123 p.
14. **Jüri Ivask.** Ion Chromatographic determination of major anions and cations in polar ice core. Tartu, 2000, 85 p.
15. **Lauri Vares.** Stereoselective Synthesis of Tetrahydrofuran and Tetrahydropyran Derivatives by Use of Asymmetric Horner-Wadsworth-Emmons and Ring Closure Reactions. Tartu, 2000, 184 p.
16. **Martin Lepiku.** Kinetic aspects of dopamine D_2 receptor interactions with specific ligands. Tartu, 2000, 81 p.
17. **Katrin Sak.** Some aspects of ligand specificity of P2Y receptors. Tartu, 2000, 106 p.
18. **Vello Pällin.** The role of solvation in the formation of iotsitch complexes. Tartu, 2001, 95 p.
19. **Katrin Kollist.** Interactions between polycyclic aromatic compounds and humic substances. Tartu, 2001, 93 p.

20. **Ivar Koppel.** Quantum chemical study of acidity of strong and superstrong Brønsted acids. Tartu, 2001, 104 p.
21. **Viljar Pihl.** The study of the substituent and solvent effects on the acidity of OH and CH acids. Tartu, 2001, 132 p.
22. **Natalia Palm.** Specification of the minimum, sufficient and significant set of descriptors for general description of solvent effects. Tartu, 2001, 134 p.
23. **Sulev Sild.** QSPR/QSAR approaches for complex molecular systems. Tartu, 2001, 134 p.
24. **Ruslan Petrukhin.** Industrial applications of the quantitative structure-property relationships. Tartu, 2001, 162 p.
25. **Boris V. Rogovoy.** Synthesis of (benzotriazolyl)carboximidamides and their application in relations with *N*- and *S*-nucleophyles. Tartu, 2002, 84 p.
26. **Koit Herodes.** Solvent effects on UV-vis absorption spectra of some solvatochromic substances in binary solvent mixtures: the preferential solvation model. Tartu, 2002, 102 p.
27. **Anti Perkson.** Synthesis and characterisation of nanostructured carbon. Tartu, 2002, 152 p.
28. **Ivari Kaljurand.** Self-consistent acidity scales of neutral and cationic Brønsted acids in acetonitrile and tetrahydrofuran. Tartu, 2003, 108 p.
29. **Karmen Lust.** Adsorption of anions on bismuth single crystal electrodes. Tartu, 2003, 128 p.
30. **Mare Piirsalu.** Substituent, temperature and solvent effects on the alkaline hydrolysis of substituted phenyl and alkyl esters of benzoic acid. Tartu, 2003, 156 p.
31. **Meeri Sassian.** Reactions of partially solvated Grignard reagents. Tartu, 2003, 78 p.
32. **Tarmo Tamm.** Quantum chemical modelling of polypyrrole. Tartu, 2003. 100 p.
33. **Erik Teinemaa.** The environmental fate of the particulate matter and organic pollutants from an oil shale power plant. Tartu, 2003. 102 p.
34. **Jaana Tammiku-Taul.** Quantum chemical study of the properties of Grignard reagents. Tartu, 2003. 120 p.
35. **Andre Lomaka.** Biomedical applications of predictive computational chemistry. Tartu, 2003. 132 p.
36. **Kostyantyn Kirichenko.** Benzotriazole – Mediated Carbon–Carbon Bond Formation. Tartu, 2003. 132 p.
37. **Gunnar Nurk.** Adsorption kinetics of some organic compounds on bismuth single crystal electrodes. Tartu, 2003, 170 p.
38. **Mati Arulepp.** Electrochemical characteristics of porous carbon materials and electrical double layer capacitors. Tartu, 2003, 196 p.
39. **Dan Cornel Fara.** QSPR modeling of complexation and distribution of organic compounds. Tartu, 2004, 126 p.
40. **Riina Mahlapuu.** Signalling of galanin and amyloid precursor protein through adenylate cyclase. Tartu, 2004, 124 p.

41. **Mihkel Kerikmäe.** Some luminescent materials for dosimetric applications and physical research. Tartu, 2004, 143 p.
42. **Jaanus Kruusma.** Determination of some important trace metal ions in human blood. Tartu, 2004, 115 p.
43. **Urmas Johanson.** Investigations of the electrochemical properties of polypyrrole modified electrodes. Tartu, 2004, 91 p.
44. **Kaido Sillar.** Computational study of the acid sites in zeolite ZSM-5. Tartu, 2004, 80 p.
45. **Aldo Oras.** Kinetic aspects of dATPαS interaction with $P2Y_1$ receptor. Tartu, 2004, 75 p.
46. **Erik Mölder.** Measurement of the oxygen mass transfer through the air-water interface. Tartu, 2005, 73 p.
47. **Thomas Thomberg.** The kinetics of electroreduction of peroxodisulfate anion on cadmium (0001) single crystal electrode. Tartu, 2005, 95 p.
48. **Olavi Loog.** Aspects of condensations of carbonyl compounds and their imine analogues. Tartu, 2005, 83 p.
49. **Siim Salmar.** Effect of ultrasound on ester hydrolysis in aqueous ethanol. Tartu, 2006, 73 p.
50. **Ain Uustare.** Modulation of signal transduction of heptahelical receptors by other receptors and G proteins. Tartu, 2006, 121 p.
51. **Sergei Yurchenko.** Determination of some carcinogenic contaminants in food. Tartu, 2006, 143 p.
52. **Kaido Tämm.** QSPR modeling of some properties of organic compounds. Tartu, 2006, 67 p.
53. **Olga Tšubrik.** New methods in the synthesis of multisubstituted hydrazines. Tartu. 2006, 183 p.
54. **Lilli Sooväli.** Spectrophotometric measurements and their uncertainty in chemical analysis and dissociation constant measurements. Tartu, 2006, 125 p.
55. **Eve Koort.** Uncertainty estimation of potentiometrically measured ph and pK_a values. Tartu, 2006, 139 p.
56. **Sergei Kopanchuk.** Regulation of ligand binding to melanocortin receptor subtypes. Tartu, 2006, 119 p.
57. **Silvar Kallip.** Surface structure of some bismuth and antimony single crystal electrodes. Tartu, 2006, 107 p.
58. **Kristjan Saal.** Surface silanization and its application in biomolecule coupling. Tartu, 2006, 77 p.
59. **Tanel Tätte.** High viscosity $Sn(OBu)_4$ oligomeric concentrates and their applications in technology. Tartu, 2006, 91 p.
60. **Dimitar Atanasov Dobchev**. Robust QSAR methods for the prediction of properties from molecular structure. Tartu, 2006, 118 p.
61. **Hannes Hagu**. Impact of ultrasound on hydrophobic interactions in solutions. Tartu, 2007, 81 p.

62. **Rutha Jäger.** Electroreduction of peroxodisulfate anion on bismuth electrodes. Tartu, 2007, 142 p.
63. **Kaido Viht.** Immobilizable bisubstrate-analogue inhibitors of basophilic protein kinases: development and application in biosensors. Tartu, 2007, 88 p.
64. **Eva-Ingrid Rõõm.** Acid-base equilibria in nonpolar media. Tartu, 2007, 156 p.
65. **Sven Tamp.** DFT study of the cesium cation containing complexes relevant to the cesium cation binding by the humic acids. Tartu, 2007, 102 p.
66. **Jaak Nerut.** Electroreduction of hexacyanoferrate(III) anion on Cadmium (0001) single crystal electrode. Tartu, 2007, 180 p.
67. **Lauri Jalukse.** Measurement uncertainty estimation in amperometric dissolved oxygen concentration measurement. Tartu, 2007, 112 p.
68. **Aime Lust.** Charge state of dopants and ordered clusters formation in CaF_2:Mn and CaF_2:Eu luminophors. Tartu, 2007, 100 p.
69. **Iiris Kahn**. Quantitative Structure-Activity Relationships of environmentally relevant properties. Tartu, 2007, 98 p.
70. **Mari Reinik.** Nitrates, nitrites, N-nitrosamines and polycyclic aromatic hydrocarbons in food: analytical methods, occurrence and dietary intake. Tartu, 2007, 172 p.
71. **Heili Kasuk.** Thermodynamic parameters and adsorption kinetics of organic compounds forming the compact adsorption layer at Bi single crystal electrodes. Tartu, 2007, 212 p.
72. **Erki Enkvist.** Synthesis of adenosine-peptide conjugates for biological applications. Tartu, 2007, 114 p.
73. **Svetoslav Hristov Slavov**. Biomedical applications of the QSAR approach. Tartu, 2007, 146 p.
74. **Eneli Härk.** Electroreduction of complex cations on electrochemically polished Bi(*hkl*) single crystal electrodes. Tartu, 2008, 158 p.
75. **Priit Möller.** Electrochemical characteristics of some cathodes for medium temperature solid oxide fuel cells, synthesized by solid state reaction technique. Tartu, 2008, 90 p.
76. **Signe Viggor.** Impact of biochemical parameters of genetically different pseudomonads at the degradation of phenolic compounds. Tartu, 2008, 122 p.
77. **Ave Sarapuu.** Electrochemical reduction of oxygen on quinone-modified carbon electrodes and on thin films of platinum and gold. Tartu, 2008, 134 p.
78. **Agnes Kütt.** Studies of acid-base equilibria in non-aqueous media. Tartu, 2008, 198 p.
79. **Rouvim Kadis.** Evaluation of measurement uncertainty in analytical chemistry: related concepts and some points of misinterpretation. Tartu, 2008, 118 p.
80. **Valter Reedo.** Elaboration of IVB group metal oxide structures and their possible applications. Tartu, 2008, 98 p.

81. **Aleksei Kuznetsov.** Allosteric effects in reactions catalyzed by the cAMP-dependent protein kinase catalytic subunit. Tartu, 2009, 133 p.
82. **Aleksei Bredihhin.** Use of mono- and polyanions in the synthesis of multisubstituted hydrazine derivatives. Tartu, 2009, 105 p.
83. **Anu Ploom.** Quantitative structure-reactivity analysis in organosilicon chemistry. Tartu, 2009, 99 p.
84. **Argo Vonk.** Determination of adenosine A_{2A}- and dopamine D_1 receptor-specific modulation of adenylate cyclase activity in rat striatum. Tartu, 2009, 129 p.
85. **Indrek Kivi.** Synthesis and electrochemical characterization of porous cathode materials for intermediate temperature solid oxide fuel cells. Tartu, 2009, 177 p.
86. **Jaanus Eskusson.** Synthesis and characterisation of diamond-like carbon thin films prepared by pulsed laser deposition method. Tartu, 2009, 117 p.
87. **Marko Lätt.** Carbide derived microporous carbon and electrical double layer capacitors. Tartu, 2009, 107 p.
88. **Vladimir Stepanov.** Slow conformational changes in dopamine transporter interaction with its ligands. Tartu, 2009, 103 p.
89. **Aleksander Trummal.** Computational Study of Structural and Solvent Effects on Acidities of Some Brønsted Acids. Tartu, 2009, 103 p.
90. **Eerold Vellemäe.** Applications of mischmetal in organic synthesis. Tartu, 2009, 93 p.
91. **Sven Parkel.** Ligand binding to 5-HT_{1A} receptors and its regulation by Mg^{2+} and Mn^{2+}. Tartu, 2010, 99 p.
92. **Signe Vahur.** Expanding the possibilities of ATR-FT-IR spectroscopy in determination of inorganic pigments. Tartu, 2010, 184 p.
93. **Tavo Romann**. Preparation and surface modification of bismuth thin film, porous, and microelectrodes. Tartu, 2010, 155 p.
94. **Nadežda Aleksejeva.** Electrocatalytic reduction of oxygen on carbon nanotube-based nanocomposite materials. Tartu, 2010, 147 p.
95. **Marko Kullapere.** Electrochemical properties of glassy carbon, nickel and gold electrodes modified with aryl groups. Tartu, 2010, 233 p.
96. **Liis Siinor.** Adsorption kinetics of ions at Bi single crystal planes from aqueous electrolyte solutions and room-temperature ionic liquids. Tartu, 2010, 101 p.
97. **Angela Vaasa.** Development of fluorescence-based kinetic and binding assays for characterization of protein kinases and their inhibitors. Tartu 2010, 101 p.
98. **Indrek Tulp.** Multivariate analysis of chemical and biological properties. Tartu 2010, 105 p.
99. **Aare Selberg.** Evaluation of environmental quality in Northern Estonia by the analysis of leachate. Tartu 2010, 117 p.
100. **Darja Lavõgina.** Development of protein kinase inhibitors based on adenosine analogue-oligoarginine conjugates. Tartu 2010, 248 p.

101. **Laura Herm.** Biochemistry of dopamine D_2 receptors and its association with motivated behaviour. Tartu 2010, 156 p.
102. **Terje Raudsepp.** Influence of dopant anions on the electrochemical properties of polypyrrole films. Tartu 2010, 112 p.
103. **Margus Marandi.** Electroformation of Polypyrrole Films: *In-situ* AFM and STM Study. Tartu 2011, 116 p.
104. **Kairi Kivirand.** Diamine oxidase-based biosensors: construction and working principles. Tartu, 2011, 140 p.
105. **Anneli Kruve.** Matrix effects in liquid-chromatography electrospray mass-spectrometry. Tartu, 2011, 156 p.
106. **Gary Urb.** Assessment of environmental impact of oil shale fly ash from PF and CFB combustion. Tartu, 2011, 108 p.
107. **Nikita Oskolkov.** A novel strategy for peptide-mediated cellular delivery and induction of endosomal escape. Tartu, 2011, 106 p.
108. **Dana Martin.** The QSPR/QSAR approach for the prediction of properties of fullerene derivatives. Tartu, 2011, 98 p.
109. **Säde Viirlaid.** Novel glutathione analogues and their antioxidant activity. Tartu, 2011, 106 p.
110. **Ülis Sõukand.** Simultaneous adsorption of Cd^{2+}, Ni^{2+}, and Pb^{2+} on peat. Tartu, 2011, 124 p.
111. **Lauri Lipping.** The acidity of strong and superstrong Brønsted acids, an outreach for the "limits of growth": a quantum chemical study. Tartu, 2011, 124 p.
112. **Heisi Kurig.** Electrical double-layer capacitors based on ionic liquids as electrolytes. Tartu, 2011, 146 p.
113. **Marje Kasari.** Bisubstrate luminescent probes, optical sensors and affinity adsorbents for measurement of active protein kinases in biological samples. Tartu, 2012, 126 p.
114. **Kalev Takkis.** Virtual screening of chemical databases for bioactive molecules. Tartu, 2012, 122 p.
115. **Ksenija Kisseljova**. Synthesis of aza-β^3-amino acid containing peptides and kinetic study of their phosphorylation by protein kinase A. Tartu, 2012, 104 p.
116. **Riin Rebane.** Advanced method development strategy for derivatization LC/ESI/MS. Tartu, 2012, 184 p.
117. **Vladislav Ivaništšev.** Double layer structure and adsorption kinetics of ions at metal electrodes in room temperature ionic liquids. Tartu, 2012, 128 p.
118. **Irja Helm.** High accuracy gravimetric Winkler method for determination of dissolved oxygen. Tartu, 2012, 139 p.
119. **Karin Kipper.** Fluoroalcohols as Components of LC-ESI-MS Eluents: Usage and Applications. Tartu, 2012, 164 p.
120. **Arno Ratas.** Energy storage and transfer in dosimetric luminescent materials. Tartu, 2012, 163 p.

121. **Reet Reinart-Okugbeni**. Assay systems for characterisation of subtype-selective binding and functional activity of ligands on dopamine receptors. Tartu, 2012, 159 p.
122. **Lauri Sikk.** Computational study of the Sonogashira cross-coupling reaction. Tartu, 2012, 81 p.
123. **Karita Raudkivi.** Neurochemical studies on inter-individual differences in affect-related behaviour of the laboratory rat. Tartu, 2012, 161 p.
124. **Indrek Saar.** Design of GalR2 subtype specific ligands: their role in depression-like behavior and feeding regulation. Tartu, 2013, 126 p.
125. **Ann Laheäär.** Electrochemical characterization of alkali metal salt based non-aqueous electrolytes for supercapacitors. Tartu, 2013, 127 p.
126. **Kerli Tõnurist.** Influence of electrospun separator materials properties on electrochemical performance of electrical double-layer capacitors. Tartu, 2013, 147 p.
127. **Kaija Põhako-Esko.** Novel organic and inorganic ionogels: preparation and characterization. Tartu, 2013, 124 p.
128. **Ivar Kruusenberg.** Electroreduction of oxygen on carbon nanomaterial-based catalysts. Tartu, 2013, 191 p.
129. **Sander Piiskop.** Kinetic effects of ultrasound in aqueous acetonitrile solutions. Tartu, 2013, 95 p.
130. **Ilona Faustova**. Regulatory role of L-type pyruvate kinase N-terminal domain. Tartu, 2013, 109 p.
131. **Kadi Tamm.** Synthesis and characterization of the micro-mesoporous anode materials and testing of the medium temperature solid oxide fuel cell single cells. Tartu, 2013, 138 p.
132. **Iva Bozhidarova Stoyanova-Slavova.** Validation of QSAR/QSPR for regulatory purposes. Tartu, 2013, 109 p.
133. **Vitali Grozovski**. Adsorption of organic molecules at single crystal electrodes studied by *in situ* STM method. Tartu, 2014, 146 p.
134. **Santa Veikšina**. Development of assay systems for characterisation of ligand binding properties to melanocortin 4 receptors. Tartu, 2014, 151 p.
135. **Jüri Liiv.** PVDF (polyvinylidene difluoride) as material for active element of twisting-ball displays. Tartu, 2014, 111 p.
136. **Kersti Vaarmets.** Electrochemical and physical characterization of pristine and activated molybdenum carbide-derived carbon electrodes for the oxygen electroreduction reaction. Tartu, 2014, 131 p.
137. **Lauri Tõntson**. Regulation of G-protein subtypes by receptors, guanine nucleotides and Mn^{2+}. Tartu, 2014, 105 p.
138. **Aiko Adamson.** Properties of amine-boranes and phosphorus analogues in the gas phase. Tartu, 2014, 78 p.
139. **Elo Kibena**. Electrochemical grafting of glassy carbon, gold, highly oriented pyrolytic graphite and chemical vapour deposition-grown graphene electrodes by diazonium reduction method. Tartu, 2014, 184 p.

140. **Teemu Näykki.** Novel Tools for Water Quality Monitoring – From Field to Laboratory. Tartu, 2014, 202 p.
141. **Karl Kaupmees.** Acidity and basicity in non-aqueous media: importance of solvent properties and purity. Tartu, 2014, 128 p.
142. **Oleg Lebedev**. Hydrazine polyanions: different strategies in the synthesis of heterocycles. Tartu, 2015, 118 p.
143. **Geven Piir.** Environmental risk assessment of chemicals using QSAR methods. Tartu, 2015, 123 p.
144. **Olga Mazina.** Development and application of the biosensor assay for measurements of cyclic adenosine monophosphate in studies of G protein-coupled receptor signalinga. Tartu, 2015, 116 p.
145. **Sandip Ashokrao Kadam.** Anion receptors: synthesis and accurate binding measurements. Tartu, 2015, 116 p.
146. **Indrek Tallo.** Synthesis and characterization of new micro-mesoporous carbide derived carbon materials for high energy and power density electrical double layer capacitors. Tartu, 2015, 148 p.
147. **Heiki Erikson.** Electrochemical reduction of oxygen on nanostructured palladium and gold catalysts. Tartu, 2015, 204 p.
148. **Erik Anderson.** *In situ* Scanning Tunnelling Microscopy studies of the interfacial structure between Bi(111) electrode and a room temperature ionic liquid. Tartu, 2015, 118 p.
149. **Girinath G. Pillai.** Computational Modelling of Diverse Chemical, Bio-chemical and Biomedical Properties. Tartu, 2015, 140 p.
150. **Piret Pikma.** Interfacial structure and adsorption of organic compounds at Cd(0001) and Sb(111) electrodes from ionic liquid and aqueous electrolytes: an *in situ* STM study. Tartu, 2015, 126 p.
151. **Ganesh babu Manoharan.** Combining chemical and genetic approaches for photoluminescence assays of protein kinases. Tartu, 2016, 126 p.
152. **Carolin Siimenson**. Electrochemical characterization of halide ion adsorption from liquid mixtures at Bi(111) and pyrolytic graphite electrode surface. Tartu, 2016, 110 p.
153. **Asko Laaniste.** Comparison and optimisation of novel mass spectrometry ionisation sources. Tartu, 2016, 156 p.
154. **Hanno Evard.** Estimating limit of detection for mass spectrometric analysis methods. Tartu, 2016, 224 p.
155. **Kadri Ligi.** Characterization and application of protein kinase-responsive organic probes with triplet-singlet energy transfer. Tartu, 2016, 122 p.
156. **Margarita Kagan.** Biosensing penicillins' residues in milk flows. Tartu, 2016, 130 p.
157. **Marie Kriisa.** Development of protein kinase-responsive photo-luminescent probes and cellular regulators of protein phosphorylation. Tartu, 2016, 106 p.
158. **Mihkel Vestli.** Ultrasonic spray pyrolysis deposited electrolyte layers for intermediate temperature solid oxide fuel cells. Tartu, 2016, 156 p.

159. **Silver Sepp**. Influence of porosity of the carbide-derived carbon on the properties of the composite electrocatalysts and characteristics of polymer electrolyte fuel cells. Tartu, 2016, 137p.
160. **Kristjan Haav**. Quantitative relative equilibrium constant measurements in supramolecular chemistry. Tartu, 2017, 158 p.
161. **Anu Teearu**. Development of MALDI-FT-ICR-MS methodology for the analysis of resinous materials. Tartu, 2017, 205 p.
162. **Taavi Ivan**. Bifunctional inhibitors and photoluminescent probes for studies on protein complexes. Tartu, 2017, 140 p.
163. **Maarja-Liisa Oldekop**. Characterization of amino acid derivatization reagents for LC-MS analysis. Tartu, 2017, 147 p.